Influence of process parameters variation and sulfur-poisoning on a commercial steam-reforming catalyst

Fabian Pollesböck
0735432

MASTERARBEIT

eingereicht am

Universitäts-Masterstudiengang

Industrieller Umweltschutz, Entsorgungstechnik und Recycling

an der Montanuniversität Leoben

im Oktober 2013

Externe Betreuer: Dr. Jitka Hrbek, Dr. Reinhard Rauch
Technische Universität Wien
Betreuer: Ao.Univ.-Prof. Christian Weiß
Institut für Verfahrenstechnik des Industriellen Umweltschutzes

Die Eidesstattliche Erklärung muss unterschrieben und mit Datum versehen in Ihrer Abschlussarbeit eingebunden werden.

EIDESSTATTLICHE ERKLÄRUNG

Ich erkläre an Eides statt, dass ich diese Arbeit selbständig verfasst, andere als die angegebenen Quellen und Hilfsmittel nicht benutzt und mich auch sonst keiner unerlaubten Hilfsmittel bedient habe.

Datum 28.10.2013

Unterschrift Verfasser/in
Fabian, Pollesböck
Matrikelnummer: 0735432

Affirmation

First I want to say thank you to my dear parents, who always guided and supported me throughout my intricate academic career.

Then I want to thank my supervisors Jitka Hrbek and Reinhard Rauch from the Technical University of Vienna and Christian Weiß from the Montanuniversität Leoben for giving me the opportunity to write this thesis outside of my home university and helping me to get to know another academic institution.

Furthermore I would like to mention Silvester Fail, who helped me a lot with the test rig apparatus for my experiments and the discussion about the results. Also Nicolas Diaz and Harald Zeman were really great office colleagues.

Abstract

Influence of process parameters variation and sulfur-poisoning on a commercial steam-reforming catalyst

The goal of this work was to investigate a commercial catalyst based on noble metals, in terms of its performance for steam reforming of product gas from a dual fluidized bed biomass gasification plant. The experiments were carried out on a laboratory scale unit, consisting of a glass tube with an inner diameter of 8 mm and a height of 1000 mm, where the cylindrical hollow catalyst pellets were placed inside. The feed gasflow was around 40 L/h under atmospheric pressure. The process parameters were varied within their possible ranges. The reactor temperature was set between 700 °C and 900 °C, the spacevelocity (SV) ranged from 6000 h^{-1} to 11 000 h^{-1} and the steam-to-carbon ratio (S/C) was varied between 1 and 3. Four different feedstock gases with varying amounts of dihydrogen sulfide (H_2S) were used for the experiments.

The thermodynamic equilibrium concentrations couldn't be reached during the experiments with the tested catalyst. The highest conversion rates for methane were about 60 %, which corresponded to a methane concentration of 3 % in the output stream. The trends suggested that higher temperatures than 900 °C would lead to even higher conversion rates, but the temperature was restricted due to material limitations. The steam-to-carbon ratio influenced primarily the hydrogen yield, which increased with more steam in the inlet. A maximum methane conversion was reached at an S/C-ratio of around 2. The spacevelocity had little influence on the resulting gas composition, however the conversion rates increased slightly at lower spacevelocities. On the contrary, the influence of H_2S in the input gas had significant influence on the reforming reactions. Even at low concentrations of 50 ppm H_2S and an exposure time of 20 min, the conversion rates dropped. Higher sulfur concentrations ($\geq$ 100 ppm) caused the conversion rate of methane to fall even below 10 %.

The results of this study are intended to be used for advanced simulation models for steam reforming including sulfur-components. Since gas mixtures from biological feedstocks usually contain a large amount of sulfur components, fundamental research for an efficient treatment of these gases for applications in chemical industry or mobility is required.

Kurzfassung

Einfluss der Prozessparameter-Variation und Schwefel-Vergiftung auf einen kommerziellen Katalysator zur Dampfreformierung

Der Schwerpunkt dieser Arbeit war es, einen kommerziellen Katalysator auf Edelmetall-Basis, im Hinblick auf seine Leistung zur Dampfreformierung von Produktgas aus einer Zweibett-Wirbelschicht Biomasse-Vergasungsanlage zu untersuchen. Die Versuche wurden im Labormaßstab auf hohlen, zylinderförmigen Katalysator-Pellets mit einem Durchmesser von 8 mm bei einem Gas-Durchfluss von rund 40 L/h unter atmosphärischem Druck durchgeführt. Die Prozessparameter wurden innerhalb der möglichen Intervalle eingestellt: Die Reaktor-Temperatur variierte von 700 °C bis 900 °C, die Raumgeschwindigkeit (spacevelocity, SV) von 6000 h^{-1} bis 11 000 h^{-1} und das Dampf-zu-Kohlenstoff Verhältnis (steam-to-carbon ratio, S/C) von 1 bis 3. Es wurden vier verschiedene Gase für die Experimente verwendet, die jeweils ähnliche Zusammensetzungen, aber unterschiedliche Mengen an Schwefelwasserstoff (H_2S, Dihydrogensulfid) aufwiesen.

Das thermodynamisch mögliche Gleichgewicht wurde bei den durchgeführten Versuchen nicht erreicht. Der maximale Umsatz von Methan lag bei etwa 60 %, was einer Methan-Konzentration von ca. 3 % im Austritts-Gas entsprach. Eine Erhöhung der Temperatur würde den Trends zufolge zu besseren Ergebnissen führen, aber diese konnten aufgrund der Heizleistung des Reaktors und den werkstoffbedingten Limitierungen nicht erreicht werden. Höhere Dampf-zu-Kohlenstoff Verhältnisse lieferten generell eine erhöhte Wasserstoff-Ausbeute und setzte das Verhältnis von H_2/CO nach oben. Ein maximaler Methan-Umsatz wurde jedoch schon bereits bei einem S/C-Verhältnis von 2 erreicht. Die Raumgeschwindigkeit hatte in den vorliegenden Versuchen einen geringen Einfluss auf die Umsätze. Es wurden aber tendenziell bessere Umsätze bei niedrigeren Raumgeschwindigkeiten, somit bei längeren Verweilzeiten, festgestellt. Bei Tests mit schwefelwasserstoffhaltigen Gasen, wurden bereits leichte Umsatzeinbrüche bei einer Konzentration von 50 ppm H_2S und einer Testdauer von ca. 20 min festgestellt. Bei höheren Schwefelkonzentrationen ($\geq$ 100 ppm) sank der Umsatz von Methan drastisch ab und fiel unter 10 %.

Die Ergebnisse dieser Arbeit sollen zur Erstellung von Simulationsmodellen für die Dampfreformierung von schwefelhaltigen Gasgemischen eingesetzt werden. Da Produktgase aus Biomasse-Anlagen meist hohe Schwefelanteile aufweisen, ist Grundlagen-Forschung im Bereich der Aufbereitung dieser Gase für Einsatzbereiche wie chemische Industrie oder Mobilität notwendig.

Contents

1 Introduction

It seems like a postulate of modern society, that more consumption leads to an increased well-being. This means not only being able to eat as much food as possible whenever somebody wants to, but also to consume whatever products and services. The basic problem is, that in contrary to food consumption it is really hard satisfy the demand for goods and services of human beings and thus there no universally accepted limits have been accepted so far. Although it was stated by the Club of Rome already in the 1970s, that an unlimited growth of material consumption cannot be possible on a physically limited planet[1], the believe in science and technology have kept the producing industries on growing without respecting any physical or ecological borders. But it was also declared in this report, that a state of ecological and economic stability can be reached, where all necessary human material needs are satisfied and quality of life is high.

Although the complete depletion of cheap energy from fossil fuels haven't occurred yet, there are new problems on the political agenda now, which force the global human society to rethink modern lifestyle. One of the main issues is definitely the human caused global warming due to the large amount of emitted CO_2 in the atmosphere, which brings up severe, global ecological consequences, which endangers current well-being of plants, animals and humans. And the availability of non-renewable resources, on which economy nowadays depends very much, will come to an end sooner or later and this problem has not overcome yet.

Nowadays the gross domestic product and the energy consumption per capita seem to be unlinked, meaning that economic development can happen independently from energy consumption, for example due to advanced technology which requires less energy[2, p. 15]. But often energy intense industries were outsourced to developing countries, thus the direct energy consumption in western countries was reduced in the official balance, but the products, which are bought in western states, still require a lot of energy to be produced.

1.1 Energy Use in Austria

The total energy consumption in Austria was 1458 PJ in 2010, which corresponds to an annual per capita energy consumption of around 4000 kg of crude oil equivalent[3]. This corresponds to an increase of energy use of 39 % since 1990. 71 % of the Austrian gross national energy consumption is covered by fossil fuels.

Nowadays renewable energies have a fraction of around 26 % (20 years ago it was 22 %) of the total energy consumption and it still seems hard to increase this fraction despite all efforts which are made by companies, citizen and politics[3].

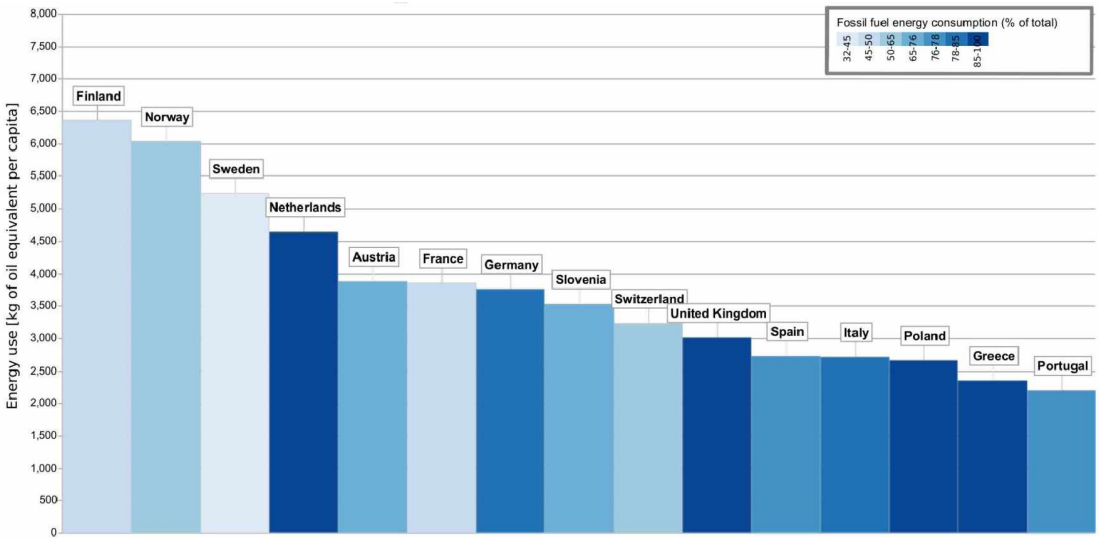

Figure 1.1: Primary energy use in 2011 (before transformation to other end-use fuels) in kilograms of oil equivalent, per capita[4, 5]

The electrical energy demand has been rising steadily, although most devices became more energy efficient, the increasing amount of various electric gadgets, automatization and the still ongoing triumph of omnipresent microelectronic devices everywhere have kept the demand for electricity growing. Around 60 % of the gross electric energy demand in Austria is produced by hydro power and another 11 % from other renewable energy sources [6]. Anyway since 2001 Austria has been depending on electric imports to satisfy the ever growing need for energy.

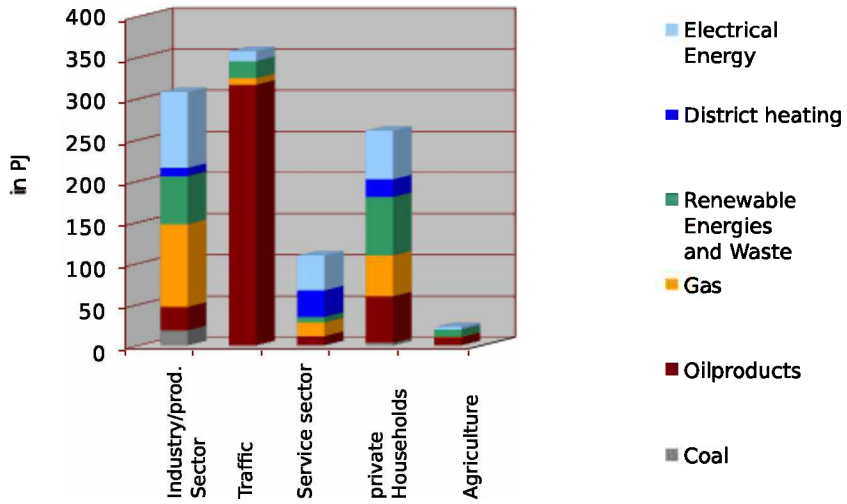

Figure 1.2: Energetic final consumption of particular sectors by energy carriers in 2009 [2, p. 21]

As can be seen in Fig. 1.2, the largest sector for primary energy consumption in Austria is transportation with around 33 % of the total energy demand[3]. This is also the sector with the highest percentage of fossil fuels (95 %). Since 1990 the consumption of energy in the transportation sector rose for 71 %, which is primary due to the fact, that there are 41 % more cars, high growth rates in transport of goods and especially due to the rapid growth of air traffic (increase of 110 %)[2].

Since many years a lot of effort has been done in research and development of new ways of transportation but up to now, there were no revolutionary inventions in transportation technology so far. Electric powered cars seem to be a promising option, but they still lack in energy density of the storage tanks, recharging rates of the accumulators and they are still far more expensive than regular automobiles. The long promised hydrogen powered car unfortunately had been promised for a long time and is unfortunately still far away from series production. Thus, besides primarily reducing the demand for individual transportation, which would have the highest impact on energy usage, it is necessary to reduce the carbon footprint right now and find alternative, renewable fuels for the already established technology of transportation.

As there are still ongoing trends towards more flexibility and high mobility in society, it is most probable that there will be no significant changes in energy consumption by just providing more energy efficient technology. Energy consumption depends mostly on the behavior of people and their will to change towards a lower consumption economy. But also advancements in technology will accompany the path of society towards a sustainable energy future. To keep the currently established technology, but to transform it towards a renewable energy basis, one possibility is to use fuels based on biomass.

1.2 Biofuels

Biomass is defined as biological material derived from living or recently dead organisms. This includes different plants, animals and their by-products, such as biodegradables wastes which can be used as fuels. Excluded from this definition is biomass, which had been transformed by geological processes into substances such as oil or coal[7].

Biofuels can be either solid, liquid or gaseous energy carriers, which are derived from different sources of biomass. Not only the rising oil prices have put the spotlight on biofuels and other renewable energy sources. Also energy safety, independence from foreign imports and environmental issues like global warming are high on the political agenda. This energy source cannot replace oil at the moment and fully satisfy our high energy demand, due to insufficient available land area. However the conversion of biomass from different sources (including waste) can be, in conjunction with less consumption and other alternative energy sources, a promising pathway to make our society less dependent on fossil fuels and reduce the impacts of global warming.

1.3 Goals Definition

There are different ways to produce biofuels from various biological feedstocks. Some of them are described in more detail in the next chapter 2.1. Process technology provides knowledge and experience for the conversion of different feedstocks, but compared to traditional energy carriers like coal and oil, there are still many challenges yet to be mastered for biomass energy.

The goal of this thesis was to investigate the performance of a commercial steam reforming catalyst for the reforming of product gas from biomass gasification for the production of liquid or gaseous fuels. Therefore the catalyst had been tested under different process conditions on laboratory scale. The experimental parameters such as temperature and feedstock gases were as close as possible to real process conditions. The results shall provide a better overall understanding of steam reforming reactions, possible usage of this commercial steam reforming catalyst on a larger scale and for the planning and simulation of industrial steam reforming reactors.

In the wider context this knowledge shall lead to an improved production of sustainable fuels, especially for the transportation sector, which will reduce the large amount of used fossil energy in this sector.

2 Fundamental Principles

2.1 Biomass Gasification

Biomass is one promising pillar for a renewable energy system in central Europe, due to its availability and still not yet fully developed potential. In general biomass can be all substances with an organic origin, thus including all living animals and plants, their residuals (e.g. excrements), dead (but not yet fossil) animals and plants (e.g. straw) and to a large extend all substances, which result from the use of organic matter (e.g. organic waste, paper and wood pulp, vegetable oil,...). Biomass can be separated in primary products, which originate from direct photolytic use of solar energy (basically all plants) and secondary products, which get their energy by converting primary products to higher organisms (e.g. animals and their excrements, sewage sludge, etc.) One of the great advantages of biomass is the easy handling and storage compared to other renewable energies like thermal solar energy or photovoltaics. Apart from burning biomass as the easiest way to make use of biomass energy, which had been practised for thousands of years, there are various other possibilities to gain high value energy from biomass[7, p. 5]:

Thermo-chemical conversion Biomass can be refined by applying heat to obtain solid, liquid or gaseous secondary fuels. The main processes are gasification, pyrolysis and carbonization. The primary goal is to produce an energy carrier, which is easy transportable and has a high energy density. Sometimes also certain chemical properties (e.g. gas composition) are pursued.

Physico-chemical conversion The basis for physico-chemical conversion are oleiferous plants, which can be modified with physical methods (cutting, mixing, pressing, filtration, etc.) to gain vegetable oil. The most prominent representative is for example rapeseed-oil, which can be processed to rapeseed methyl ester (RME), which can be used in most modern diesel engines and has the advantage to be biologically degradable[8].

Bio-chemical conversion These processes include all bio-chemical conditioning, which includes the help of microorganisms and enzymes. Most widespread used is the fermentation of sugars, starch or cellulose with the help of yeast to ethanol (C_2H_5OH). This mixture then is purified by rectification and dehydration and pure ethanol can be used as fuel in gasoline engines or incineration plants. Furthermore microorganisms produce a methane-rich biogas during the anaerobic decomposition of organic substance. After gas cleaning and conditioning, this gas then can be used in gas engines or even as natural gas substitute.

Biofuels cannot replace oil completely and fully satisfy our high demand for energy at the moment, mainly due to insufficient available land area for growing the amount of

needed biomass. However the conversion of biomass from different sources (including waste) can be, in conjunction with other alternative energy sources, a promising pathway to make our society less dependent on fossil fuels.

Especially useful would be a conversion of biomass to high energy density fuels to replace at least partly one of the main energy consumer of fossil fuels: transportation.

2.1.1 Principles of Thermal Biomass Gasification

The basic principle of gasification is a thermo-chemical conversion of the carbon from the solid biomass into some energy-rich gas using a gasification medium. Usual operating temperatures range from 700 °C to 1200 °C and the gasifier is operated at substoichiometric conditions ($0<\lambda<1$)[9]. There is no ideal, universal gasifier and ideal gasifying medium. It always depends on the desired composition of the product gas and the type of feedstock biomass.

The produced gas contains mostly CO (carbon monoxide), CO_2 (carbon dioxide), CH_4 (methane), H_2 (hydrogen) and depending on the gasification process sometimes also N_2 (nitrogen). The amount of the different gas fractions vary strongly depending on the feedstock, the gasification medium and the process conditions. The resulting gas is usually called product gas and sometimes also synthesis gas, syngas or low calorific value gas (LCV). In this thesis, the gas mixture derived from biomass gasification is called product gas. The term synthesis gas is usually misleading, because synthesis gas just contains CO and H_2.

2.1.2 CHP-Plant in Güssing

As the experiments of this thesis were intended to obtain data regarding the reforming of product gas from the biomass gasification plant in Güssing, the plant shall be described in few words.

The combined heat and power (CHP) plant in Güssing was built in 2000 and started operation in April 2002 to produce heat and electricity from biomass (wood chips). The produced heat is fed into the district heating grid of the town and the electricity is fed into the national power network. The CHP plant has a total fuel power of 8 MW, an electrical output of 2 MW and 4.5 MW of thermal power. The electrical efficiency is around 25 %, the thermal efficiency 56.3 %, both together resulting in an overall efficiency of 81.3 %[10]. The hourly product gas production is around 2500 m^3/h (measured at standard conditions).

The plant uses wood chips as a feedstock, which are gasified in a dual fluidized bed (DFB) gasification system towards a high quality product gas. The system was developed by the Institute of Chemical Engineering (Technical University of Vienna) and the AE Energietechnik. The product gas contains mainly hydrogen and carbon monoxide. The average product gas composition, after cleaning before entering the gas engine, is shown in Tab. 2.1.

Component		
Water content	[vol-%]	~10
H_2	[vol-%]	35 - 45
CO	[vol-%]	22 - 26
CO_2	[vol-%]	20 - 22
CH_4	[vol-%]	~10
C_2H_4	[vol-%]	2 - 3
N_2	[vol-%]	1.2 - 2
H_2S	[vol-ppm]	~150

Table 2.1: Average gas composition of product gas from Güssing [10, 11]

The gasification is based on the dual fluidized bed (DFB) concept, which means that two separate fluidized chambers, which are connected by a chute, are used to produce a high quality product gas, which is poor in nitrogen. The DFB concept is illustrated in Fig. 2.1.

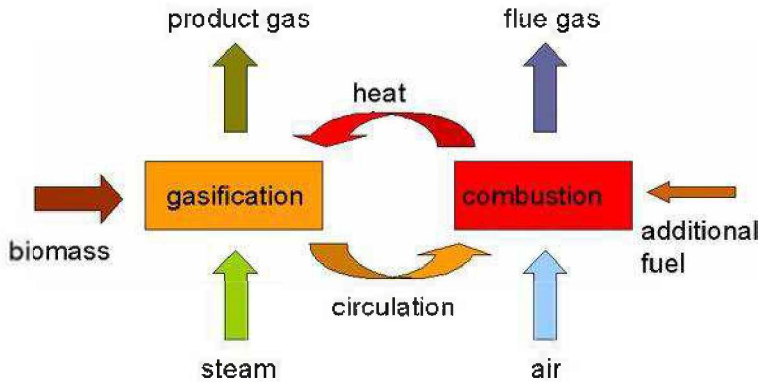

Figure 2.1: Principle of the dual fluidized bed concept [12]

In the gasification chamber the biomass is fluidized with hot bed material and steam at approx. 850 °C. High temperatures in the gasification chamber lead to biomass drying, devolatilization (pyrolysis) and finally the gasification of carbon in the presence of process steam. By-products and unwanted components like H_2S and tars are also produced in this process. After gasification the bed material and non-gasified carbon are moved to the combustion chamber, which is fluidized with preheated air. In doing so, the carbon is oxidized at around 930 °C. This combustion heats up the bed material, which provides the necessary heat for the strongly endothermic gasification reactions by recirculation to the gasification chamber.

The product gas is cooled down to approximately 150 °C in a series of heat exchangers. Then the particles are removed by a baghouse filter. Undesired tars are removed by a

rapeseed methyl ester (RME) scrubber, which also cools down the gas to around 40 °C[10].

The flowsheet diagram of the CHP in Güssing can be seen in Fig. 2.2.

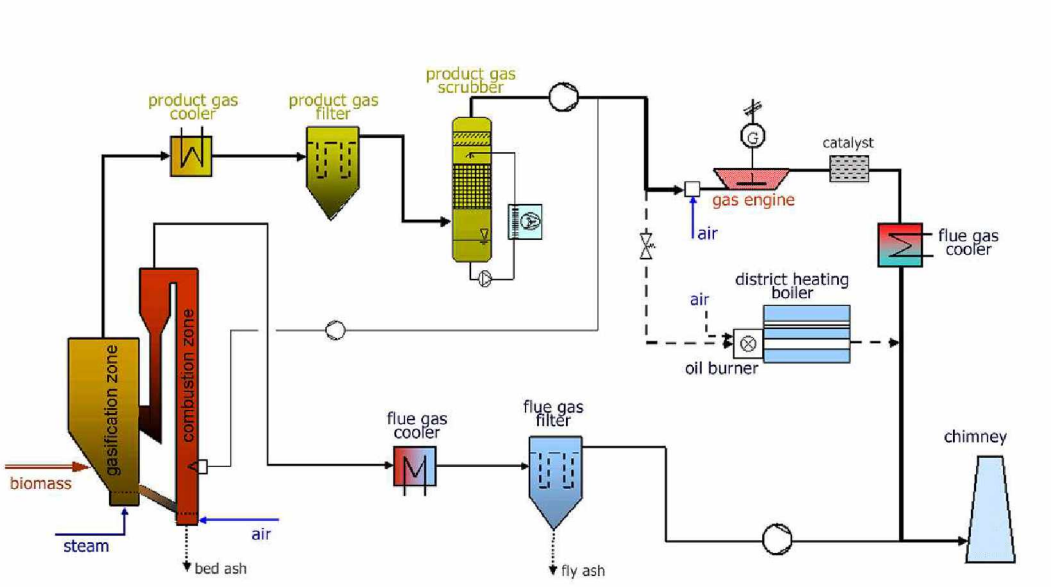

Figure 2.2: Simplified flow chart of the biomass CHP plant Güssing [13]

2.2 Catalysis

A substance which increases the rate of a chemical reaction without being consumed is called a catalyst. The overall standard Gibbs energy is not changed [14], thus a catalyst changes the kinetics of a reaction but not the thermodynamics. The equilibrium constant of the complete reaction is not affected.

Due to the presence of the catalyst usually the chemical bond of a molecule is loosened, which leads to a lower activation energy of the overall reaction. There is the distinction between homogeneous catalysis, when only one phase is present and heterogeneous catalysis, in which the reaction takes place at the interface between phases.

2.2.1 Homogeneous Catalysis

In a homogeneous catalytic reaction, the reactants and catalysts are all in the same phase. Usually all substances are dissolved in a liquid solvent. The main drawback of this type of catalysis is the need for a special separation of the catalyst from the products and reactants. Examples for technical processes are enzymatic reactions, polymerization-reactions in organometallic chemistry and acid-/base-catalyzed reactions for esterification.

2.2.2 Heterogeneous Catalysis

The heterogeneous catalysis has much more technical importance than the homogeneous catalysis and is widely used in all industries. More than 90% of all chemical processes depend on some heterogeneous catalytic reaction and they are fundamental of the synthesis of 60% of all chemical products [15, p. 249]

Most industrial use of heterogeneous catalysis is between either a gaseous or liquid reactant and products and a solid catalyst. Thus the main focus will be here on solid catalysts. These can consist of metals, oxides, sulfides, carbides, nitrides, acids, salts, basically any type of material. They come in various forms and can be loose particles, or small particles on a support. As catalyst carrier can serve a porous powder, such as aluminum oxide particles or large monolithic structures like ceramics.

For the development of a successful solid catalyst several important properties have to be implemented[16]:

- High activity per unit of volume in the reactor
- High selectivity towards the desired product at the conversion levels used in the reactor, and the lowest possible selectivity to byproducts that generate waste problems
- Sufficiently long life time, resistance to deactivation
- Possibility to regenerate, particularly if deactivation is fast

- Sufficient thermal stability against sintering, structural change or volatilization inside the reaction environment (e.g. when steam is a byproduct of the reaction)
- High mechanical strength with respect to crushing (e.g. under the weight of the catalyst bed or during the shaping process)
- High attrition resistance (resistance to mechanical wear, especially for applications in fluidized bed reactors)

Reaction Mechanism

The heterogeneous catalytic reaction takes place in three steps (illustrated in Fig. 2.3):

1. **bonding**: The reactants are chemisorbed on the catalyst surface and form bonds with the catalyst in a spontaneous reaction. Hence, this reaction is exothermic and the free energy is lowered
2. **reaction**: The reaction of the bond molecules take place while they are adsorbed on the solid surface. This step is constrained by the activation energy, which is however much lower than for the uncatalyzed reaction.
3. **separation**: In the last step the product separates from the catalyst in an endothermic reaction, hence increasing the potential energy.

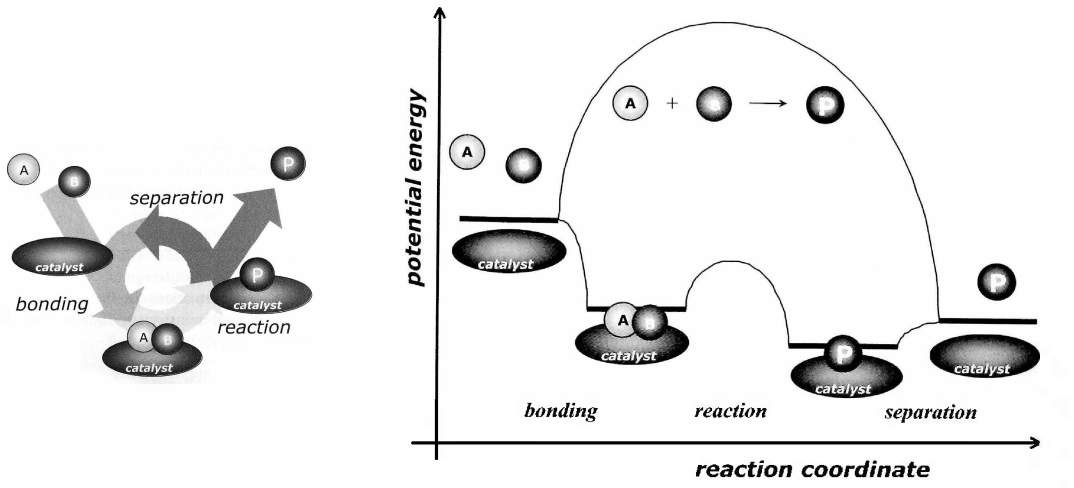

(a) Elementary steps of the catalytic reaction [16, p. 2]

(b) Potential energy diagram of a catalytic reaction with gaseous reactants A and B, product P and a solid catalyst [16, p. 3]

Figure 2.3: Scheme of catalytic reactions

There are several important issues which should be kept in mind when a catalyst is used:

- A catalyst accelerates both the forward and the reverse reaction. Thus also the decomposition of the product is accelerated by the catalyst if the thermodynamic conditions change.
- The reacting molecules have to be chemisorbed on the catalyst surface. If just weaker physisorption takes place, the intramolecular bonding is still too strong and the activation energy of the reaction cannot be lowered.
- All reactants taking part in the reaction should be bond equally strong to the catalyst material. Otherwise one species could poison the catalyst as it occupies all the active sites.

Characteristics

The most important parameters to characterize the performance of catalysts are[17, p. 23]:

Activity : The activity is the ability of the catalyst to accelerate the reaction of substrates to various products.

Activity can be measured (at standard conditions) in:

- **Reaction Rate** The activity can be measured as the amount of converted reactant per volume or mass of catalyst and time:

$$r = \frac{m_{reactant\ converted}}{m_{catalyst} \cdot t} \frac{[kg]}{[kg \cdot h]} \tag{2.1}$$

or

$$r = \frac{m_{reactant\ converted}}{V_{catalyst} \cdot t} \frac{[kg]}{[L \cdot h]} \tag{2.2}$$

- **Rate constant** k The speed of any chemical reaction can also be described by it's reaction constant k. This parameter is an intrinsic factor, which depends only on the temperature, pressure and the presence of a catalyst. The dimension of k depends on the order of the reaction[18].

  A general formulation of the rate constant for an arbitrary reaction like

$$a \cdot A + b \cdot B + \ldots \leftrightarrow c \cdot C + d \cdot D + \ldots \tag{2.3}$$

  is as following:

$$v = k[A]^{\alpha}[B]^{\beta} \ldots \tag{2.4}$$

  Where:

v	: is the speed of the reaction
k	: is the reaction constant
$[A], [B], \ldots$	: are the concentrations of species A, B, ...
$\alpha, \beta, \ldots$	: is the order of the reaction for species A, B, ...

The reaction constant needs to be ascertained for each reactant separately by experimental methods.

- **Activation energy** The reaction constant catalyst activity can also be measured by the (lowered) activation energy from the Arrhenius equation. In this equation the dependence on the temperature is expressed:

$$k = k_0 \cdot \exp(-\frac{E_a}{RT}) \tag{2.5}$$

- **Turnover frequency (TOF)** The turnover frequency is another possibility to indicate the catalyst activity on microscopic scale, which is the number of converted molecules per time of one active center[16, 18]:

$$TOF = \frac{number\ of\ molecules\ reacting}{t} \quad \text{per active site} \tag{2.6}$$

- **Space velocity** Also the space velocity (the gas flow divided by the catalyst volume) at which a certain conversion is obtained at a particular temperature can be used to define catalyst activity[16].

Selectivity In many cases there is not just one possible product resulting from a catalytic reaction. The ability to generate a desired product is called the selectivity of a catalyst. Usually it is given as fraction (or percentage) of all products:

$$S_i = \frac{n_{desired\ product\ i}}{n_{all\ products}} \quad \frac{[mol]}{[mol]} \tag{2.7}$$

Life The lifespan describes the total operating time the catalyst can be used before it drops below a sufficient level of activity and/or selectivity. The lifetime depends on the chemical, thermal and mechanical stability of the catalyst and it's support material. The process conditions and the presence of inhibitors and poisons are both a crucial factor. Further information regarding deactivation and poisoning are given in 2.3.4.2.

The lifetime can be given as **Turnover number (TON)**, which indicates the number of moles, one active site can convert before becoming inactive:

$$TON = number\ of\ molecules\ total\ converted/active\ site \tag{2.8}$$

On a macroscopic scale it might make more sense to give the mass of converted reactant per volume of catalyst before deactivation:

$$TON = mass\ of\ reactants\ converted/volume\ of\ catalyst \tag{2.9}$$

Catalyst support

Heterogeneous metal catalysts are often unstable and prone to sintering, especially as there are usually high temperatures needed for the desired reactions. Therefore so-called structural promoters are applied to enclose the catalyst material, e.g. by applying particles

inside the pores of an inert material. This support can all kinds of materials, which are thermally stable and chemical inert. Widespread used in industry are alumina, silica and carbon compounds [16, p. 193].

Prominent catalyst support materials are [16, p. 195]:

Alumina, Al_2O_3 Due to its excellent thermal and mechanical stability, alumina are most widely used as support material. Although there are various structures possible, just three of them are of interest as support, namely the nonporous, crystallographically ordered α-Al_2O_3, and the porous amorphous γ- and η-Al_2O_3. γ-Al_2O_3 acts as a catalyst itself for example in the Claus process for producing elemental sulfur and is also a very widely used support material, for various processes like hydrotreating, reforming, exhaust cleaning, water-gas shift, dehydration, hydrogenation and many more. It offers a high surface area ($50\,m^2/g$ to $300\,m^2/g$), pore volumes of about $0.6\,cm^3/g$, mesopores between 5 nm and 15 nm, high thermal stability and the possibility to be shaped into stable extrudates and pellets.

α-Alumina, which is the only crystalline form is highly stable and mainly used in high temperature applications, such as steam reforming, or in cases when low surface areas are needed.

Silica, SiO_2 Silica is a good support for reactions taking place at low temperatures ($<$ 300 °C), such as hydrogenation, polymerizations or some oxidations. Compared with alumina, silica has lower thermal stability and tends to form volatile hydroxides in steam at elevated temperatures, which limits its application as a support.

Titania, TiO_2 Titania are used for high temperature applications, like DeNOx with V_2O_5 as active material.

Carbon Porous carbons are used for noble metal catalysts, mainly in liquid hydrogenation reactions of organic compounds. Surface areas may be as high as $1500\,m^2/g$ with micropores smaller than 1 nm. One advantage is the easy recoverability of the expensive noble metals.

Shaping Depending on the process and the type of reactor different shaped catalyst support have to be used. In general it is a good approach to press powder of small particles into larger bodies. As a rule of thumb, the density of a powder is increased by a factor of three by pressing it into a solid pellet shape, thus resulting in higher catalytic activity per volume of catalytic bed.

Figure 2.4: Examples of the various forms of shaped catalysts[19].

Usual shapes for large reactors, when high mechanical strength is required, are pellets (1.5 mm to 10 mm in diameter), rings (6 mm to 20 mm) and multichanneled pellets (20 mm to 40 mm). Also ceramic monoliths (honeycomb shaped) are well-established catalyst design.

Mass Flow and Heat Transfer

The common reactors for catalytical reactions of fluid reactants and solid catalysts are either fixed bed reactors or fluidized bed. The latter type is especially used when the catalyst material is stable to abrasion and there is a need for turbulent, uniform particle mixing. The fluidized bed reactor is more difficult to operate at stable process conditions. It is used usually for catalytic cracking in the petroleum industry and also for biogas production from biomass (see also 2.1).

Thus for most catalytic reactions in chemical industry a fixed bed is used, which is easier to calculate and to operate. The normal setting is a catalyst-packed bed with a gaseous or liquid media flowing through. Within the bed heat transfer and mass flows have to be considered, however on the reactor-wall just heat transfer takes place, usually due to external heating or cooling, depending on the chemical reaction.

The packed bed with the solid-fluid-system can be seen as a quasi-homogeneous media on a macro scale, where the diffusion coefficient is strongly dependent on the flow-conditions within the bed. Also for the heat transfer on scope of the whole bed, one has to consider the liquid flow to be able to find a thermal conductivity for the modified Fourier equation[15, p. 258].

On the catalyst surface the mass- and heat-transfer is limited by hydrodynamic boundary layer around the catalyst pellet. This small-scale transfer is called outer diffusion or film diffusion. Within one catalyst particle there are also several steps of mass- and heat-transfer taking place. The reactants and products have to be transported to and from the active centers and also depending on the reaction enthalpy, heat energy has to be provided or removed. There are seven micro-scale sub-steps needed for a successful reaction on a porous catalyst, which are illustrated in Fig. 2.5:

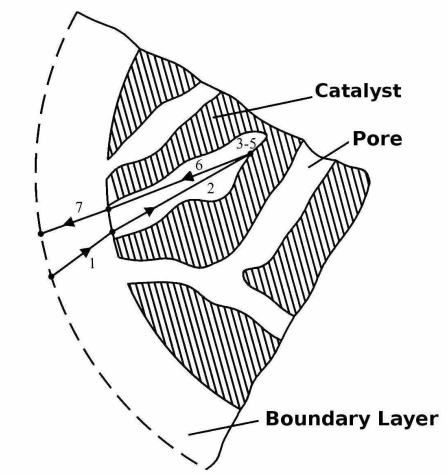

Figure 2.5: Seven steps of heterogeneous catalysis on a solid particle [15, p. 260]

1. Outer diffusion of the reactants from the drifting gas-phase through the boundary layer towards the outer catalyst surface
2. Diffusion through the pores from the outer surface towards the active centers on the inner catalyst surface
3. Adsorption of the reactants on active catalyst material
4. Chemical reaction of the reactants
5. Desorption of the products and remaining reactants
6. Diffusion through the pores to the outer catalyst surface
7. Mass transfer through the boundary layer to the gas-phase

Depending on the process parameters (flow, reactants, catalyst material, catalyst support material, etc.) a catalytic reaction can be limited by outer diffusion, pore diffusion or by chemical reaction. If a reaction is in the kinetic domain, thus not limited by boundary layer-diffusion, the conversion-rate is independent from the linear flow-velocity. On the other hand, a reaction is diffusion-controlled (or diffusion-limited), when the reaction-rate or conversion is influenced by the turbulence or the velocity of the fluid [15, p. 260].

2.3 Steam Reforming

Steam reforming is one of the basic chemical processes to produce hydrogen. The basic process was developed in the early 20th century in Germany to obtain hydrogen from coal, primarily for ammonia synthesis. In 1917 the Haber-Bosch process was developed and introduced in industry in 1930. Thus the demand for cheap hydrogen rose for the large quantity of ammonia needed, mainly to produce fertilizers for industrial agriculture[20]. The industrial breakthrough of steam reforming happened in the 1950s when it became possible to use naphtha as a feedstock due to the operation of tubular reformers at high pressure. Thus a by-product of oil refining became a valuable source for hydrogen as the first large-scale naphta reforming plant was built in 1959[17, p. 225f]. As natural gas became available in large quantities, methane was used as the preferred feedstock, because this process is more economic, due to higher hydrogen yields and less unwanted by-products. Nowadays around 49 % of the industrially produced hydrogen are derived from natural gas, 29 % from liquid hydrocarbons and 18 % from coal[21]. The latest development of catalysts for natural gas and substitute natural gas has focused on extending catalyst life, inhibiting carbon forming reactions, improving activity and by improving the physical properties [16, p. 306].

The product of the steam reforming process is called synthesis gas (also syngas), which is a mixture of H_2 and CO (and CO_2). Syngas can be used for many different chemical processes, e.g. the synthesis of higher alcohols, mainly methanol (by hydroformylation), hydrogenation of unsaturated compounds or the direct reduction of iron ore in metallurgical industry. Methanol itself is a source for various other chemical products like acetic acid, dimethyl ether (DME), formaldehyde, methyl-tert-butyl ether (MTBE), liquid hydrocarbons, etc. Also the high hydrogen content of syngas can be further purified by permeable membranes and/or pressure swing adsorption (PSA), which could be one pillar for a hydrogen energy economy. The oil crisis in 1970s showed also the benefits of flexible feedstocks in chemical industry. Synthesis gas can be produced from almost any carbon containing resource, which means both from coal, natural gas, liquid fuels and also from biomass. Thus syngas can be one key element for a flexible chemical industry, as it allows various conversion from one feedstock to another as illustrated in Fig. 2.6.

Still nowadays the most important application for hydrogen is the production of ammonia (50 %), then followed by applications in refineries (22 %) and the methanol synthesis (14 %)[23]. Around 96 % of the globally produced hydrogen is directly based on fossil fuels, mainly methane with around 50 % and the rest from liquid fuels or coal[21]. Thus the main process for producing hydrogen is still steam reforming although there are various alternative pathways like electrolysis, biological processes or thermochemical conversion, these processes are not yet economically reasonable and often still in an experimental state of development.

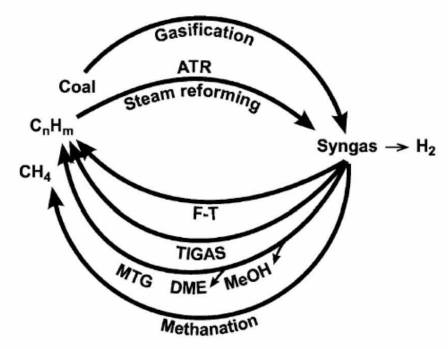

Figure 2.6: The synfuel cycle: ATR: autothermic reforming; F-T: Fischer-Tropsch synthesis; TIGAS: Topsoe integrated gasoline synthesis; MTG: Mobil methanol to gasoline process; DME: dimethyl ether; MeOH: methanol; Methanation: for substitute natural gas (SNG) production[22]

2.3.1 Basic Reactions

There are two reversible, highly endothermic main reactions (eq. 2.10) for the steam reforming of methane.

$$CH_4 + H_2O \leftrightarrow CO + 3\ H_2 \qquad \Delta H^{\ominus}_{298} = +206,2\ kJ\,mol^{-1} \tag{2.10}$$

$$CH_4 + 2\ H_2O \leftrightarrow CO_2 + 4\ H_2 \qquad \Delta H^{\ominus}_{298} = +165,0\ kJ\,mol^{-1} \tag{2.11}$$

As steam reforming can be also applied for higher hydrocarbons (widely applied in industry for naphthas), the general formula can be described as:

$$C_nH_m + nH_2O \leftrightarrow nCO + (n + \frac{1}{2}m)\ H_2 \qquad \Delta H^{\ominus}_{298} > 0 \tag{2.12}$$

(2.13)

Also so called dry reforming (eq. 2.14) takes place when temperatures are high enough. This reforming reaction received considerable attention for several advantages, including a lower H_2/CO ratio of 1 and the possible reuse of CO_2 from combustion processes. The major problem encountered in pure dry reforming, is the enhanced carbon deposition on the catalyst which leads to rapid deactivation[24].

When abundant steam is present, the dry reforming reaction just plays a minor role, due to the fact that the reactions including H_2O have lower reaction enthalpies:

$$CH_4 + CO_2 \leftrightarrow 2\ CO + 2\ H_2 \qquad \Delta H^{\ominus}_{298} = +247,4\ kJ\,mol^{-1} \tag{2.14}$$

If a higher hydrogen-yield is needed, more water is added and the water-gas shift reaction (eq. 2.15) converts additional carbon monoxide and steam to hydrogen and carbon dioxide. Due to the high process temperatures and the exothermic reaction enthalpy of the water-gas shift reaction, this conversion just plays a minor role during the reforming. Thus usually the water-gas shift reaction takes place in an additional downstream reactor: [16, p. 305ff]

$$CO + H_2O \leftrightarrow CO_2 + H_2 \qquad \Delta H^{\ominus}_{298} = -41,2\ kJ\,mol^{-1} \qquad (2.15)$$

The forward steam reforming reactions (eq. 2.10) are endothermic and result in more gaseous moles in the product, thus favored by high temperatures and low pressures.

2.3.2 Thermodynamics

Usually the process takes place at very high temperatures up to 1000 °C. The thermodynamic reason for the very high temperatures can be seen clearly in Fig. 2.7

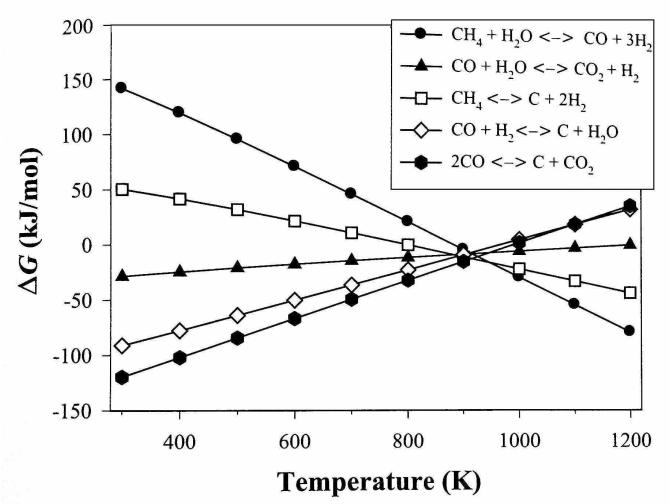

Figure 2.7: Gibbs free energy change for steam reforming and related reactions [16, p. 307]

Usual reaction temperatures in industrial processes range from 800 °C to 1000 °C. Traditionally the reactors have a vertical, tubular design and are operated at moderate pressures at 25-35 bar, which allows a compact construction of the reactor with decent conversion rates. The tubes are loaded with catalysts and surrounded by furnaces, where additional fuel (usually methane) is burned to reach the very high temperatures. New approaches to more sophisticated reactors use a burner at the reactor entrance and the heat is provided by oxidation of some fractions of the feedstock. This process is called auto thermal reforming[16, p. 306].

2.3.3 Catalysts Material

Since around 40 years the most widely used catalyst, due to it's low costs, availability and good catalytic properties, is nickel. The catalyst activity is pending on the metal surface area, i.e. the number of active sites on the catalyst. Thus a generally high dispersion of metal particles is favored, which makes a high number of the active particles available to the reactants. Usually this is achieved by precipitating the active material as small crystallites from a soluble salt on the refractory support, which must be sufficiently porous to allow access of the gas to the nickel surface. Alternatively the metal can be incorporated by impregnating a preformed catalyst support with a solution of a salt, which is subsequently decomposed by heating to the oxide [17, 25]. There are many other and more advanced catalyst preparation methods, which are not discussed here in detail. Usual dispersions for nickel catalysts are around 2 % to 5 % with metal particles of 20 nm to 50 nm[25]. The Ni particles are commonly dispersed on an Al_2O_3 and/or $AlMgO_4$ spinel. The active metal area is rather low, with an order of just a few m^2g^{-1}[16]. To obtain the catalytic activity the nickel oxides must be reduced to the metal by using hydrogen in the start-up phase of the reactor[17].

There is still a lot of research going on, especially due to always improving knowledge about microscopic mechanisms from surface chemistry, to improve the catalysts towards higher activity, higher selectivity and longer lifetime. Basically there are two ways to enhance the process: to find a better material, size and distribution of the active material or to improve the support material.

Active Material Other transition metals such as palladium (Pd), platinum (Pt), ruthenium (Ru), rhodium (Rh) or iridium (Ir) can also be used and show to some extent very good reforming properties (see Tab. 2.2). The biggest drawback however, is the price of this rare materials, which result in higher catalyst costs even though less amount is needed. But as catalyst preparation methods are always improving, there may be a chance of using precious material due to the fact, that far less active substance is needed. For example Ru and Rh show high selectivity towards carbon-free operation, i.e. they show high reforming rates combined with low carbon formation rates[26]. Other reactive metals like iron and cobalt are also in principle active, but they oxidize easily under process conditions[16, p. 306].

Support Other approaches are to add special promoters to the catalyst support material, which makes the whole catalyst less susceptible towards coke formation. One example is to add reducible oxides like ZrO_2 and La_2O_3 to the usual Al_2O_3 carrier, which results in high activity and higher stability towards carbon deposition[27]. Another way is to add alkali, like potassium to the support, which is already implemented on industrial scale[28].

Catalyst metal content (wt%)	Relative rate
Ni (16)	1.0
Ru (1.4)	2.1
Rh (1.1)	1.9
Pd (1.2)	0.4
Ir (0.9)	1.1
Pt (0.9)	0.5

Table 2.2: Relative activities (activity Metal/activity Nickel ratio) for steam reforming of methane, T=550 °C, S/C=4 [mol/mol], p=1 bar [26]

2.3.4 Catalyst Deactivation

Catalyst deactivation describes the loss of catalytic activity and/or selectivity over time. It is a great and continuing concern in commercial catalytic processes, as quoted by Jens R. Rostrup-Nielsen of Haldor Topsøe[29]:

> In most of the reactions, I have studied the catalytic activity was not the decisive factor, but rather secondary phenomena such as sulphur poisoning, carbon formation and sintering.

There are many different ways for deactivation and in general it is inevitable, but it can be slowed and sometimes avoided, if the mechanisms are identified. Thus it is necessary to understand the causes of deactivation and develop process conditions and/or catalysts, which are more resistant to the harsh conditions for steam reforming. The most common mechanisms of catalyst deactivation are summarized in Tab. 2.3.

Mechanism	Type	Definition	Example
Fouling	Mechanical	physical deposition of species from fluid phase on the catalytic surface and in the pores	Carbon deposition
Poisoning	Chemical	blocking of sites by strong chemisorption	H_2S poisoning
Thermal degradation	Thermal	thermally induced loss of catalytic surface area, support area, and active phase–support reactions	Sintering
Attrition/crushing	Mechanical	breakdown of the catalyst (support) particles can lead to blockage of the reformer tubes	
Phase transformation	Chemical	Reaction of fluid with catalytic phase to produce inactive phase	Oxidation

Table 2.3: Mechanisms of catalyst deactivation[17, 25, 30]

2.3.4.1 Carbon Deposition

In steam reforming one of the main issues is carbon deposition, as there are many reactions where solid carbon (basically graphite) can be formed from the gaseous components (see Fig. 2.7). In general the probability of carbon formation increases with decreasing oxidation potential (mainly due to lower steam content)[16].

The most common chemical reactions for coke formation are thermal cracking (eq. 2.16), disproportionation (eq. 2.17) and CO reduction (eq. 2.18)[17]:

$$CH_4 \leftrightarrow C + 2H_2 \tag{2.16}$$
$$2CO \leftrightarrow C + CO_2 \tag{2.17}$$
$$CO + H_2 \leftrightarrow C + H_2O \tag{2.18}$$

There are three typical kinds of carbon deposition: pyrolytic carbon, encapsulating carbon and whisker or filamentous carbon[31]. Pyrolytic carbon is usually formed by thermal cracking of hydrocarbons above 600 °C. Encapsulating carbon is obtained by slow polymerization of unsaturated hydrocarbons at temperatures below 500 °C. Whisker carbon, which are long filaments of graphitic carbon with the catalyst particle on the top (see Fig. 2.8), is produced at temperatures above 450 °C. The adsorbed hydrocarbon dissociates on the catalyst surface into carbon atoms. Then the carbon atom diffuses through the catalyst particle and nucleates into the fibre at the rear interphase and detaches the nickel particle from the support[32]. While the first two types of carbon cover the catalyst particle surface and deactivate the catalyst particle, whiskers don't deactivate directly, but they block the catalyst pores and increase the pressure drop to unacceptable levels[33]. At high temperatures the main morphology of carbon is those of whiskers. The diameter of the whisker is determined by the catalytic particle from which it grows[16].

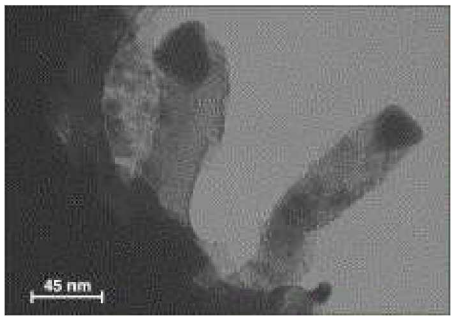

Figure 2.8: Carbon whisker with nickel crystal at the end [32]

A similar technique is applied to produce single walled carbon nano-tubes, which attracted substantial interest because of their high mechanical strength and interesting electronic behavior. For steam reforming, carbon filament growth can lead to severe

problems like blocking of the reactor and, due to the high strength of the whiskers, to destruction of the catalyst. This again may lead to hot spots inside the reactor due to the large amount of supplied heat for the endothermic reactions.

Several approaches have been taken to avoid this problem of carbon formation. Avoiding the thermodynamical region for carbon deposition is an obvious one, but this restricts the available parameter space severely. Especially as temperature and steam amount vary much in large reactors. Another approach is to develop a process or a catalyst which is less susceptible to carbon deposition.

SPARG Process The SPARG (Sulfur PAssivated ReforminG) process uses findings from surface science, which indicated that a much larger amount of nickel atoms are needed for forming carbon whiskers than for reforming of hydrocarbons. Thus by adsorbing sulfur atoms on the the nickel sites, the thermodynamical potential for carbon formation is increased from just a few kJ/mol to about 35 kJ/mol for around 80 % sulfur coverage[34]. Unfortunately sulfur is also a strong poison for the reforming reaction, meaning that it deactivates the catalyst completely if all active sites are covered. But luckily the carbon formation is influenced much stronger by the deactivation of some nickel particles, which leads to an overall enhanced selectivity for the reforming reaction. The decrease in activity is compensated by using more catalysts and/or higher temperatures.

Unfortunately H_2S has to be added to the feedstock continuously as the adsorbed sulfur is hydrogenated and removed from the catalyst. This results in a product gas, which contains H_2S, which calls for another purification step[16].

Gold–Nickel Alloy Catalysts Single gold atoms, which have no effect on the steam reforming reaction, can be alloyed with nickel to form a structure of randomly distributed Au-atoms all over the nickel surface. This means that gold can be used to break up the large ensembles of Ni-atoms, which favor carbon deposition. Experimental results confirmed, that gold-enhanced nickel catalysts perform much better regarding deactivation through carbon[16].

Although this studies were published already in 1998, this catalyst is not yet widely used in industry. This is most probably due to the higher costs for catalysts which are Au-dotted, both for material costs of the noble metal and the fabrication costs of the catalyst.

2.3.4.2 Sulfur Poisoning

Sulfur is present in organic and/or organic sulphides in nearly all naturally occurring feedstocks. The main sulfur-containing component is H_2S (hydrogen sulfide), which concentration depends very much on the feedstock, e.g. 4 ppm in natural gas from the North Sea[16], 200 ppm to 1400 ppm in naphthas[17] and around 150 ppm for product gas from biomass gasification in Güssing[10, 11].

Sulfur usually has to be removed to a level of about 0.2 ppm to 0.5 ppm prior to the reforming process as it is a very strong nickel catalyst poison. The removal is done usually by hydrodesulfurization, converting the sulfur present in thiols, thiophenes or COS into H_2S, which then can be adsorbed stochiometrically by ZnO up to 400 °C before the reactor [16, 17, p. 306].

The catalyst is more sensitive to sulfur poisoning at lower temperatures, as shown in Fig. 2.9a. This is due to the fact, that the poisoning process may be described as a simple exothermic adsorption process, which is less likely to take place at higher temperatures.

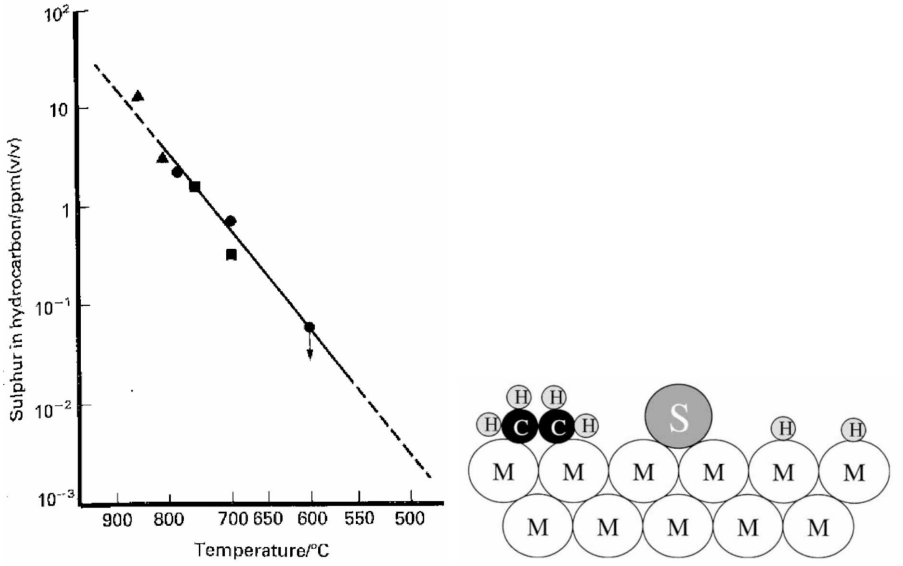

(a) Minimum sulfur concentration to poison nickel at different temperatures. • heptane, ■ naphtha, ▼ methane [17]

(b) Conceptual model of poisoning by sulfur atoms of a metal surface [30]

Figure 2.9

As basically all sulfur containing compounds from the feed are converted into H_2S, the mechanism can be described as chemisorption of hydrogen sulfide on the nickel catalyst[35]. In general the group 8 metal catalysts are all susceptible to sulfur poisoning, but nickel is even more sensitive than others. The chemisorption mechanism including occupation of one nickel site was investigated in detail by Rostrup-Nielsen [1968] for temperatures above 400 °C and can be described as a formula as shown in eq. 2.19 [36]. Thus the S-atom detaches from the hydrogen and occupies the active site.

$$H_2S(gas) + Ni_{surface} \leftrightarrow Ni_{surface} - S + H_2(gas) \tag{2.19}$$

As the equation above suggests, it is in principle possible to reverse the chemisorption of sulfur, by applying hydrogenation, to recover the catalyst, but the driving force

is very small. Sulfur may be also removed by oxidation of the catalyst[25, 36]. Due to the exothermic nature of the adsorption, the sulfur removal is increased at higher temperatures. It is also important to decrease the sulfur content in the feed to let the sulfur atoms desorb back into the gas with low H_2S partial pressure.

There are new developments of catalysts, which should be more resistant towards sulfur poisoning. One approach is to dope conventional nickel catalysts with noble metals and metal oxides like Re, Mo, Co, Ru, Rh, WO_3, Y_2O_3. Another way is to use just noble metals like Pd, Ru, Rh or combinations of these with rare earths like yttrium or lanthanum as active material, which are then less susceptible towards sulfur chemisorption[37–39].

2.3.4.3 Thermal Degradation

Thermally induced deactivation of catalysts may come from loss of surface area due to crystallites growth of the active material (Fig. 2.10b) or due to phase transformation which leads to pore collapse of the support material (Fig. 2.10b). This two processes are usually referred to as "sintering". These reactions usually take place at high reaction temperatures above 500 °C and are generally accelerated by water vapor, which is always present at steam reforming processes[30, 40]. There are three basic mechanisms of metal crystallite growth: crystallite migration, atomic migration and vapor transport (at very high temperatures). Crystallite migration is the transport of whole particles on the support followed by collision and coalescence. Atomic migration involved detachment of metal atoms from particles, which then are captured by larger crystallites.

Sintering increases exponentially with temperature and also depends very much on the present atmosphere. For example oxidizing conditions are worse than reducing or inert atmospheres for supported metal catalysts. The temperature at which the solid phase becomes mobile also depends very much on factors like size, morphology and texture of the particles and support. For example highly porous γ-Al_2O_3 is more sensitive to sintering than α-alumina[41].

In general effects due to thermal degradation are irreversible and thus it is of high concern to keep reaction temperatures as low as possible. Active metals and their support material with melting points above 1700 °C can show signs of sintering even at temperatures half of their melting point[40].

2.3.5 Other Reforming Processes

There are mainly just two other processes for reforming of hydrocarbons, which are used in industry and shall be described here briefly: Partial oxidation (POX) and autothermal reforming (ATR). Other new processes, which are not yet in a applicable state include also pyrolysis, plasma reactors or unmixed combustion[42].

Partial Oxidation (POX) The reforming of hydrocarbons is a highly endothermic process, thus one approach is to oxidize some of the hydrocarbons to generate the

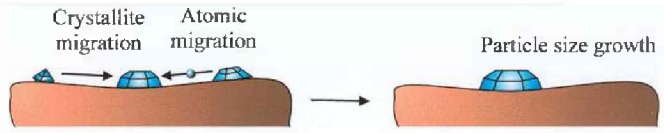

(a) Sintering of the active metal particles

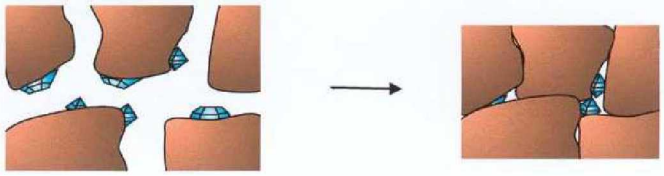

(b) Sintering and solid-solid phase transitions of the support

Figure 2.10: Sintering mechanisms [41]

necessary heat for the catalytic reforming process. Partial oxidation is usually used when liquid fuels are reformed. For example there are just 17 % of the lower heating value of diesel needed, to reach temperatures of up to 870 °C for the process. The formula for methane partial oxidation is shown in eq. 2.20 [24].

$$CH_4 + \frac{1}{2}O_2 \leftrightarrow CO + 2\,H_2 \qquad \Delta H^{\ominus}_{298} = -35.9\ kJ\,mol^{-1} \tag{2.20}$$

Of course there are many additional other oxidation pathways possible, but this reaction is the valid representative and shows the endothermic nature of the partial oxidation. The optimum operating conditions as found in literature for CH_4 partial oxidation reforming are at 0.5 O_2/CH_4 ratio, 1200 °C and 1 atm. Investigations promised a reduction of required energy of 10-15% and a the capital investment could be reduced by 25-30% by partial oxidation[24].

The biggest drawback however is, that either an cost intensive cryogenic air separation plant is needed to produce pure oxygen for the combustion or that the whole plant must be designed for huge volume flows, due to the additional nitrogen from the ambient air.

Autothermal Reforming (ATR) Autothermal reforming is basically a combination of endothermic steam reforming and exothermic partial oxidation. Hereby the advantages of both processes are combined - on one hand the higher hydrogen yield through steam reforming and the supply of energy through partial oxidation. It should also be mentioned that by autothermal reforming of methane, a almost complete CH_4 conversion can be achieved within a few milliseconds.

Certainly there are special requirements for the used catalysts. They must be able to perform both well for steam reforming as they should promote the water-gas shift reaction

and they should be resistant against carbon deposition from the oxidation reactions[32]. The catalyst must also withstand very high temperatures due to the exothermic reaction inside the reactor.

Autothermal reforming is already widely used in industry, mainly to convert natural gas to synthesis gas for the production of ammonia and methanol. Haldor Topsøe has built for example more than 30 autothermal reformers since 1985[43].

Further research is going on especially in the field of autothermal reforming of diesel, which should take place "onsite" in a fuel cell[44].

2.3.6 Uses of Synthesis Gas

The three main applications of synthesis gas, which is produced by steam reforming, are the methanol synthesis, the hydroformylation of alkenes to alkohols and aldehydes and the Fischer-Tropsch synthesis to produce synthetic fuels[16]. As methanol synthesis and synthesis of larger hydrocarbons are mainly interesting to substitute fossil fuels as energy carriers, these two processes with their products and by-products are shown in Fig. 2.11.

The synthesis pathways are not described here in detail, because the main objective was to research the production of synthesis gas.

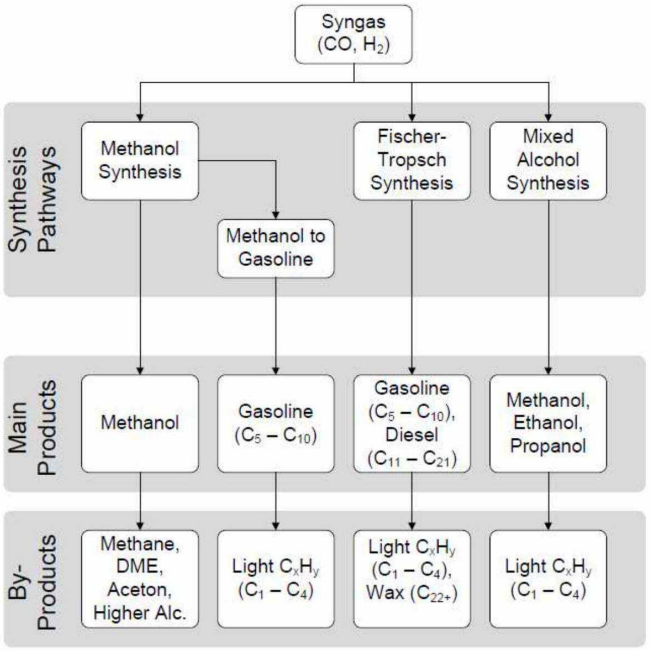

Figure 2.11: Different synthesis pathways with its products and by-product [10, p.12]

3 Experimental Setup

The main apparatus used for the experiments was the test rig for chemical kinetics of the Institute of Chemical Engineering, TU Wien. The test rig was fed with different feedstock gases and operated at various process conditions to test the catalyst performance. The following section gives a detailed explanation of the experimental equipment and the testing conditions.

3.1 Test Rig for Chemical Kinetics

3.1.1 Flowsheet

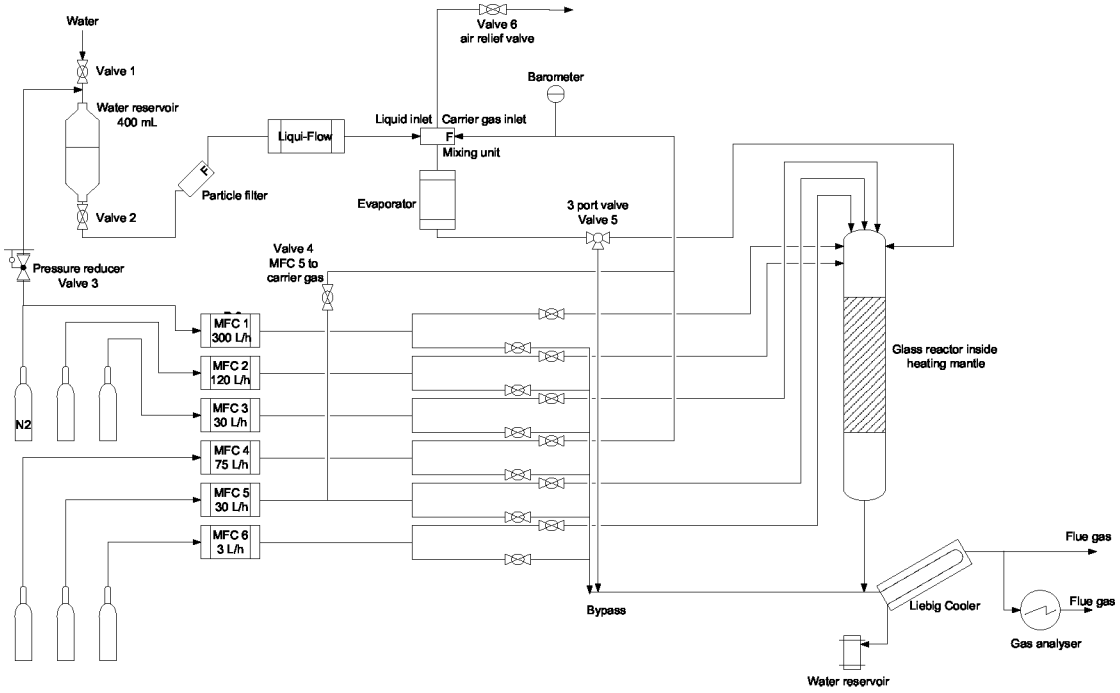

Figure 3.1: Flowchart of the kinetics test rig

The flowsheet of the kinetics test rig is shown in Fig. 3.1. As can be seen in the chart, it was possible to connect up to six different gas-sources to the different mass-flow controllers (MFCs) of the test rig. One of these gas-sources was connected to the reservoir of deionized water to act as a carrier-gas for the vapor-stream. This carrier-gas had to

be a clean and as far as possible inert gas, otherwise the evaporator could be damaged. Before the evaporator the deionized water was cleaned by a micro-filter to avoid plugging of the equipment. The pressure in the water-system had to be exactly 1 bar, so the Liqui-Flow® device could operate with high accuracy.

The MFCs should be operated between 10 % and 90 % of their maximum flow-rate to obtain most precise flow-rates. Thus it was crucial to select the right MFC for each gas-component, depending on the required gas-mixture. Each gas channel was controlled by two valves, to select either the reactor or the bypass as output for the channel. It would be possible to open both valves, but then the output would be undefined, because the gas stream would split up in undefined proportions. All gas-channels including the vapor-stream were joined inside the reactor before the catalysts. The reactor itself is explained in more detail in the subsequent sections. The vapor-stream pipe was equipped with special insulation and additional electric heating, so the water couldn't condensate on the way to the reactor.

After the reactor the excess-water was condensed in a Graham condenser. The water was collected in a reservoir for further analysis. The dry gas-stream then entered to the 5-component gas analyzer. This was accomplished by an additional pump, which always delivered exactly 40 L/h to the gas analyzer, independent of the actual volume-flow through the reactor. Therefore the analyzer was connected via bypass-loop to the reactor output. One had to consider this setup and bear in mind, that if the volume-flow was less than 40 L/h, it would take more time until the current concentration reaches the gas analyzer. Thus the flow of 40 L/h was taken as a general minimum flow-rate of the system.

3.1.2 Reactor Parameters

The components and the geometries of the reactor of the test rig are shown in Fig. 3.2a. The gas- and vapor-flows entered the reactor on the top. To prevent condensation of the steam and to pre-heat the gases, the first 44 cm was heated by a self-regulated electric heating tape to a temperature of 120 °C. This first part of the reactor was made of stainless steel and connected to the glass-reactor by a high temperature polymer tube.

On the next 20 cm of the reactor was another heating tape located, which was regulated by a thermocouple to a temperature of around 130 °C. This part of the reactor was insulated by a mineral wool cylinder with aluminum foil on the outside. The outer diameter was $d_{ins,out} = 15\,cm$ and the wall-thickness was $s_{ins,wall} = 4.5\,cm$.

The main reforming reaction took place in a tubular fixed-bed glass-reactor which was surrounded by the electric heating shell, which provided the necessary thermal energy. The reactor tube material was quartz glass (Silux) with an outer diameter of 12 mm, a wall thickness of 1 mm and a length of 100 mm. Inside the reactor 12 pieces of the cylindrical catalysts were placed in the upper third of the heating shell. Before and after the catalysts thermocouples type-K (temperature-range from −200 °C to 1350 °C) were placed to measure the exact inlet- and outlet-gas-temperature.

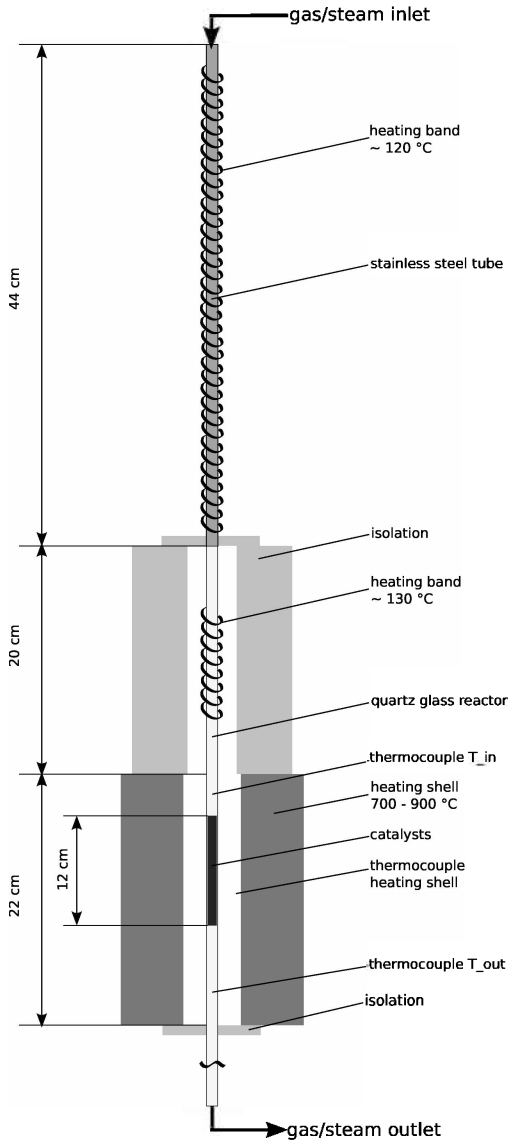

(a) Scheme of the reactor

(b) Open heating shell with reactor at 800 °C

Figure 3.2: Reactor of the test rig

The heating shell and the insulation material were all placed on a metal plate with a hole in the middle, where the glass-reactor goes through. The hole was insulated with glass wool to reduce the stack effect inside the heating shell. The reactor-outlet was then connected to the condenser and further to the analytical equipment.

3.1.3 Equipment

The used test rig was equipped with following devices:

- **Electric cylindrical heating shell**: A ceramic, cylindrical, 860 W electric heater provided the needed thermal energy for the desired reforming reactions. The set-temperature was regulated by a thermocouple, which was placed in the middle of the heating shell and a digital controller, which was located on the side of the test rig.

  The heating shell had following geometries: outer diameter $d_{hs,out} = 16\,cm$, inner diameter $d_{hs,in} = 5\,cm$, a wall-thickness of $s_{hs,wall} = 5.5\,cm$ and a height of $h_{hs} = 22\,cm$.
- **Mass flow controllers**
  - **MKS® Mass-Flo® Controllers**: This analog, elastomer-sealed Mass Flow Controllers (MFC), type 1179, meters the gas-flow by analyzing the thermal conductivity of the current flow. The manufacturer states an accuracy of 1 % of the full scale[45]. This type was used in MFC 1 (max. 300 l/h), 2 (max. 120 l/h) and 3 (30 l/h) of the test rig.
  - **Bronkhorst® Digital Mass Flow Controllers (MFC)**: This controller with thermal mass flow meters was placed in MFC 4 (max. 75 l/h), 5 (max. 30 l/h) and 6 (3 l/h) of the apparatus. The accuracy is about ± 1 %. Usually MFCs should be operated between 10 % and 90 % of their maximum flow rate[46].
  - **Bronkhorst® Liqui-Flow®**: This high-tech flow meter controlled the water-flow of the evaporator with an accuracy of ±1 %. Maximum flow-rates range from 0.1 g/h to 100 g/h[47].
  - **Bronkhorst® Controlled Evaporator Mixer**: The used CEM-device (W-202-330-P) had an electrical heating power of 10 W and a maximum liquid flow of 30 g/h. The maximum gas-flow was 4 l/min and the maximum temperature was 200 °C[48].
- **Elster Kromschröder BK-G2,5 gas meter**: (Q_{max}=4 m^3/h; Q_{min}=25 L/h; V=1.2 dm^3; p_{max}=0.5 bar) This gas meter was used to measure the total dry gas outlet flow. The gas meter contains two chambers with movable diaphragms. Each chamber is filled alternately and the movement of the diaphragms is transfered to the analog display by a magnetic coupling. The device is designed to meter exactly the volumes of towngas, natural gas, propane, butane air or other inert gases. It is said to be very stable, robust and accurate even at low gas flows [49].
- **Rosemount NGA 2000 MLT 4 gas analyzer**: 5-component gas analyzing device for H_2, CO, CO_2, CH_4 and O_2. H_2 is measured by a thermal conductivity sensor by a Wheatstone Bridge. CO, CO_2 as well as CH_4 are measured by the absorption of infrared radiation. The gas-specific wavelengths of the absorption bands characterize the type of gas and the height of the absorption-peak gives a measure of the concentration of the component measured. [50]

- **LabVIEW®-Automation Software Version 8.5.1**: An particular LabVIEW® application was used to control and supervise all temperatures and massflows in the test rig. It was possible to set the different setpoints for each MFC, the Liqui-Flow® controller and the evaporator temperature. Also the calibration of each MFC for the different gases had to be done by selecting the gas correction factor (GCF). Various graphs were used to display the current inlet- and outlet-temperature as well as the steam temperature. The 5-component gas analyzer was also linked to the application, so the measured outlet concentrations were displayed in real-time. A screenshot of the application can be seen in Fig. 3.3.
- **Graham condenser**: The used condenser was a Liebig cooler with the coolant (distilled water) flowing through spiral coil. The direction of the vapor-loaded gas was in counter-current to the water. The coolant was cooled in an electric cooling system to a temperature of 4 °C.
- **Thermometer**: A regular thermometer was used to measure the ambient air temperature.

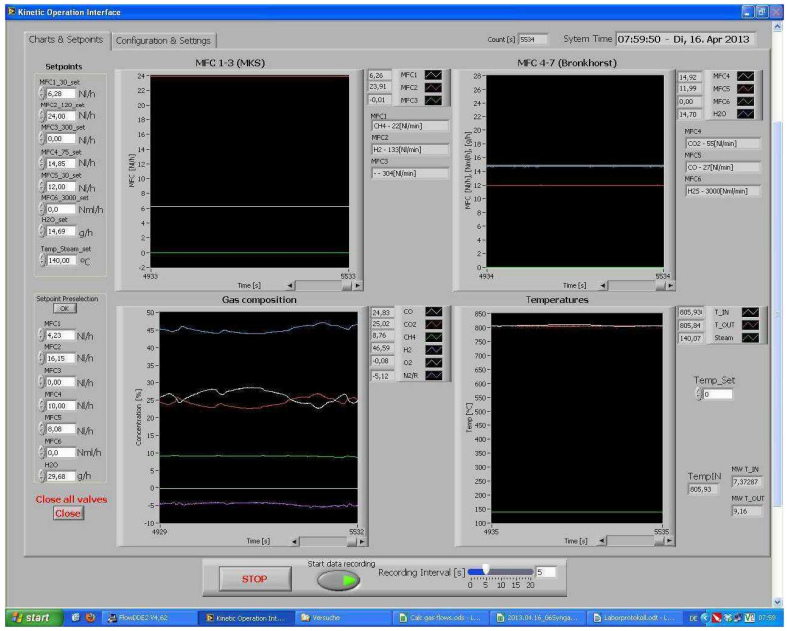

Figure 3.3: Screenshot of the LabVIEW® application

3.2 Catalyst

The used catalyst was developed and sold as a special reforming-catalyst which should be more resistant against usual deactivation mechanisms like coking and sulfur-poisoning. The active materials on the ceramic support were various noble metals, which exact composition was subject of trade secrets of the manufacturer. Common noble metal elements used for reforming usually include rhodium, ruthenium, iridium, platinum and palladium (see section 2.3.3). The loading of the catalyst with active material was around 1 %.

The glass-reactor of the test rig for chemical kinetics was filled every time with 12 pieces of hollow-cylindrical catalyst and positioned as can be seen in Fig. 3.2a. The average weight of the 12 catalyst cylinders was 6.5 g. The shape and the dimensions of the catalyst are shown in Fig. 3.4. Thus the resulting the bulk density was calculated as shown in formula 3.1

$$\rho_b = \frac{M_{catalysts}}{V_{catalysts-bed}} = 0.862\,\mathrm{g/cm^3} \tag{3.1}$$

The same catalyst was also investigated in the master thesis of Cerezo. With the material data from this thesis, a particle density of $\rho_\mathrm{p} = 3.081\,\mathrm{g/cm^3}$ could be calculated [51, p.21]. This corresponds well to the usual density of the support material, which ranges from $2.64\,\mathrm{g/cm^3}$ for SiO_2 to $3.42\,\mathrm{g/cm^3}$ for Al_2O_3 [52, 53]. Furthermore an effective diffusion coefficient $\mathrm{D_e} = 6.58 \times 10^{-6}\,\mathrm{m^2/s}$ was used in the thesis mentioned before.

Regarding poisoning in literature was found, that for example catalyst decay which is due to poisoning at a level of 1 part in 10^9, then one year of catalyst use in the plant could be simulated in the use of 50 ppm of poison for 10 min. However adsorption and subsequent reactions will be quite different under these two set of conditions[17, p. 65]. Therefore the arranged experiments were carried out with elevated sulfur concentrations to obtain results for catalyst deactivation in less time.

Property	Unit	Value
Outer diameter	mm	8
Inner diameter	mm	3
Height	mm	8

Figure 3.4: Shape and parameters of one single catalyst cylinder

3.3 Feedstock Gases

For the executed experiments three different feedstock-gases were used to test the catalyst-performance for various gas compositions. The exact gas compositions can be seen in Tab. 3.1:

Gas Mixture 1 Actually provided as an calibration gas for the 5-component gas analyzer, this gas was used as a clean gas mixture, which had a similar composition as the product gas from Güssing, but without any catalyst-poisons. The vendor of the gas bottle was Air Liquide Austria GmbH.

Gas Mixture 2 The gas mixture 2, which was created by mixing pure gases using the mass-flow controllers, was the primary gas mixture for testing the performance of the catalyst. The mass-flow controllers mixed the raw gases to obtain the right compositions for getting a mixture which is similar to the product gas from Güssing. The used gas bottles were methane 2.5 ($\geq$99.5 % CH_4), nitrogen 5.0 ($\geq$99.999 % N_2), hydrogen 5.0 ($\geq$99.999 % H_2), carbon dioxide technical ($\geq$99.5 % CO_2) and carbon monoxide standard (>98 % CO).

H_2S Gas Mixture To test the catalyst activity with sulfur-poisoned gas, hydrogen sulfide was added to the gas mixture 2. The H_2S-concentrations ranged from 25 ppm to 200 ppm. The default H_2S content for the parameters-study was 166 ppm in the dry gas (100 ppm in wet gas). The used H_2S-gas bottle contained an actual value of (10 130 $\pm$ 300) ppm H_2S and nitrogen as residual component.

Product Gas The product gas from the biomass-gasification plant in Güssing was stored in a gas bottle. The real gas composition was tested with a gas chromatograph in Güssing on 17.01.2013 and the results are shown in Tab. 3.1

Component	molar percentages [%]			
	Gas Mixture 1	Gas Mixture 2	H_2S Gas Mixture	Product Gas
CO	22.2	21	21	18.7
CO_2	20.7	26	26	23.3
CH_4	11	11	11	9.2
C_2H_4	2	0	0	2.2
C_2H_6	0.5	0	0	0.25
H_2	40.1	42	42	41.8
N_2	3.1	0	0	4.7
Sulfur	0	0	0.0025 - 0.02	0.009

Table 3.1: Compositions of used gases

3.4 Input and Output Parameters

The parameters which were used to gain comparable reaction-conditions as well as the parameters to obtain values for the interpretation of the results of the different experiments are described here. These definitions are widely consistent with the cited literature.

3.4.1 Input-Parameters

The following parameters were used to describe the conditions under which the reactions took place. Each parameter was varied within its possible range, which was limited by the minimum and maximum throughput of the mass-flow controllers and the maximum possible temperature of the test rig.

T Temperature
: The temperature was measured by type-K thermocouples and recorded automatically by Labview®. The experimental temperature ranged from 700 °C to 900 °C, because higher temperatures could damage the test rig apparatus. The maximum temperature of 900 °C was difficult to keep at a steady-state, due to high heat convection at this elevated temperatures as well as thermal fatigue of the stressed parts of the apparatus (sintering of the metal inlet tubes and embrittlement of the polymer hose were detected).

S/C Steam to carbon ratio in reactor, which is the ratio of total number of steam-molecules to the number of carbon atoms in the feed gas. The S/C ratio indicates primarily the tendency for coking. As explained in 2.3.4.1 coking is less probable when there is more oxygen available through H_2O. CO_2 doesn't affect the carbon formation and thus only CO and CH_4 are relevant for the S/C ratio[25, p. 53].

$$S/C = \frac{\dot{n}_{H_2O,in}}{\dot{n}_{CH_4,in} + \dot{n}_{CO,in}} \left[\frac{mol/h}{mol/h}\right] \tag{3.2}$$

SV The spacevelocity (also Gas Hourly Space Velocity, GHSV) is a measure for the dwell time of the reactants on the catalyst. It is defined as the ratio of the standardized volume-flow of the wet inlet-gas to the catalyst volume. As it is very difficult in industrial scale to calculate the exact volume of a packed bed of catalyst-pellets, the volume is calculated by using the total volume of the catalytic bed in the reactor.

$$SV = \frac{\dot{V}_{in,wet}}{V_{cat}} \; [h^{-1}] \tag{3.3}$$

3.4.2 Output-Parameters

These parameters were used to analyze and interpret the results from the various experiments:

X_i Conversion of substance i

$$X_i = \frac{\dot{n}_{i,in} - \dot{n}_{i,out}}{\dot{n}_{i,in}} * 100\ [\%] \tag{3.4}$$

The conversion describes the amount of converted moles per second related to the inlet-amount of moles per second of substance i. The parameter can have either a positive (in case of reaction-products) or negative (in case of reactants) value.

H_2/CO

$$H_2/CO = \frac{Y_{H_2,out}}{Y_{CO,out}}\ [-] \tag{3.5}$$

This parameter is the ratio of H_2-concentration and CO-concentration after the reactor. It is an important parameter for further fuel processing, e.g. a good value for mixed alcohols synthesis is 1.5.

H_2-Selectivity

$$S_{H2} = \frac{\dot{n}_{H2,out} - \dot{n}_{H2,in}}{\dot{n}_{CH4,in} - \dot{n}_{CH4,out}}\ [-] \tag{3.6}$$

In general the selectivity describes the ratio between the generation of a desired product and the consumption of one of the main reactants of the process. The H_2-selectivity is the ratio between the moles of H_2 created and the moles of CH_4 used by the steam reforming reaction. As hydrogen is (besides CO) one of the main products of the reforming process, this parameter is an interesting measure for the effectiveness of the process. But the production of hydrogen needs not necessarily result just from the reaction of methane with steam (steam reforming reaction, see eq. 2.10), but can also result from converting carbon monoxide and water to hydrogen and CO_2 (water-gas shift reaction, see eq. 2.15). Still the H_2-selectivity can be used to give a measure for the overall hydrogen-yield from methane.

3.4.3 Volume Flows

The total volume flow (L/h) of the inlet- and the outlet-stream was important to be able to calculate the massflows from the measured concentrations. As the total number of molecules and thus the total volume increased during the reaction in the reformer, the inlet- and outlet-streams were not equal. Therefore each stream had to be measured independently.

Inlet The inlet volume flow was determined by the summation of the average flow of the gas massflow-controllers and the addition of the gasified water-stream, so no extra measurement was needed. This calculation is shown in Eq. 3.7.

$$\dot{V}_{in} = \sum \dot{V}_{gas,i}[\mathrm{L/h}] + \dot{m}_{water}[\mathrm{g/h}]\frac{22.414[\mathrm{L/mol}]}{18.02[\mathrm{g/mol}]} \tag{3.7}$$

Several extra bypass-measurements were arranged to verify the accuracy of the massflow-controllers (MFC) with the Elster Kromschröder gas meter. Therefore the value measured by the gas meter (the volume was corrected from ambient air temperature to the standard-temperature of 0 °C, see 3.5.1) was compared to the measured value by the massflow-controllers for different gases and different massflows. The exact time and value of the gas meter was determined by taking pictures of the analog display. Further the measurement took about 45 min to be able to compensate temporary fluctuations within the volume flow and the measurement.

As can be seen in Table 3.2 the difference between these measured values was very little and could be neglected. Thus in all experiments the MFC-values could be taken for the volume-flow of the inlet gases.

Gas	**Gas Meter-Value** [l/h]	**MFC-Value** [l/h]	**Measurement Error** [l/h]	[%]
Gas Mixture 2	46.96	46.23	0.73	1.55
Gas Mixture 2	33.32	34.15	−0.8	−2.40
Product Gas	34.53	35.05	0.52	1.50

Table 3.2: Consistency of gas meter and MFCs

Outlet The outlet volume flow was measured by the analog Elster Kromschröder gas meter and in contrast to the other experimental data not automatically recorded on the computer. During the first experiments the value of the gas meter display and the corresponding time was written in the spreadsheet by hand. The time of the measurement was recorded in minute-scale, which was not accurate enough for this data as was found out later. The recording of the gas flow improved during the experiments and for the last experiments the gas meter display was photographed to have very accurate values for both the time and the display of the gas meter.

Then the corresponding volume flow was calculated as shown in eq. 3.8

$$\dot{V}_{out} = \frac{V_{gas\,meter,end} - V_{gas\,meter,start}}{t_{end} - t_{start}} \tag{3.8}$$

3.5 Important Definitions

3.5.1 Standard Conditions

The standard conditions for temperature and pressure in this document refers to the physical normal conditions (German "Normalbedingungen") as defined in DIN 1343 and ÖNORM A 2732 for reference conditions and normal conditions. These documents define the normal temperature at T_N=273.15 K (0 °C) and normal pressure at p_N=101.325 kPa (1 atm). Therefore all volumes or volume flows below are given at these normal conditions.

3.5.2 H_2 and CO_2 Interference Error

The Rosemount NGA 2000 5-component gas analyzer had a cross sensitivity for H_2 and CO_2, which is due to the measurement with a thermal conductivity detector (TCD). The device had an internal correction of this interference error, but the gas concentration values on the digital COM output, which was connected to LabVIEW, were without this correction. The correct values were only available through the analog output of the device. After being aware of this deviation, a laptop was connected to the analog output, to record the real concentrations of H_2 and CO_2. For all further experiments, the data was recorded simultaneously both on the computer of the test rig and the additional laptop.

To correct the values from earlier experiments, it was necessary to determine the internal correction factors of the gas analyzer. Therefore 4567 datapoints from both the analog and the digital output were used to find the parameters for the linear equation shown in eq. 3.9, which depended on the hydrogen as well as on the carbon dioxide concentration.

$$c_x = c^0_{H2} \cdot k_x + c^0_{CO2} \cdot l_x + d_x \tag{3.9}$$

Where:

x : is either H_2 or CO_2
c_x : is the corrected concentration for gas x
c^0_{H2} : is the original, digital concentration for H_2
c^0_{CO2} : is the original, digital concentration for CO_2
k_x : is the multiplication factor for H_2 to get the corrected value for gas x
l_x : is the multiplication factor for CO_2 to get the corrected value for gas x
d_x : is the distance to the ordinate for gas x

The unknown multiplication factors and the distance to the ordinate were calculated by using the *LINEST*-function of LibreOffice Calc. Due to the many datapoints it was possible to find accurate values for all parameters and a good coefficient of determination ($R^2_{CO2} = 0.986$ and $R^2_{H2} = 0.992$). The average difference from the values calculated from the uncorrected values to the values corrected internally by the analyzer was for CO_2 just $\overline{\Delta x}_{CO2} = -1.003 \times 10^{-5}$ and for H_2 $\overline{\Delta x}_{H2} = -1.714 \times 10^{-5}$.

3.5.3 Estimation of Unused Steam

The test rig for chemical kinetics had a water reservoir to collect unreacted H_2O after the reactor. The gas-flow was cooled down to about 4 °C, thus all water should be removed. As the duration of one experiment was in average only about 10 min, the accuracy of the amount of water was crucial to the usability of these results.

The main problem with the exact measurement was, that there was always small amount of water left in the tubes and in the last part of the reactor. After comparing the hydrogen-balance with the theoretical residual water content, one had to conclude, that the determination of the unused steam was not accurate enough.

3.5.4 Mass Balances

Both the inlet stream and the reformed gas stream consisted of a mixture of CO, CO_2, CH_4, H_2 and H_2O. As mentioned before it was difficult to measure the exact amount of unused steam, therefore the mass balances were only specified for the dry gas. The mass balance was calculated on atomic base, thus each molecule containing either carbon, hydrogen or oxygen was weighted depending on how many atoms are included.

Carbon For the carbon mass balance, all carbon containing main components were summed up, i.e. CO, CO_2 and CH_4. Other higher hydrocarbons with very low concentrations were not taken into account. The general equation, considering all possible reactions with carbon components is shown in eq. 3.10.

$$\dot{n}_{CH4,in} + \dot{n}_{CO,in} + \dot{n}_{CO2,in} = \dot{n}_{CH4,out} + \dot{n}_{CO,out} + \dot{n}_{CO2,out} + \dot{n}_{C,deposit} \quad (3.10)$$

It was possible, that carbon deposition (coking) took place due to reactions explained in 2.3.4.1, but during these experiment no carbon was detected in the reactor. There were no signs of solid carbon like black powder or small black particles on the catalyst. Furthermore there was no increase in weight of the catalysts before and after the reforming experiments, which gave another evidence, that no relevant carbon deposition took place. Therefore the term $\dot{n}_{C,deposit}$ was set to zero and removed from the balance, which then lead to equation 3.11 where both in- and outlet massflows were known.

$$\dot{n}_{CH4,in} + \dot{n}_{CO,in} + \dot{n}_{CO2,in} = \dot{n}_{CH4,out} + \dot{n}_{CO,out} + \dot{n}_{CO2,out} \quad (3.11)$$

This equation 3.11 was used to affirm the exactness of the measured massflows.

Hydrogen The hydrogen mass balance is given in eq. 3.12. Unfortunately it was not possible to detect the amount of reacted H_2O $\dot{n}_{H2O,reacted}$ with any measurement device, but it could be calculated since all other terms are given.

$$4\,\dot{n}_{CH4,in} + 2\,\dot{n}_{H2O,reacted} + 2\,\dot{n}_{H2,in} = 4\,\dot{n}_{CH4,out} + 2\,\dot{n}_{H2,out} \quad (3.12)$$

Oxygen Also for the oxygen mass balance it was not possible to estimate the exact amount of reacted water, but it was possible to calculate it from the balance in eq. 3.13.

$$\dot{n}_{CO,in} + 2\,\dot{n}_{CO2,in} + \dot{n}_{H2O,reacted} = \dot{n}_{CO,out} + 2\,\dot{n}_{CO2,out} \quad (3.13)$$

3.5.5 Measurement of Plausibility

To evaluate the plausibility of the experiments several uncertainties were take into account:

High reactor load At high space velocities, the chemical equilibrium could not be reached due to kinetic limitations of the absorption and reaction of the molecules on the catalyst.

Irregular reactor flow Due to an irregular reactor flow, some molecules might be able to pass the reactor without sufficient catalyst contact. However it is hard to distinguish between high reactor load and irregular reactor flow.

Further reactions There are still large amount of water vapor present in the gas, when the reformed gas mixture is cooled down in the unheated tube after the reactor. Under these conditions the water-gas shift reaction can occur and further formation of H_2 and CO_2 can take place.

Accuracy of data General impreciseness of experimental found data, which can either result from errors in calculations, inexactness of measurements or human mistakes while acquiring data.

Simulation data Comparison with simulation data from HSC gave further conclusions about the plausibility.

4 Experimental Results

The following pages explain how the experiments were arranged and the results are presented in detail.

4.1 Main Reactions

The four primary reactions taking place in the steam reforming reactor are following:

$$CH_4 + H_2O \leftrightarrow CO + 3\ H_2 \qquad \Delta H^{\ominus}_{298} = +206.2\,\text{kJ/mol} \qquad (4.1)$$

$$CH_4 + 2\ H_2O \leftrightarrow CO_2 + 4\ H_2 \qquad \Delta H^{\ominus}_{298} = +165.0\,\text{kJ/mol} \qquad (4.2)$$

$$CH_4 + CO_2 \leftrightarrow 2\ CO + 2\ H_2 \qquad \Delta H^{\ominus}_{298} = +247.4\,\text{kJ/mol} \qquad (4.3)$$

$$CO + H_2O \leftrightarrow CO_2 + H_2 \qquad \Delta H^{\ominus}_{298} = -41.2\,\text{kJ/mol} \qquad (4.4)$$

Due to the high CO_2 fraction in the inlet gas, apart from steam reforming, also dry reforming (eq. 4.3) took place in the reformer. As can be seen, this reaction has a lower enthalpy than 4.1 and is therefore less probable to take place if enough water is present. Just at low S/C ratios, where little steam was present, dry reforming would take place at elevated temperatures. Also the equilibrium of the water-gas shift reaction (eq. 4.4) was affected by the amount of steam in the inlet.

4.2 Study of Parameters

To obtain comparable performance-results for the tested commercial catalyst, different process-conditions were applied in the test rig. The three parameters, which could be varied were *temperature*, the *steam-carbon-ration* and the *spacevelocity*. For all of them different boundaries had to be taken into account, which limited the range of possible variation:

Temperature The examined range of temperature was from 700 °C to 900 °C. At lower temperatures than 700 °C the reaction was too slow to show significant conversion rates. The upper temperature boundary was at around 900 °C due to limits of the material. Both the quartz-glass reactor and other parts like the polymer tubes above the reactor showed signs of wear due to the high temperatures.

The experimental default temperature was set to 850 °C.

Steam-to-carbon ratio (S/C) The steam-to-carbon ratio was limited by the maximum water mass flow of 30 g/h of the Bronkhorst® Controlled Evaporator Mixer. As the gas composition was constant and the spacevelocity should be around 10 000 h^{-1}, the highest steam-to-carbon ratio which could be achieved was around 3.0.

The default S/C ratio was set to 2.0.

Spacevelocity (SV) The gas hourly spacevelocity (GHSV or SV) ranged from around 6000 h^{-1} to 11 000 h^{-1}. The total dry gas volume flow shouldn't get below 40 L/h, as then the gas analyzer wouldn't get enough gas volume to supply confident results. Therefore the minimum spacevelocity was set to 6000 A possibility to reach lower spacevelocities would have been to increase the catalyst volume, but there was not enough space for more than 12 pieces of catalyst cylinders in the quartz reactor. A glass reactor with a larger diameter could be an alternative, but there was no high temperature resistant reactor available at the moment of the experiments. The upper limit of the spacevelocity range was set by the maximum flow rate of the evaporator as mentioned above.

The default spacevelocity was 10 000.

For the following experiments always one parameter was varied while the others were kept constant to obtain information about the influence of the varied value.

4.3 Experimental Procedure

For each experiment, first the reactor had to be heated up to the needed temperature. Therefore the whole system was flushed with nitrogen at 20 L/h while heating up the reactor. The temperature was increased by approximately (4 to 5) °C/min. After reaching the desired temperature the needed influent components (usually CO, CO_2, CH_4, H_2 and water) were set up to bypass the reactor to be measured in the 5-component gas analyzer. This was necessary to obtain a real gas composition, which then could be compared with the effluent after the steam reforming. After reaching a steady-state in bypass-mode, the valves of the inlet gases were switched, so all gases were flowing through the reactor. Then again it took some minutes to reach a steady-state, which was usually retained for about 10 min. Then a new configuration was set up in LabVIEW to carry out the next experiment.

Progress The trends in concentrations and temperature are described here for one exemplary case of product gas at a spacevelocity of 9000, S/C=2 and a temperature of T=850 °C. The corresponding graphs are shown in Fig. 4.1.

1. **Bypass measurement** All valves of the gas streams were set to bypass to measure the real concentrations of the inlet gases. This concentrations were very stable and could be readout clearly from the graphs. Also one can see that the temperatures in the reactor before the catalysts (T_in) and after the catalysts (T_out) differed

Figure 4.1: Example of one experiment (product gas at SV=9000, SC=2, T=850 °C

a lot. This due to the fact, that during bypass measurement there was no gas flow through the reactor and thus the heat ascended and was retained in the reactor.

2. **Switching to reactor** After approx. 360 s the valves were switched towards the reactor and the changes in temperature and concentrations are obvious. First there was a rapid increase of hydrogen and CO which went along with a decrease of CO_2 and CH_4. Also the inlet and outlet temperatures decreased respectively increased to approach each other.
3. **Steady-state** A steady-state was reached after approx. 600 s total time in this case. This can be seen best at the concentration of methane, which showed a very uniform concentration of around 6 %. All other concentrations fluctuated, especially CO and CO_2. Their concentration depended much on the reactor temperature where a direct correlation with T_in was observable. Therefore the average value (arithmetic mean) for each gas component was calculated to obtain one specific value as a result for the experiment. The standard deviation of each component's concentration shouldn't exceed 2 %, otherwise the range of variation would be too large.

   For this case following values were detected: CO=(19.1 ± 1.7) %, CO_2=(18.5 ± 1.2) %, CH_4=(6.3 ± 0.1) %, H_2=(42.4 ± 0.6) %, O_2=(-0.02 ± 0.05) % at a temperature of 849 °C (average of T_in and T_out).
4. **Next experiment** Then the valves were switched back to bypass and the values for the MFCs in LabVIEW for the next point of measurement were set. This was either a variation of the amount of water in the stream (variation of S/C ratio) or the total flow (variation of spacevelocity). For variation of the temperature all streams were kept constant and only the reactor temperature was changed.

4.4 Results for Feedstock Gases

In this section the influence of the different feedstock gases are presented and discussed. For each gas several different test cases were carried out to obtain data for the catalyst performance. The feedstock gases were gas mixture 1 (4.4.1), gas mixture 2 (4.4.2), H_2S gas mixture (4.4.3) and product gas (4.4.4).

For each gas and each varied parameter both the conversion X and the concentration c are shown for all gas components in different graphs. The legend on the right side of the graph shows which gas is represented by which symbol. Further a simulation of the equilibrium composition was done with HSC by minimizing the Gibbs enthalpy. The equilibrium results are represented by a continuous line in the graphs below. To be able to compare the outcomes from HSC, which include also water vapor in the simulation, it was necessary to remove the fraction of water from the simulation to obtain the dry gas concentrations (see eq. 4.5). Then these results for the gas compositions from the experiments and the equilibrium composition in HSC were compared with each other.

$$c_{x,dry} = \frac{c_x}{100 - c_{H2O}} \cdot 100\ [\%] \tag{4.5}$$

Where:

x : is the gas component (CO, CO_2, CH_4, H_2 and N_2)
$c_{x,dry}$: the dry gas concentration of x in percent
c_x : the original percentage of component x from HSC
c_{H2O} : the percentage of water in the equilibrium result

4.4.1 Gas Mixture 1

The ready-mixed gas, which actually served as a calibration gas for the 5-component analyzer, was used for the first experiments on the test rig. The gas composition as described by the manufacturer as well as the average data obtained for the experiments from bypass-measurements with the gas analyzer of the test rig can be seen in Tab. 4.1.

The N_2 fraction of the data obtained from the analyzer was significantly higher than in the gas composition from the manufacturer due to two reasons: first of all there was a stream of 3 L/h of N_2 added as a carrier gas stream for the water vapor. Additionally other gas components like C_2H_4 and C_2H_6 couldn't be detected by the gas analyzer and thus they were included in this N_2 and residuals fraction. Due to the lack of information about the exact composition of this residual fraction, it was not further displayed and discussed in the diagrams below. This nitrogen and residuals fraction reached a significant concentration (around 20 % for gas mixture 1) due to the addition of nitrogen as a carrier gas. Therefore it was necessary to remove this part and re-calculate all other gas compositions. This calculation was similar to the removal of H_2O from the results from HSC as described above and the equation is shown in eq. 4.6.

$$c_{x,N2\,removed} = \frac{c_x}{100 - c_{N2}} \cdot 100\ [\%] \tag{4.6}$$

Where:

x : is the gas component (CO, CO_2, CH_4 or H_2)
$c_{x,N2\,removed}$: the gas concentration of x in percent without N_2
c_x : the percentage of component x with N_2
c_{N2} : the percentage of N_2 from the measurement

Component	CO	CO_2	CH_4	C_2H_4	C_2H_6	H_2	N_2
vendor-data [vol-%]	22.2 ± 0.4	20.7 ± 0.4	11.0 ± 0.2	2.0 ± 0.4	0.50 ± 0.01	40.1	3.1 ± 0.1
gas analyzer [vol-%]	18.6 ± 0.3	17.2 ± 0.2	9.5 ± 0.1	-	-	33.9 ± 0.3	20.8 ± 1.0[1]

Table 4.1: Average gas composition of gas mixture 1

The results for the experiments with gas mixture 1 are shown in the various graphs of 4.2 to 4.5.

Variation of Temperature The temperature was varied for the gas mixture 1 at two different steam-to-carbon ratios. In both cases it was obvious, that the conversion of methane as well as the amount of produced hydrogen rose with higher temperatures. As can be seen in Fig. 4.2b both methane and hydrogen concentrations didn't reach the level of thermodynamic equilibrium, but at higher temperatures they converged towards it. The hydrogen concentration showed a maximum at around 700 °C, but this value wasn't reached in the experiment, probably due to limitations in reaction and diffusion kinetics. For temperatures of 700 °C and higher, the concentration of methane should be close to zero according to the thermodynamic equilibrium, but with the tested catalyst it was not possible to reach this low concentrations. The trend shows, that with higher temperatures it could be possible to get towards the equilibrium results, but the used test apparatus wouldn't withstand these severe conditions. The results for CO- and CO_2-concentrations were close to the data from the equilibrium.

In the experiment with a higher S/C ratio of 3.2 it was noticeable, that the methane and hydrogen conversion were significantly higher (Fig. 4.3a). The equilibrium hydrogen concentration showed a maximum at around 650 °C (see Fig. 4.3b). The experimental hydrogen concentration converged towards the equilibrium at higher temperatures. The CO and CO_2 concentrations were not so close to the values from the equilibrium as they were at lower S/C ratios. The equilibrium showed an intersection point of the two lines at around 840 °C, which was in the first case already at around 650 °C.

[1] Also including other gas components, which were not detectable by the used analyzer for this experiments

Further it was apparently noticeable, that a higher S/C-ratio resulted in better conversion rates of methane and in a higher H_2-content, even at lower temperatures. This fact can also be seen in the next graphs, where the S/C-ratio was varied.

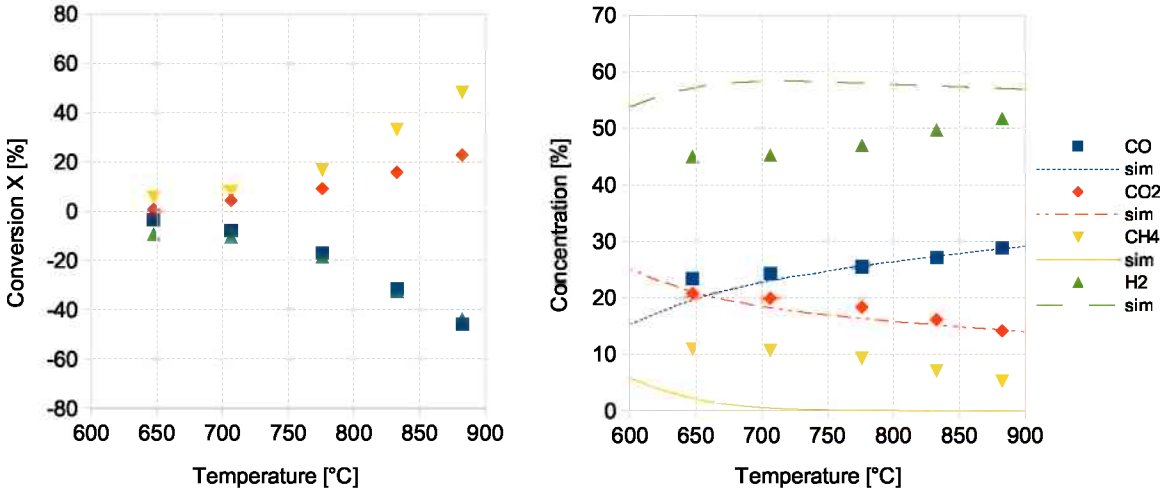

(a) Gas conversion (b) Gas concentration

Figure 4.2: Variation of temperature (gas mixture 1), S/C=1.6, SV=10 000 h^{-1}

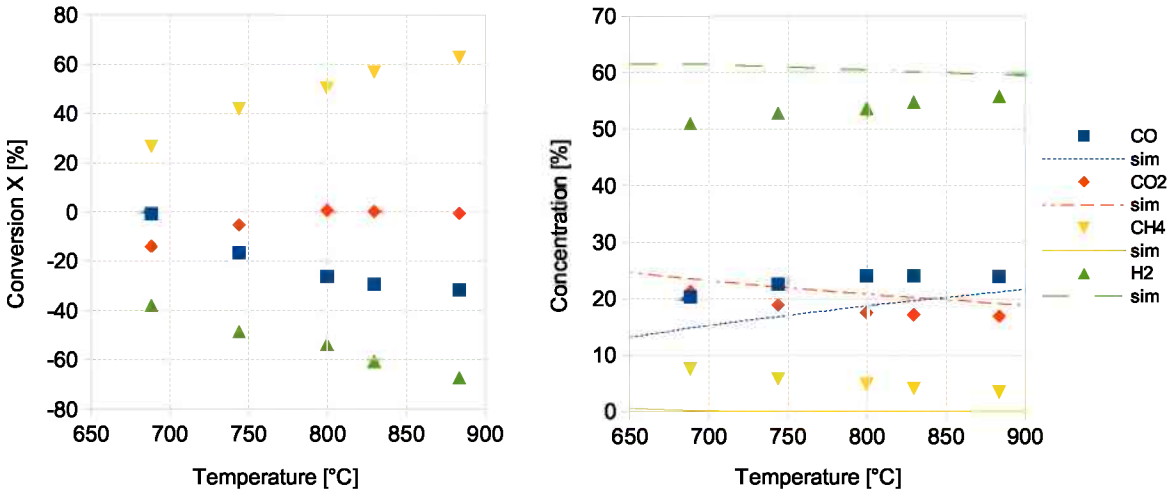

(a) Gas conversion (b) Gas concentration

Figure 4.3: Variation of temperature (gas mixture 1), S/C=3.2, SV=10 000 h^{-1}

Variation of Steam-to-Carbon Ratio The steam to carbon ratio was varied from 0.7 to 3.0. Although the S/C ratio is primary a parameter for coking tendency it can be seen in the experimental results, that both the conversion of methane and hydrogen increased at higher S/C ratios. This was on one hand due to the higher availability of water for the reforming of methane and on the other hand because of the water-gas shift reaction. Due to the latter reaction the CO-concentration was lower at higher S/C ratios as can be seen clearly in Fig. 4.4b.

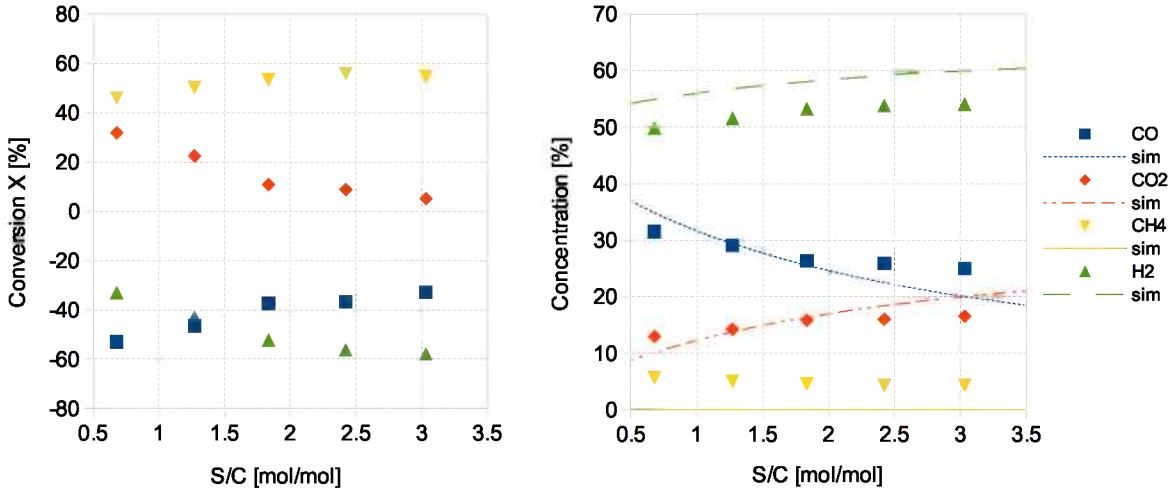

(a) Gas conversion **(b)** Gas concentration

Figure 4.4: Variation of steam-carbon-ratio (gas mixture 1), T=830 °C, SV=10 000 h^{-1}

Variation of Spacevelocity The gas hourly spacevelocity (Fig. 4.5) had little influence on the gas conversion rates compared to the other parameters. It is evident, that lower spacevelocities resulted in better conversion of methane and higher amounts of hydrogen, due to the fact, that more molecules could get in contact with the catalyst at lower gas velocities.

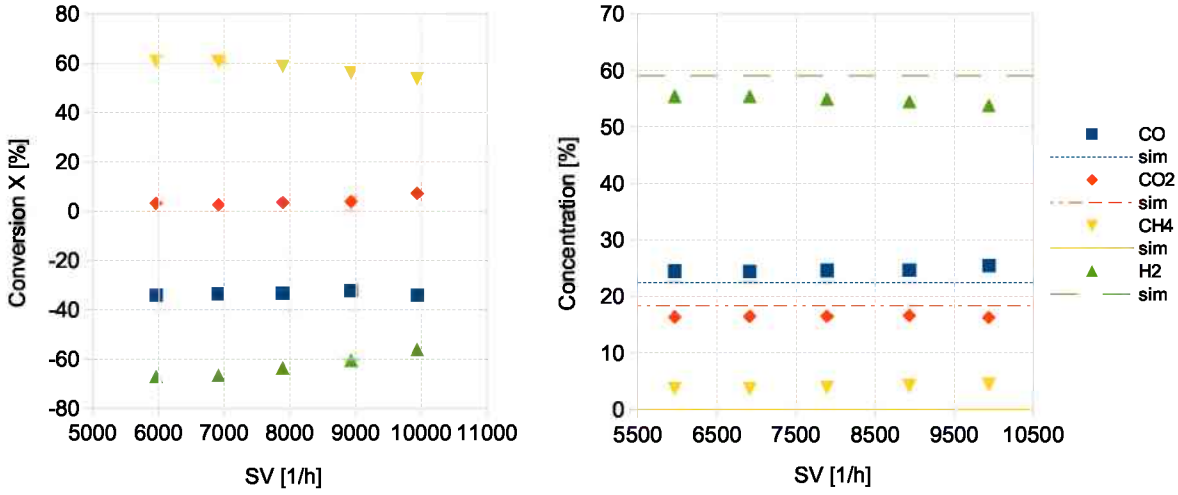

(a) Gas conversion **(b)** Gas concentration

Figure 4.5: Variation of spacevelocity (gas mixture 1), S/C=2.4, T=820 °C

4.4.2 Gas Mixture 2

The artificial mixed gas from pure gas bottles was another source for testing catalyst properties. Here the pure gas components CO, CO_2, CH_4 and H_2 were used to create a synthetic product gas mixture. The massflow controllers were set up to obtain a gas composition which was as constant as possible and close to the real composition of the product gas from the biogas plant. The targeted concentrations and the real concentrations measured by the gas analyzer are shown in Tab. 4.2.

No additional nitrogen had to be added because the pure CO_2 served as an inert carrier gas for the steam from the evaporator.

Component	CO	CO_2	CH_4	H_2	N_2
target [vol-%]	21	26	11	42	0
gas analyzer [vol-%]	22.0 ± 0.3	26.3 ± 0.2	11.5 ± 0.1	39.6 ± 0.9	0.7 ± 0.8[1]

Table 4.2: Average gas composition of gas mixture 2

[1] Also including other gas components, which were not detectable by the used analyzer

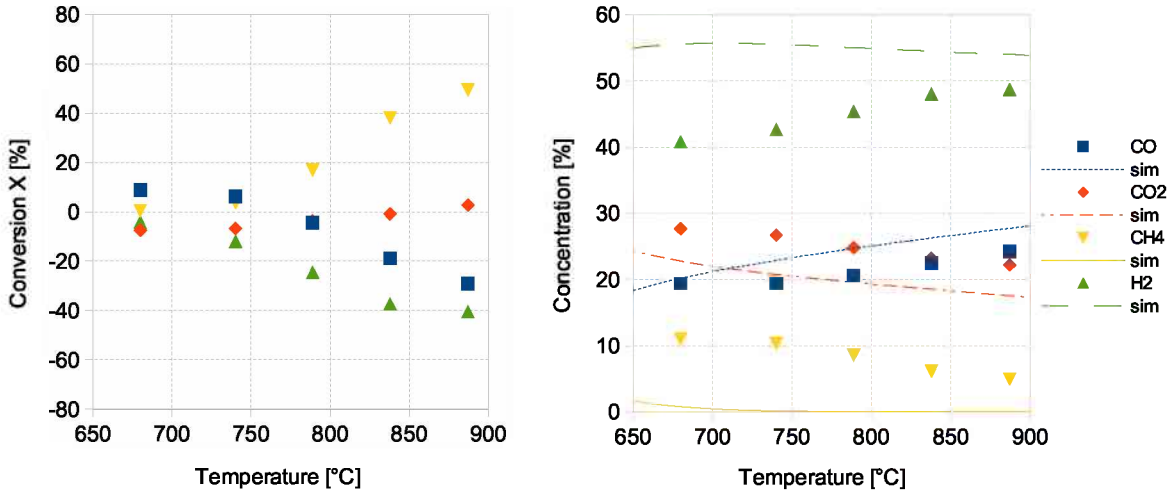

(a) Gas conversion (b) Gas concentration

Figure 4.6: Variation of temperature (gas mixture 2), S/C=1.9, SV=10 000 h^{-1}

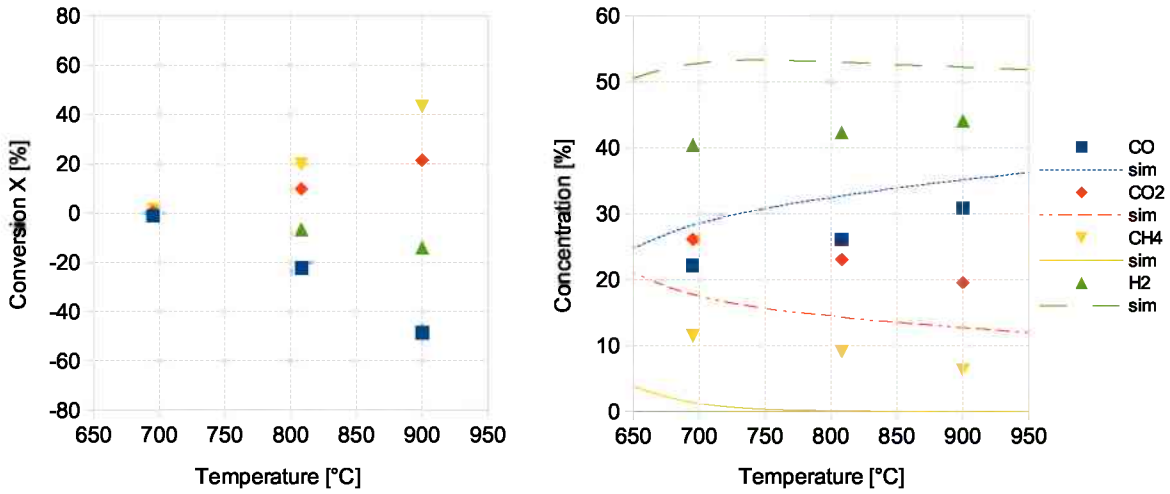

(a) Gas conversion (b) Gas concentration

Figure 4.7: Variation of temperature (gas mixture 2), S/C=1.0, SV=10 000 h^{-1}

Variation of Temperature In Fig. 4.6 the five experiments with a S/C-ratio of 1.9 at different temperatures are shown. It can be clearly seen that the conversion of CH_4 rose with higher temperatures (Fig. 4.6a). At lower temperature some CO_2 was produced and CO was consumed, whereas at temperatures beyond 800 °C this was reversed. This was due to the water-gas shift reaction.

Again, like in the previous results, it could be observed, that with higher temperatures the experimental results were closer to the concentrations from the equilibrium (Fig.

4.6b). Also by comparing the results from Fig. 4.7 and Fig. 4.8 it is clear that a higher S/C ratio resulted in higher conversion of methane and more hydrogen.

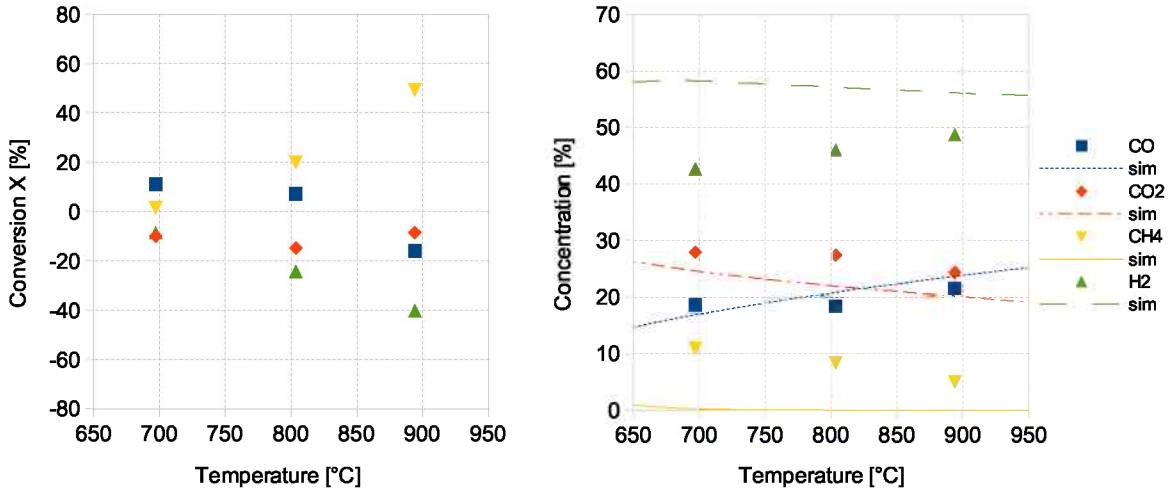

(a) Gas conversion **(b)** Gas concentration

Figure 4.8: Variation of temperature (gas mixture 2), S/C=2.9, SV=10 000 h^{-1}

Variation of Steam-to-Carbon Ratio The experiments with different steam-to-carbon ratios at the same temperature (850 °C) showed that especially the hydrogen yield rose with more water in the inlet-stream (Fig. 4.9). The hydrogen conversion changed from −30 % at S/C=1 to −60 % at S/C=3, thus the conversion doubled within this examined range. The change of the conversion of methane was not so significant, but still it increased around 10 % (Fig. 4.9a).

At low S/C ratios CO_2 was consumed, while it was produced at higher S/C ratios (higher than 1.5). Due to the fact, that the hydrogen and CO_2 concentration rose and the CO concentration was less at higher S/C ratios, the most probable explanation for this observation is the water-gas shift reaction (Fig. 4.9b).

There were no observations of carbon deposition on the catalyst (no significant change in weight before and after the experiments and no visual sign of carbon powder).

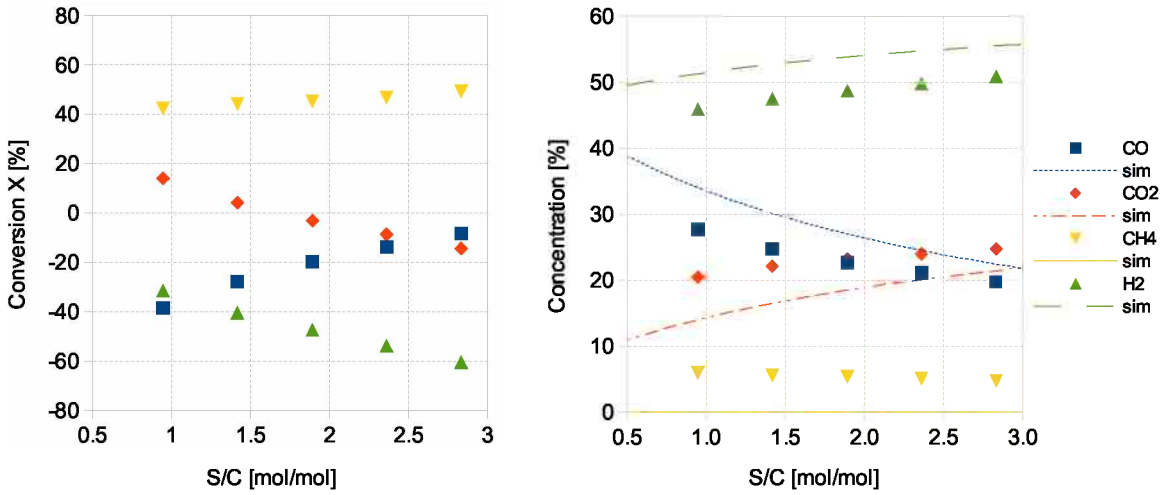

(a) Gas conversion (b) Gas concentration

Figure 4.9: Variation of S/C (gas mixture 2), T=850 °C, SV=10 000 h^{-1}

Variation of Spacevelocity The variation of the gas hourly spacevelocity showed less impact on the gas concentrations than the other parameters. Although it could be observed, that the reforming products were closer to the equilibrium concentration, the influence within the varied range of spacevelocity was small. Between spacevelocities of 6000 h^{-1} and 11 000 h^{-1} the methane conversion decreased around 12 % (from 57 % to 45 %) and the hydrogen conversion decreased around 3 % (from −52 % to −49 %).

It would also be interesting to carry out experiments at spacevelocities lower than 6000 h^{-1} to see if the catalyst performs better and the equilibrium concentrations can be reached.

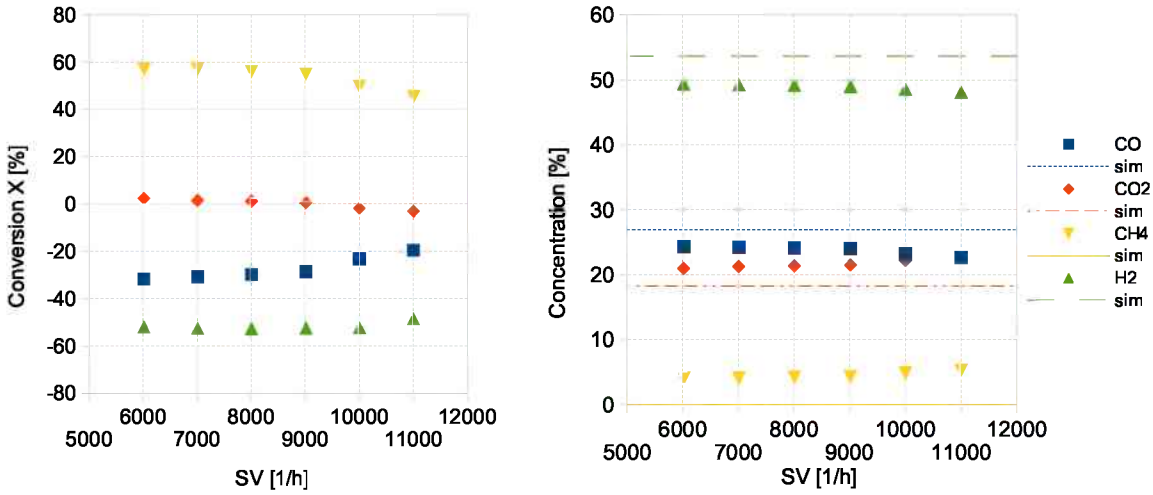

(a) Gas conversion (b) Gas concentration

Figure 4.10: Variation of spacevelocity (gas mixture 2), S/C=1.9, T=850 °C

4.4.3 H_2S Gas Mixture

The mixed gas from pure gas bottles with addition of H_2S was used to test specific poisoning of the catalyst. Therefore a certain amount of H_2S from a bottle containing nitrogen and H_2S (H_2S concentration of $(10\,130 \pm 300)$ ppm) was dosed to the gas-mixture, which was explained before in section 4.4.2. The average gas concentrations for the experiments with an H_2S concentration of 163 ppm in the dry gas, for which the parameters temperature, spacevelocity and steam-to-carbon ratio were varied, is given in Tab. 4.3.

Component	CO	CO_2	CH_4	H_2	N_2
gas analyzer [vol-%]	21.4 ± 0.2	25.9 ± 0.3	11.9 ± 0.1	37.2 ± 0.7	3.8 ± 0.3[1]

Table 4.3: Average gas composition of H_2S gas mixture

[1] Also including other gas components like H_2S, which were not detectable by the used analyzer for this experiments

Variation of H_2S-concentration The experiment with increasing hydrogen sulfide concentration showed at which point the immediate poisoning of the catalytic activity started. As can be seen in Fig. 4.11a a first significant drop of about 5 % in conversion rate of methane and hydrogen was detected at 50 ppm H_2S. Then at the next concentration of 75 ppm the conversion of hydrogen was reduced considerably to around −4 %. Methane had at this point a conversion of 10 %, showing a drop of 25 % compared to 50 ppm of H_2S. From this point on all conversion rates got closer towards zero percent. Methane still showed the highest conversion rate of around 4 % at 200 ppm H_2S in the feedstock gas.

Due to the short exposure time of the catalyst of around 20 min per experiment no exact information can be given, regarding poisoning when the catalyst is used at low H_2S-concentrations for a longer period of time. Most probably the reactive sites on the catalyst will be also occupied by sulfur molecules and thus resulting in a deactivation of the catalytic activity similar to high H_2S-concentrations for a short time. It can be concluded, that already at a concentration of 75 ppm of H_2S the catalyst was poisoned, so the reforming reaction was significantly slowed down.

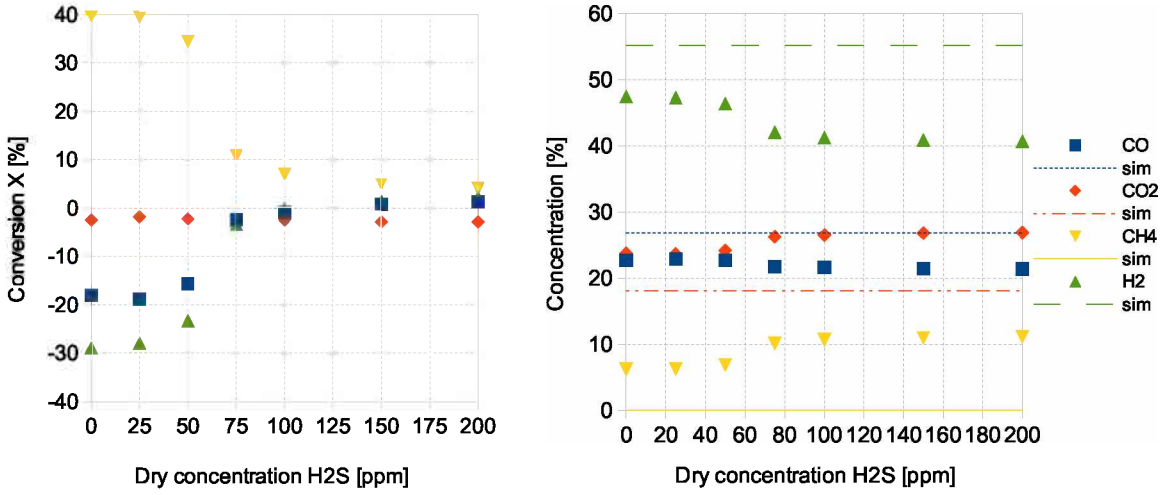

(a) Gas conversion **(b)** Gas concentration

Figure 4.11: Variation of H_2S concentration (H_2S gas mixture), S/C=1.9, T=850 °C, SV=10 000 h^{-1}

Variation of Temperature As can be seen in Fig. 4.12a the conversion was much lower in comparison with the results of gas mixture 2. The catalyst became more active at temperatures higher than 850 °C, but nevertheless the conversion of methane was 50 % at 887 °C (S/C=1.9) without H_2S and just 17 % with 163 ppm H_2S in the feedstock gas. Similar drops in conversion rates were also detected for the conversion of hydrogen (−10 % conversion instead of −40 % without H_2S). The conversion of CO and CO_2 were not so much affected. The CO conversion dropped from −30 % at 887 °C down to −13 %, which was probably due to the fact, that less CO was produced because less methane was reformed. However the CO_2 conversion seemed not to be affected at all by H_2S.

In 4.12b the outlet concentrations were compared with the equilibrium data. For all temperatures the concentrations were even further away from the equilibrium concentrations and the experimental results were just close to the inlet composition. Only at high temperatures around 887 °C the results showed a significant change in the gas composition.

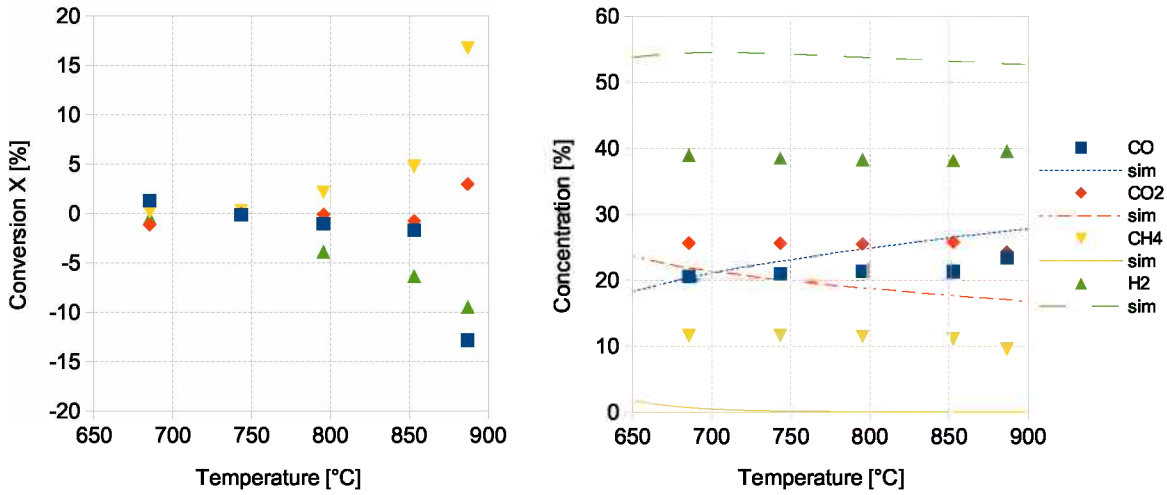

(a) Gas conversion (b) Gas concentration

Figure 4.12: Variation of temperature (H_2S gas mixture), S/C=1.9, SV=10 000 h^{-1}

Variation of Steam-to-Carbon Ratio The experiments for different S/C ratios with poisoned gas were carried out at temperatures of 850 °C. Again the capability of the reactor to promote the reforming reaction was reduced, which can be seen in Fig. 4.13a. The conversion of methane kept staying very low again. It was influenced more by the temperature than by the amount of steam in the inlet. Also CO and CO_2 were converted in very low amounts, but a tendency towards less CO and more CO_2 (due to the water-gas shift reaction) could be detected. Just one runaway value could be detected at a steam-to-carbon ratio of 2.4, which occurred probably due to an inaccurate measurement because of the very low concentration changes. The hydrogen conversion became gradually more with higher S/C ratios, although no additional methane was reformed to CO and H_2. Thus it was probably again the water-gas shift reaction which lead to the higher yield in hydrogen and more CO_2 at higher steam-to-carbon ratios.

In Fig. 4.13b the concentrations are compared with the equilibrium values. All concentrations stayed nearly the same as in the inlet stream, showing that the catalyst was deactivated to a large extent. Just, as mentioned above, hydrogen and CO_2 became a little bit more and the concentration of CO decreased around 2 %.

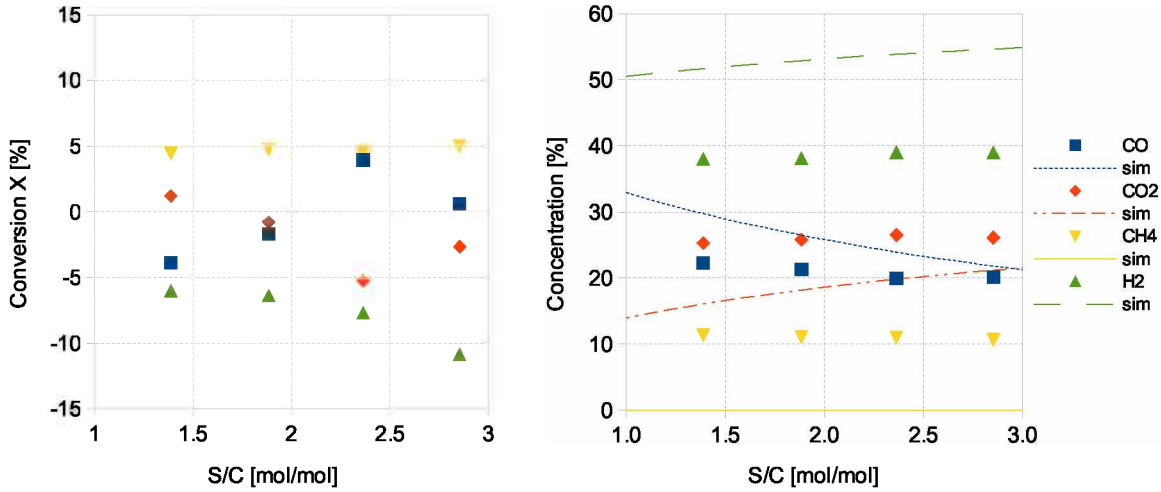

(a) Gas conversion **(b)** Gas concentration

Figure 4.13: Variation of S/C ratio (H_2S gas mixture), T=850 °C, SV=10 000 h^{-1}

Variation of Spacevelocity The conversion of methane was better at lower spacevelocities, due to the longer interaction time with the catalyst (Fig. 4.14a). Although a clear trend for the conversion of methane and hydrogen could be identified, the overall change in conversion was only around 4 % within the analyzed range of spacevelocities. Compared with other parameters the spacevelocity had a higher influence on the conversion than for example the steam-to-carbon-ratio, but significantly less influence than the temperature. The conversion of CO and CO_2 varied considerably, which was probably a result of inaccuracies in the measurement and the propagation of the error due to the little change in concentrations.

In Fig. 4.14b the gas composition of the outlet stream is shown, which was nearly the same as the inlet stream. Compared with results of the feedstock gas without H_2S the influence of the spacevelocity was even less and the concentrations were even further away from the equilibrium.

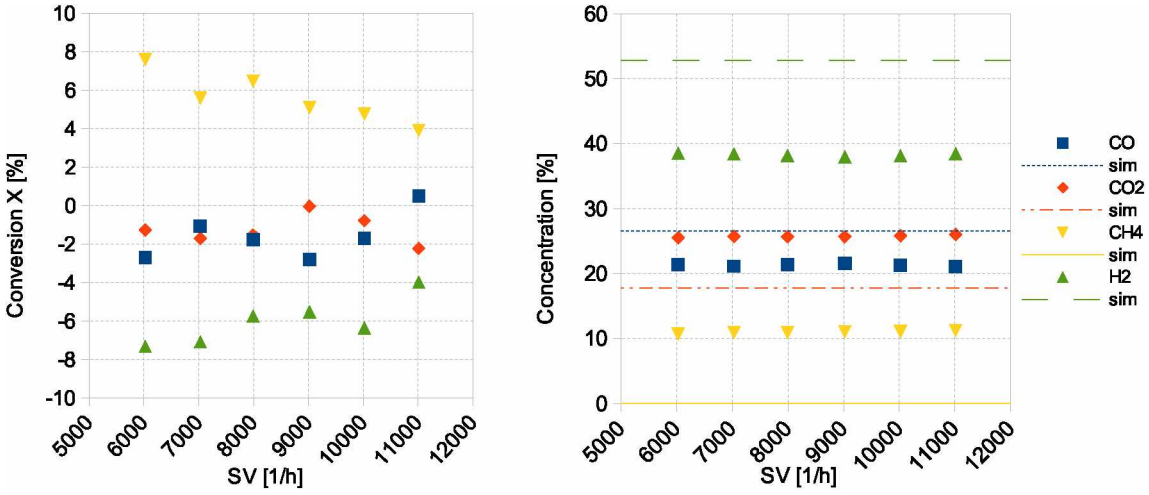

(a) Gas conversion (b) Gas concentration

Figure 4.14: Variation of spacevelocity (H_2S gas mixture), S/C=1.9, T=850 °C

4.4.4 Product Gas

The product gas from the biomass gasification plant Güssing was stored in a gas bottle to be available in the laboratory for the test rig. A gas sample was taken and analyzed using gas chromatography to identify all substances currently present in the bottle. The results showed, that the composition did not change significantly. The only component which was different from a gas sample, which would be taken directly from the plant, is H_2S. In the stored bottle just carbonyl sulfide (84 ppm COS) and thiophene (7 ppm C_4H_4S) was identified instead of H_2S. Due to the high pressure in the metal tank and the high availability of carbon and oxygen in the other gas components, the hydrogen sulfide converted primarily to COS. This had no impact on the measurement of the catalyst because the carbonyl sulfide was immediately reduced to H_2S at the high temperatures in the reactor.

Before entering the reactor the gas was diluted with N_2, which served as a carrier gas for the water vapor (see also 4.4.1). The nitrogen volume flow was about 3 L/h, which increased the amount of nitrogen measured in the outlet stream. Another reason for the higher nitrogen amount in the outlet, was that the gas analyzer couldn't detect hydrogen sulfide and higher hydrocarbons like C_2H_4 and C_2H_6. The total amount of nitrogen and residuals ranged from 16 % to 25 % in the inlet stream and from 12 % to 20 % in the outlet stream. The percentage in the outlet was lower because the total gas volume flow was increased by the reforming reaction and the amount of other hydrocarbons was reduced. It was again necessary (like for gas mixture 1 in 4.4.1) to remove the nitrogen fraction from the gas composition to remove fluctuations in the concentrations due to this residual fraction. These fluctuations were especially high for the variation of steam-to-carbon ratio. The conversion graphs were not affected because they were calculated from absolute mass flows and not from concentrations. The equation for re-calculating the concentrations of the gas components without nitrogen and other residuals is shown in eq. 4.6.

In Tab. 4.4 the composition of the product gas is shown. The first line contains the values from the GC-measurement and the second line the average gas composition from bypass measurements at the test rig.

Component	CO	CO_2	CH_4	C_2H_4	C_2H_6	H_2	H_2S	N_2
GC-data [vol-%]	18.7	23.3	9.2	2.2	0.3	41.8	0.009	4.7
gas analyzer [vol-%]	16.0 ± 0.4	20.8 ± 0.5	8.5 ± 0.2	-	-	34.3 ± 0.8	-	20.4 ± 1.9[1]

Table 4.4: Average gas composition of product gas

[1] Also including other gas components, which were not detectable by the used analyzer for this experiments

Variation of Temperature Due to the fact, that the concentration measured by the GC, which was used for the calculation of the inlet-streams, differed from the actual concentration measured by the gas analyzer of the test rig, the steam-to-carbon ratio was always a bit higher than desired and for this experiment it was around 2.4. As can be seen in Fig. 4.15a there was a steep increase of conversion rate with temperature. At lower temperatures around 700 °C the conversion of methane was just 5 % and hydrogen was −11 %. This conversion increased up to 37 % for methane and −38 % for hydrogen at 900 °C. The amount of CO rose significantly with higher temperatures. Also the CO_2 conversion increased with higher temperatures but not as much as CO.

In Fig. 4.15b the experimental concentrations are compared with the equilibrium concentrations from HSC. The methane and hydrogen concentration were getting closer to the equilibrium with higher temperatures, which indicates that the reaction was probably limited by diffusion. Therefore the overall reaction on the catalyst sped up with higher temperatures. The concentration of CO and CO_2 were also influenced by temperature and they were increasing and decreasing respectively, but they were much closer to their equilibrium composition.

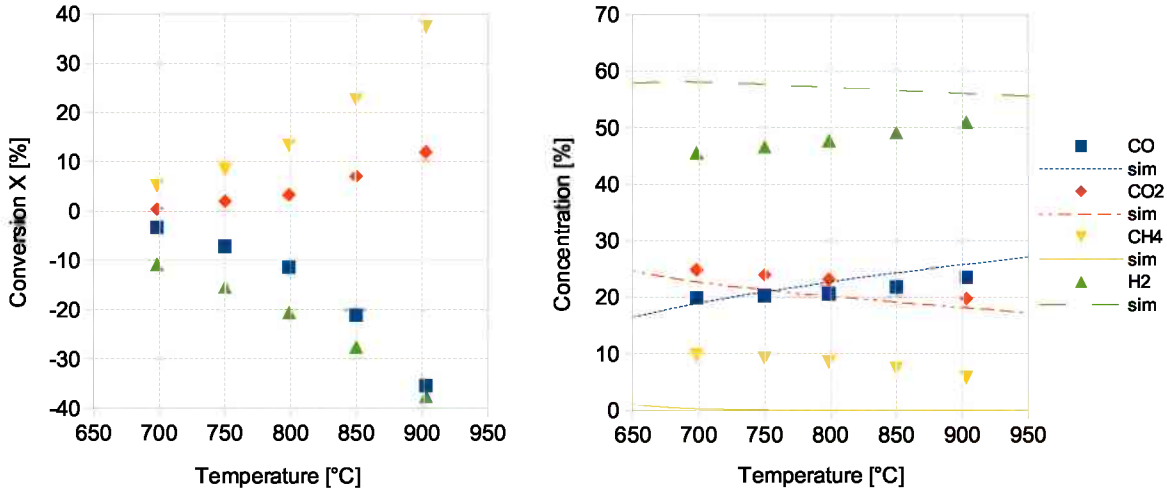

(a) Gas conversion **(b)** Gas concentration

Figure 4.15: Variation of temperature (product gas), S/C=2.4, SV=10 000 h^{-1}

Variation of Steam-to-Carbon Ratio The conversion rates of the different gases at different steam-to-carbon ratios are shown in Fig. 4.16a. Methane is clearly the component which was affected least by varying the amount of steam in the inlet. The methane conversion increased a little bit, but stayed always between 19 % and 23 %. On the other hand the hydrogen conversion rose due to the fact, that more hydrogen was produced by the steam reforming reaction (taking place at high S/C ratios) than by the dry reforming reaction (at low S/C ratios). The range for hydrogen conversion was from −17 % at S/C=1.2 to −32 % at S/C=3.7. Both CO and CO_2 conversion decreased with rising steam amount. The reason was probably that at lower H_2O concentrations the dry reforming reaction (see 2.14) was more likely to take place and hence CO_2 was consumed and CO produced. With more steam available the steam reforming reaction, which has a lower enthalpy, took place and thus just CO was produced from CH_4 and H_2O without the need of CO_2.

Taking a look at the concentrations from the experiment (Fig. 4.16b), the concentration of hydrogen increased slowly and methane decreased slightly. Due to the fact, that the distance to the equilibrium concentration always stayed rather the same, it can be concluded, that the overall methane reforming (both dry reforming and steam reforming) was not limited by a lack of water, but probably by diffusion limitations on the catalyst. The concentrations of CO and CO_2 showed both for the experimental and the equilibrium calculation results, clear trends towards less CO and more CO_2 at higher S/C ratios.

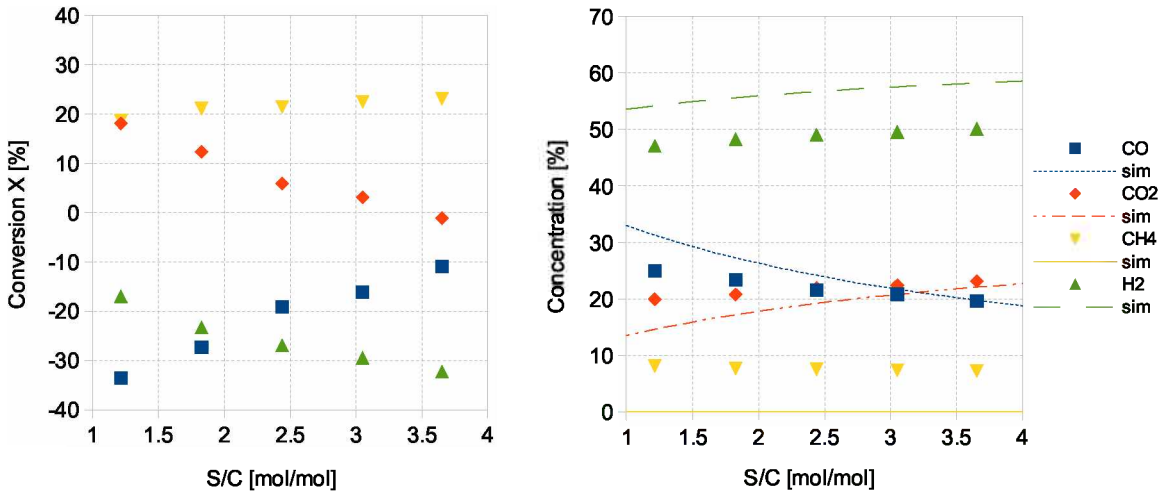

(a) Gas conversion (b) Gas concentration

Figure 4.16: Variation of S/C ratio (product gas), T=850 °C, SV=10 000 h^{-1}

Variation of Spacevelocity The spacevelocity was varied from 6000 h^{-1} to 11 000 h^{-1} to obtain data about the influence of the residence time on the reaction (Fig. 4.17). There was some influence detected for each gas component, but the only clear trend showed methane. The methane conversion changed from 27 % at 6000 h^{-1} to 23.5 % at 11 000 h^{-1}. The conversion of the other gas components CO, CO_2 and H_2 contained some runaway values, especially at 8000 h^{-1} and 9000 h^{-1}. Also for H_2 no clear trend could be identified, although the conversion should have increased at lower spacevelocities, similar to the experiments explained before. Disregarding the runaway values, the conversion of CO and CO_2 were both reduced with higher volume flows. This can be explained by the shorter residence time in the reactor, which resulted in incomplete reactions.

In Fig. 4.17b the values from the experiment were compared with the equilibrium data. For hydrogen and methane no clear trends could be identified from these curves. Only the concentrations of CO and CO_2 showed a slight trend towards less conversion at higher spacevelocities.

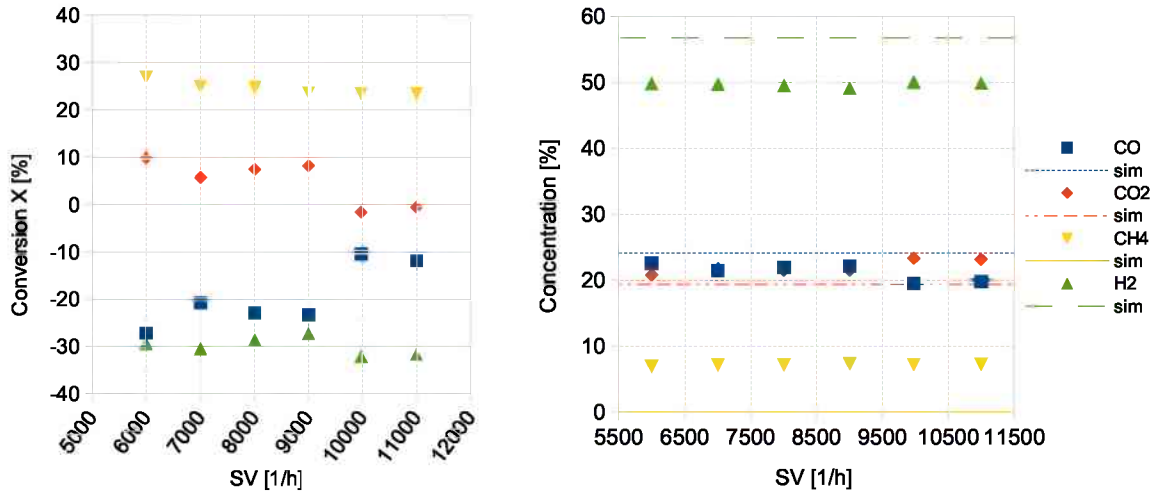

(a) Gas conversion (b) Gas concentration

Figure 4.17: Variation of spacevelocity (product gas), S/C=2.5, T=850 °C

4.5 Comparison of Feedstock Gases

In the following section the results are represented in graphs, where always one result (e.g. CH_4 conversion) is shown for the variation of one specific input parameter (e.g. temperature). One diagram contains different points for the different feedstock gases to be able to compare the results with each other.

4.5.1 Variation of Temperature

As discussed before, the temperature had a significant influence on the conversion of the gas components and on the gas concentrations in the outlet stream. In the following graphs 4.18 to 4.20 the same temperature ranges as before were analyzed, but the different feedstock gases were compared with each other on the basis of one certain output parameter.

CH_4 Conversion In Fig. 4.18 the methane conversion, which is the percentage of the converted moles CH_4 by the reforming reaction, is shown in dependence on the temperature. The highest conversion reached gas mixture 1, when the tests were carried out with a significant higher S/C ratio of 3.2. For gas mixture 1 the methane conversion was still good at lower S/C ratios, but it was already closer to gas mixture 2. The gas mixture 2 showed also good results, which were very stable and corresponded well with the results of gas mixture 1 at a similar S/C ratio. The methane conversion of gas mixture 2 didn't depend very much on the S/C ratio because the three different results for gas mixture 2 were close to each other. The product gas from Güssing showed then already lower conversion rates of methane. They differed from the best conversion rates of gas mixture 1 around 20 % to 35 %. The by far lowest methane conversion showed the gas mixture with the highest hydrogen sulfide content of 163 ppm H_2S. This H_2S gas mixture reached just conversion rates of methane of around 5 % at 850 °C and a S/C-ratio of 1.9. Both at higher and lower temperatures the conversion was always significantly lower than for feedstock gases with less H_2S.

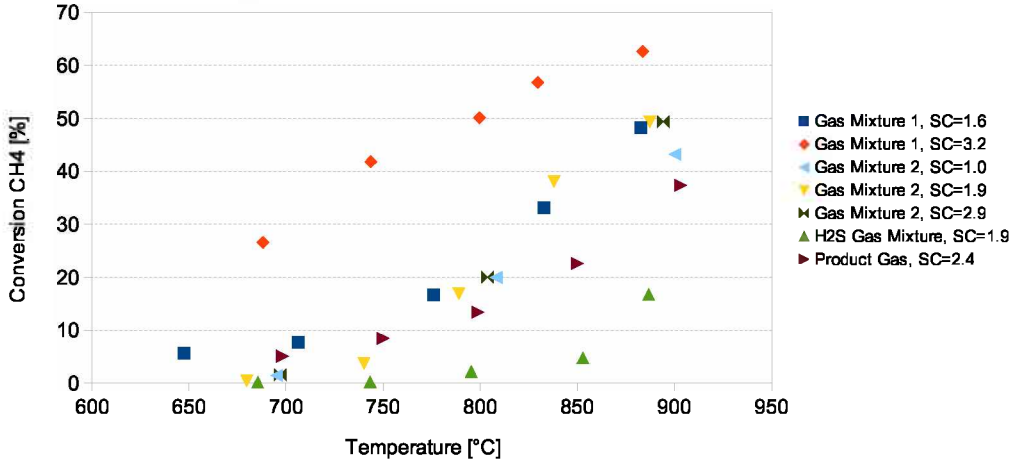

Figure 4.18: CH_4-conversion for different temperatures (SV=10 000 h^{-1})

H_2 Conversion In Fig. 4.19 the conversion of hydrogen is shown in dependence on the temperature. Again the highest conversion was reached with gas mixture 1, where a hydrogen conversion of $-63\,\%$ at $880\,°C$ was measured. One reason for this high yield was again the high S/C ratio. As can be seen the same gas mixture had much lower hydrogen conversion at lower S/C ratio. The hydrogen conversion for gas mixture 2 (with S/C of 1.9 and 2.9), gas mixture 1 (S/C of 1.6) and product gas were close to each other. The conversion was around $-30\,\%$ at $850\,°C$ and around $-40\,\%$ at $900\,°C$. The gas mixture 2 with a S/C ratio of 1.0 showed little hydrogen conversion capability. Probably there was less hydrogen in the outlet because CH_4 was consumed by dry reforming reaction, which resulted in a lower production of hydrogen. The lowest hydrogen conversion was with the H_2S poisoned feedstock gas. With hydrogen sulfide the results were about $-5\,\%$ to $-10\,\%$.

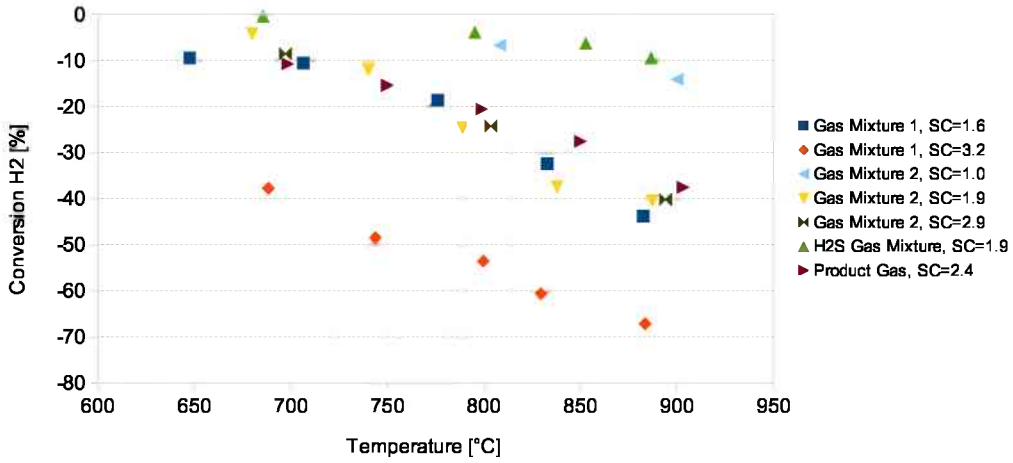

Figure 4.19: H_2-conversion for different temperatures (SV=$10\,000\,h^{-1}$)

H_2/CO-Ratio Another output parameter which was not investigated yet, is the ratio of hydrogen and carbon monoxide in the outlet (see eq. 3.5). This ratio was calculated not from the amount of moles in the outlet, but from the gas concentration. There was no additional correction for the varying amount of nitrogen in the outlet needed, because this factor would be eliminated in the fraction anyway. A desired value for this parameter should be 2.0 for most synthesis processes and 1.5 for the synthesis of mixed alcohols.

In Fig. 4.20 the resulting ratios for the different feedstock gases are represented. There were mainly two fractions, which was at a value around 2.3 for product gas (S/C=2.4), gas mixture 2 (S/C=1.9), gas mixture 2 (S/C=2.9) and gas mixture 1 (S/C=3.2) and the other one at a value around 1.8 for gas mixture 1 (S/C=1.6), H_2S gas mixture (S/C=1.9) and at even lower values gas mixture 2 (S/C=1.0). A trend could be detected, that with more steam in the inlet, the H_2/CO ratio was higher, due to the higher hydrogen conversion. It was also interesting, that even the H_2S-poisoned feedstock gas led to a similar H_2/CO ratio as the clean inlet gases with a lower steam-to-carbon ratio.

For further fuel processing the steam-to-carbon ratio was a bit too high at 850 °C. This parameter was not influenced very much by temperature, due to the fact, that with rising temperature the amount of both H_2 and CO increased, but it depended more on the steam-to-carbon ratio.

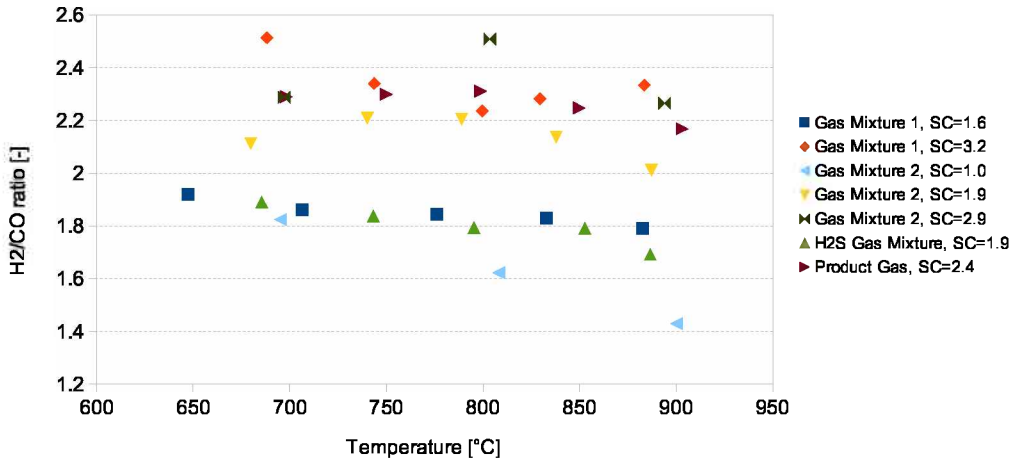

Figure 4.20: H_2/CO-Ratio for different temperatures (SV=10 000 h^{-1})

H_2-Selectivity The H_2-Selectivity is the ratio between the generated moles hydrogen and the consumed moles of methane. The theoretical value for the ratio between produced hydrogen and used methane should be 3 (based on the mole balance of the steam reforming reaction, see eq. 2.10). This value can be lower than three, which means, that probably dry reforming took place, hence less hydrogen is produced. If the H_2-selectivity is higher, then probably additional hydrogen was formed by means of the water-gas shift reaction.

In Fig. 4.21 the H_2-selectivity in dependency on the temperature is shown. The trend for all feedstock gases showed, that with higher temperature the selectivity went down, which means that the water-gas shift reaction was less probable to take place at higher temperatures. This corresponds well with the fact, that the water-gas shift reaction favors lower temperatures. Still at the default temperature of 850 °C the selectivity for hydrogen was around 4 for all feedstocks.

It could also be observed that the gases containing H_2S (H_2S gas mixture and product gas) reached higher H_2-selectivities at all temperatures. This could mean that due to the sulfur present in the inlet, the water-gas shift reaction is favored in comparison to the steam reforming reaction.

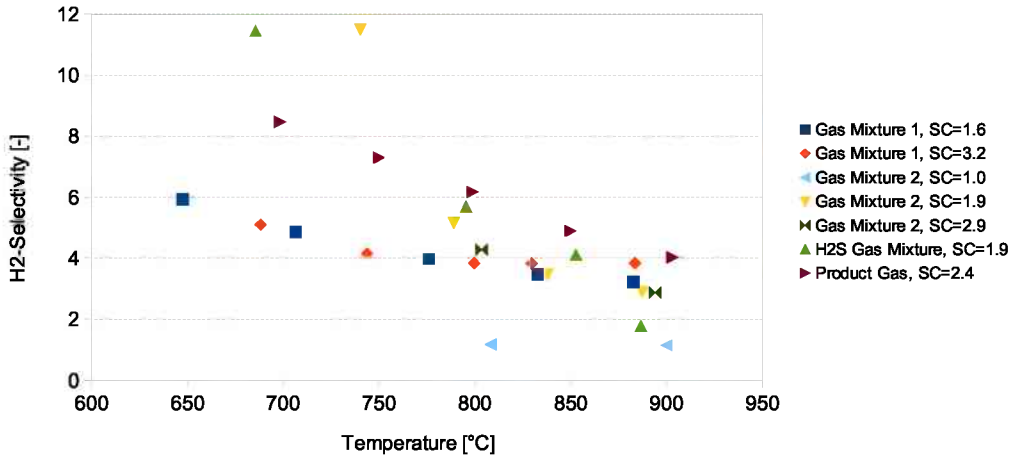

Figure 4.21: H_2-selectivity for different temperatures (SV=10 000 h^{-1})

4.5.2 Variation of Stream-to-Carbon Ratio

In the following section the variation of different steam-to-carbon ratios is discussed for various feedstocks. In each graph now just the S/C ratio was varied, while all other parameters were kept constant (spacevelocity of $10\,000\,h^{-1}$ and temperature between 830 °C to 850 °C) to obtain information about the influence of H_2O on the reactions.

CH_4 Conversion Fig. 4.22 shows the conversion of methane in dependence of steam-to-carbon ratio. As can be seen in the figure there was a huge difference between the different feedstock gases. The influence of the S/C ratio was higher for the gases, which contained no H_2S. For gas mixture 1 the methane conversion increased from 45 % to 55 % and for gas mixture 2 it increased from around 42 % to nearly 50 %. On the other hand for H_2S gas mixture the consumption of methane increased just around 0.5 % and for product gas there was a small increase of around 4 % in methane conversion.

The trend for gas mixture 1 suggests that a maximum conversion of methane was already reached at a steam-to-carbon ratio of 2.5. On the other hand gas mixture 2 showed that the methane consumption can still be increased with more water content in the inlet. Due to restrictions of the maximum massflow of water in test rig it was not possible to increase the amount of steam higher than around 3.5 at the same spacevelocity, to see if the conversion of methane could still be increased.

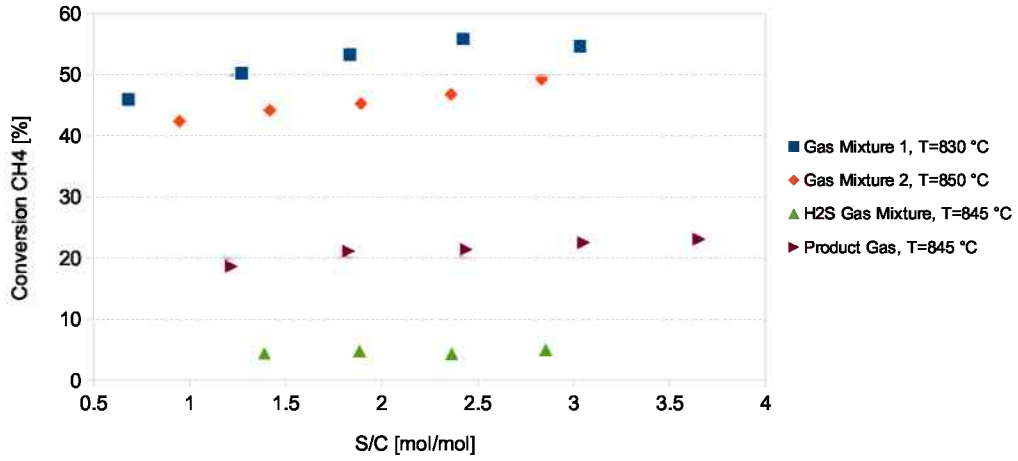

Figure 4.22: CH_4-conversion for different S/C-Ratios (SV=$10\,000\,h^{-1}$)

H_2 Conversion In Fig. 4.23 the results for the hydrogen conversion of different feedstock gases is shown. Here the influence of the steam amount was even higher than for the conversion of methane. The steepest increase showed gas mixture 2, which rose from $-32\,\%$ at S/C=0.9 to $-61\,\%$ at S/C=2.8, so it nearly doubled. The conversion of gas mixture 1 showed a similar increase, but then stagnated at an S/C ratio of around 2.5. The two gases, which contained hydrogen sulfide showed a higher yield in hydrogen with more steam in the inlet. For product gas an increase from $-17\,\%$ to $-32\,\%$ was detected, which means also a doubling of the hydrogen conversion. The conversion for H_2S gas mixture rose from $-6\,\%$ to $-11\,\%$.

Concluding it can be noted, that within the investigated range a higher amount of steam in the inlet always resulted in more hydrogen in the outlet. There is definitely a maximum, when more water vapor in the inlet won't result in more hydrogen, but this maximum couldn't be reached during this experiments.

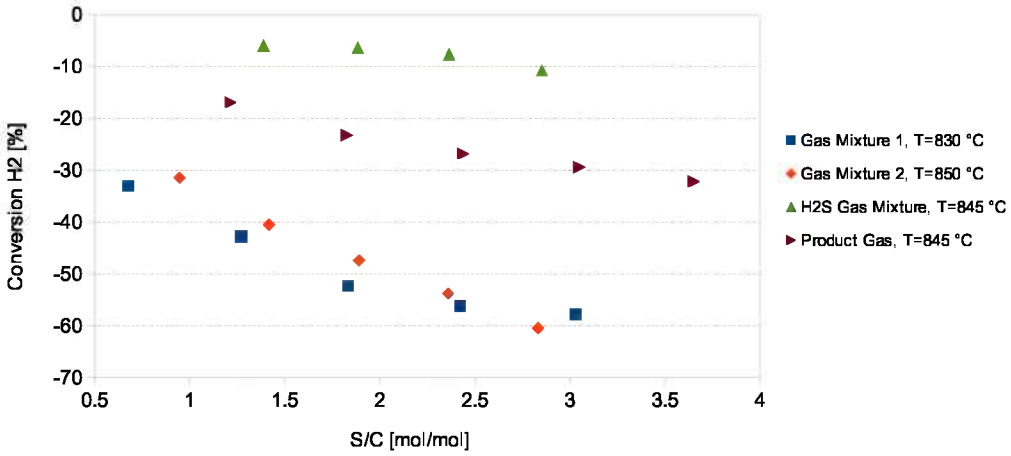

Figure 4.23: H_2-conversion for different S/C-Ratios (SV=10 000 h^{-1})

H_2/CO-Ratio Fig. 4.24 shows the hydrogen to carbon monoxide ratio in dependence on the steam-to-carbon ratio for different feedstock gases. For gas mixture 2 and product gas clear linear trends of the H_2/CO-ratio could be identified. Gas mixture 1 and H_2S gas mixture however showed a steep increase up to a S/C ratio of 2.5, then these two trends leveled out and didn't rise so much with higher S/C ratios.

In general it can be stated, that the steam-to-carbon ratio was a measure to set a desired H_2/CO-ratio. There are further measurements necessary to obtain more data to be able to make clear predictions, but the results represented in Fig. 4.24 confirmed this linear dependency.

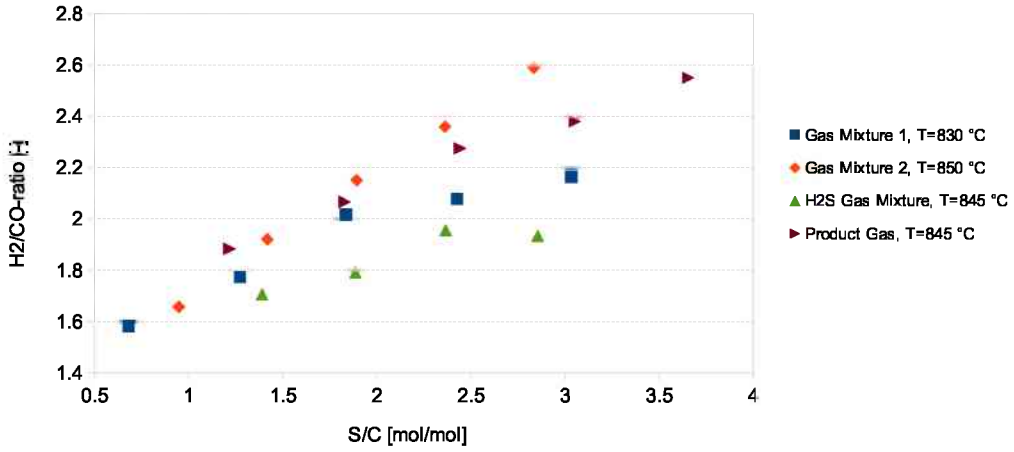

Figure 4.24: H_2/CO-Ratio for different S/C-Ratios (SV=10 000 h^{-1})

H_2-Selectivity In Fig. 4.25 the results for the H_2-selectivity in dependency on the steam-to-carbon ratio is shown. It is interesting that the H_2S poisoned gases (H_2S gas mixture and product gas) showed a high hydrogen selectivity, which meant that more hydrogen was produced from fewer moles of methane consumed. This means probably, that the produced hydrogen came mainly from the water-gas shift reaction and not from the reformation of methane. All different feedstock gases showed the tendency, that the H_2-selectivity went up at higher steam-to-carbon ratios, due to the fact that with more H_2O available the steam reforming reaction became more probable to take place than the dry reforming reaction.

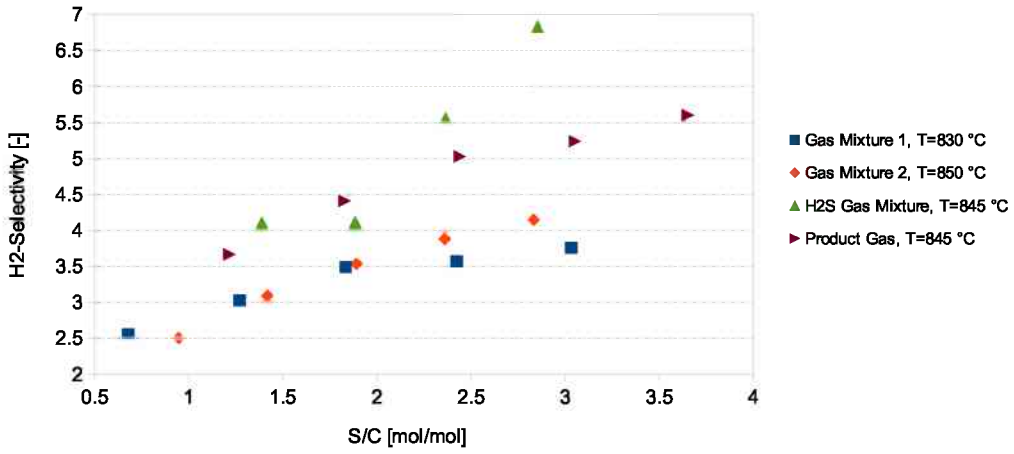

Figure 4.25: H_2-Selectivity for different S/C-Ratios (SV=10 000 h^{-1})

4.5.3 Variation of Space-Velocity

The present section shows the variation of the gas hourly spacevelocity (GHVS or SV) whilst all other parameters (temperature and steam-to-carbon ratio) were kept constant to measure the influence of the spacevelocity on the different output parameters.

CH_4 Conversion As can be seen in Fig. 4.26 the conversion of methane was not very much influenced by the variation of the spacevelocity. The influence was stronger on feedstock gases without H_2S, e.g. for gas mixture 2 the conversion decreased from 57 % at SV=6000 h^{-1} to 45 % at SV=11 000 h^{-1}.

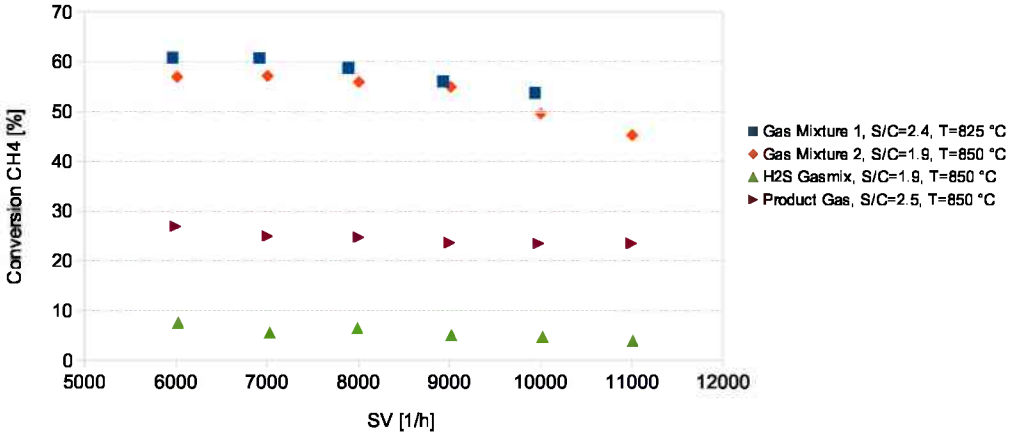

Figure 4.26: CH_4-conversion for different spacevelocities

H_2 Conversion In Fig. 4.27 the conversion of hydrogen is shown for various spacevelocities. Again the dependence on the spacevelocity was more significant for feedstocks, which contained no H_2S and which had a higher conversion of hydrogen. The highest change in hydrogen conversion showed gas mixture 1, which changed from −67 % at SV=6000 h^{-1} to −56 % at SV=10 000 h^{-1}.

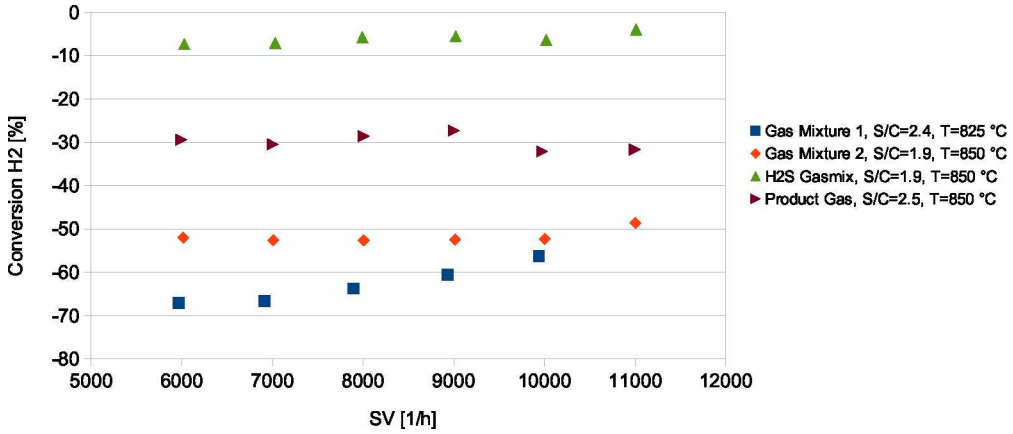

Figure 4.27: H_2-conversion for different spacevelocities

H_2/CO-Ratio Figure 4.28 shows the results for the H_2/CO ratio. It is to mention, that the lowest H_2/CO ratio was measured for H_2S gas mixture at around 1.8, then for gas mixture 2 a ratio of around 2 was measured, for gas mixture 1 the ratio was around 2.2 and for product gas around 2.3. As can be seen in the graph, the values for the H_2/CO ratio were not really constant, but the influence of the spacevelocity was rather low. The two values for product gas at high spacevelocities didn't align well to the other results, which was probably due to an inaccurate measurement.

Other parameters like the steam-to-carbon ratio affected the H_2/CO ratio much more than the spacevelocity.

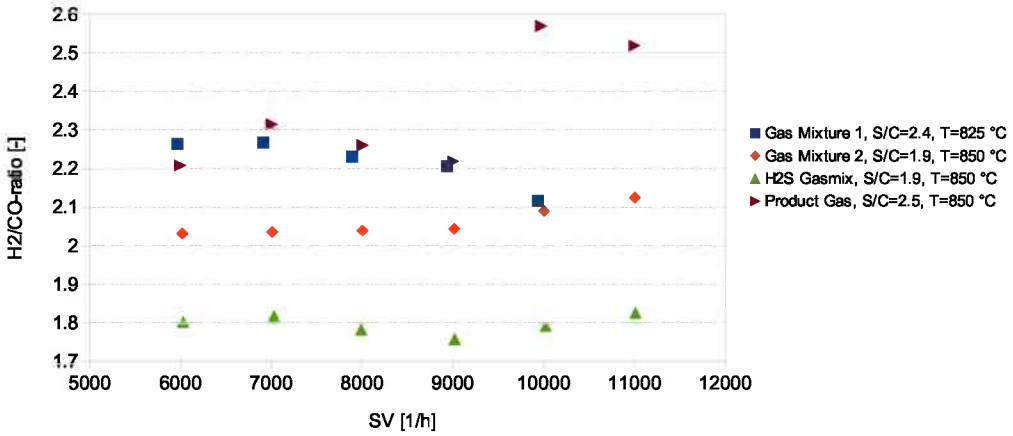

Figure 4.28: H_2/CO-ratio for different spacevelocities

H_2-Selectivity The H_2-selectivity is shown in Fig. 4.29 for various spacevelocities. Again it was hard to identify any clear trends for this parameter regarding the spacevelocity. Just gas mixture 2 showed a trend towards higher H_2-selectivity at higher spacevelocities. Also the trend of product gas went in this direction, but there were several outliers in this graph. The results for H_2S gas mixture were fluctuating very much, thus no useful information regarding this feedstock could be given.

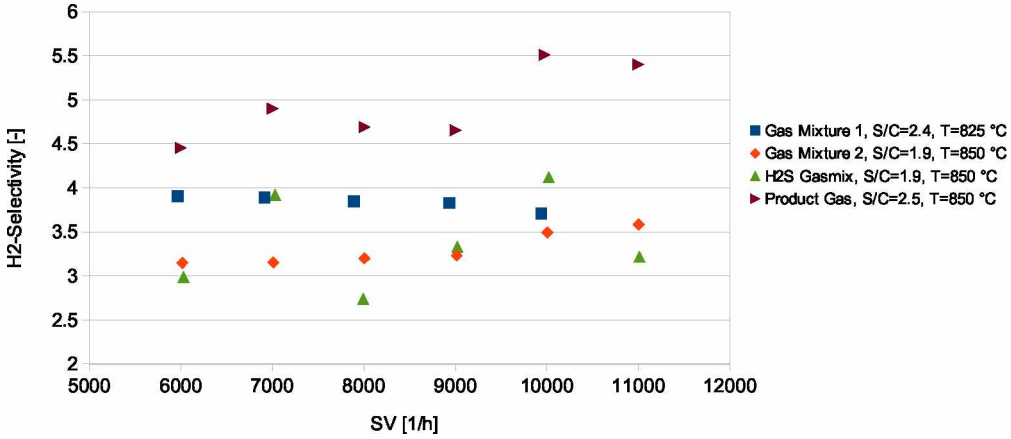

Figure 4.29: H_2-selectivity for different spacevelocities

5 Summary and Conclusions

The goal of this thesis was to analyze a commercial catalyst, based on noble metals, regarding its performance for steam reforming of product gas from dual fluidized bed biomass gasification plants. The experiments were carried out on a laboratory scale unit with a flow rate of around 40 L/h at atmospheric conditions. The hollow-cylindrical shaped catalyst pellets with a diameter of 8 mm were placed in a quartz-glass reactor. The process parameters were varied within the possible range of temperatures from 700 °C to 900 °C, spacevelocities from 6000 h^{-1} to 11 000 h^{-1} and steam-to-carbon ratios of 1 to 3. There were four feedstock gases used for the experiments, with different amounts of H_2S, which was a determining factor for the catalyst's performance.

It was shown, that the catalyst performed not as good as the thermochemical equilibrium would suggest it, but it reached conversion rates up to 60 % for methane. Especially at higher temperatures around 900 °C, which was the upper limit for the test rig, the catalyst showed higher reaction rates. The steam-to-carbon ratio in the reactor inlet influenced significantly the conversion results. Higher S/C-ratios were generally preferred, especially if the hydrogen yield should be high and to avoid coking of the catalyst. A maximum of methane conversion was reached at a S/C-ratio of around 2. The spacevelocity didn't affect the output parameters as much as the other factors, but a clear tendency towards higher conversion rates at lower spacevelocities was identified. When there was sulfur present in the feed steam, the performance dropped significantly, even at concentrations as low as 50 ppm of H_2S. At higher concentrations of H_2S (100 ppm to 200 ppm) the conversion of methane dropped even below 10 %.

Other deactivation mechanism like thermal degradation or coking couldn't be identified at the investigated operating conditions. One explanation to that is the low total operating time of the catalyst, which avoided carbon formation or sintering. Another reason for low carbon formation was that the steam-to-carbon ratio was usually higher than stoichiometrically needed. Although superheated steam is very expensive to produce, this high steam-to-carbon ratios (around 2) are also used in industry to obtain higher conversion yields and to avoid carbon formation [17, p. 234]. Furthermore the used catalyst were engineered especially to avoid common deactivation mechanisms like poisoning and coking. Therefore the active steam reforming material was not just nickel, which is well-known to be susceptible towards carbon deposition, but also other transition metals were used to enhance the stability of the reforming reaction.

The results from this thesis are intended to be used in simulation models for steam reforming of gas mixtures, which include H_2S. There was little research done till now in the field of simulation of sulfur poisoned steam reformers. As described in the beginning, Haldor Topsøe investigated the influence of sulfur on the steam reforming process in the 1980s, but since then the methods and technologies have improved considerably.

Especially not much research has been done for steam reforming of product gas from biomass gasification, which could be a possible pathway for renewable basic chemicals and sustainable energy carriers.

5.1 Subjects for Further Research

The focus of this work was to find suitable operating parameters for a steam reforming catalyst under laboratory conditions. There are still many challenges yet to be mastered and other experiments to be carried out before an economical application of this process on industrial scale for real product gas will be possible.

A lot of other commercial catalysts are available on the market and the research and development for newer, better catalytic materials is still ongoing. Especially as energy efficiency is high on the agenda of politicians and private industries nowadays, there are ambitious efforts towards better energy conversions. Hence also other materials and different commercial catalysts should be analyzed regarding their performance for steam reforming of product gas containing sulfur components.

The long-term application of the tested catalyst could not be investigated within this thesis, which is an important factor for application in large scale. There are many well-known mechanisms, which can affect the catalyst performance if it is exposed for longer time to these high temperatures, which are needed for the reforming reaction. The surface area of the catalyst can be reduced by thermal degradation, which results in less active sites and thus lowering the reaction rates. Also mechanical influences like catalyst breakdown effects the process stability. Carbon formation (coking) at nano-scale is another important issue for long-term stability but therefore special equipment such as in-situ TEM-microscope and reactors for long-time operation are needed. Although the used catalyst should be less vulnerable towards deactivation mechanisms, this needs to be tested under industrial operating conditions, which means long operating hours and high pressure of 30-40 bar. Also the influence of real product gas, which contains dust particles and tars will affect the performance and could result in clogging of the catalyst pores.

References

[1] The Club of Rome. *40 years 'Limits to Growth'*. Web. retrieved on 14.08.2013. URL: http://www.clubofrome.org/?p=326.

[2] Bundesministerium für Wirtschaft, Familie und Jugend. *Energiestatus Österreich 2011*. Web. retrieved on 02.05.2013. 2011. URL: http://www.bmwfj.gv.at/EnergieUndBergbau/Energieversorgung/Documents/Energiestatus2011_Homepage.pdf.

[3] Umweltbundesamt. *Energieeinsatz in Österreich*. Web. retrieved on 07.08.2013. Aug. 2013. URL: http://www.umweltbundesamt.at/umweltsituation/energie/energie_austria/.

[4] The World Bank. *Energy use (kg of oil equivalent per capita)*. Web. retrieved on 13.05.2013 via Google Public Data. URL: http://data.worldbank.org/indicator/EG.USE.PCAP.KG.OE?cid=GPD_26.

[5] Google. *Public Data*. Web. retrieved on 13.05.2013. URL: http://www.google.com/publicdata/.

[6] E-Control. *Stromkennzeichnungsbericht 2011*. Web. retrieven on 07.08.2013. 2011. URL: http://www.e-control.at/portal/page/portal/medienbibliothek/oeko-energie/dokumente/pdfs/Stromkennzeichnungsbericht%202011.pdf.

[7] Martin Kaltschmitt, Hans Hartmann, and Hermann Hofbauer. *Energie aus Biomasse: Grundlagen, Techniken und Verfahren (German Edition)*. 2., neu bearb. u. erw. Aufl. Springer, Nov. 2009. URL: http://amazon.com/o/ASIN/3540850945/.

[8] James H. Clark and Fabien Deswarte, eds. *Introduction to Chemicals from Biomass*. ISBN: 978-1-119-96443-8. Wiley, 2011.

[9] Barbara Rehling. "Development of the 1MW Bio-SNG plant, evaluation on technological and economical aspects and upscaling considerations". PhD thesis. Technical University Vienna, 2012.

[10] Reinhard Rauch and Gabriela Falk. *Mixed Alcohols from Biomass Steam Gasification*. Tech. rep. BIOENERGY 2020+ GmbH, 2011.

[11] Reinhard Rauch. *Renewable fuels for advanced powertrains*. Tech. rep. University of Technology Vienna, 2007. URL: http://www.eee-info.net/cms/netautor/napro4/appl/na_professional/parse.php?mlay_id=2500&xmlval_ID_DOC[0]=1000270.

[12] Institute of Chemical Engineering, TU Vienna. *The Gasification Concept*. Web. retrieved on 9.8.2013. 2011. URL: http://www.ficfb.at/basic.htm.

[13] Institute of Chemical Engineering, TU Vienna. *Description of the Biomass CHP Güssing*. Web. retrieved on 9.8.2013. 2011. URL: http://www.ficfb.at/renet_d.htm.

[14] Alan D. McNaught and Andrew Wilkinson. *Compendium of Chemical Terminology - IUPAC Recommendations.* 2 Sub. XML on-line corrected version: http://goldbook.iupac.org (2006-) created by M. Nic, J. Jirat, B. Kosata. Blackwell Scientific Publications, Oxford, 1997.

[15] Klaus Hertwig and Lothar Martens. *Chemische Verfahrenstechnik - Berechnung, Auslegung und Betrieb chemischer Reaktoren.* München: Oldenbourg Verlag, 2011.

[16] I. Chorkendorff and J. W. Niemantsverdriet. *Concepts of Modern Catalysis and Kinetics.* New York: John Wiley & Sons, 2006.

[17] M. V. Twigg. *Catalyst Handbook.* 2 Sub. Manson Pub., 1996.

[18] Karin Föttinger, Günther Rupprechter, and Yuri Suchorski. *Vorlesung Kinetik und Katalyse (165.103).* Web. E165 Institut für Materialchemie, TU Vienna. 2013. URL: https://tiss.tuwien.ac.at/course/courseDetails.xhtml?windowId=b4f&courseNr=165103.

[19] Oxeeco Technologies Pvt. Ltd. *Catalysts.* Web. retrieved on 11.8.2013. 2013. URL: http://www.oxeeco.in/catalysts.

[20] C.A. Francesco, D.A. Kramer, and L.E. Apodaca. *NITROGEN (FIXED)—AMMONIA STATISTICS.* U.S. GEOLOGICAL SURVEY, Oct. 2010. URL: http://minerals.usgs.gov/ds/2005/140/nitrogen.pdf.

[21] S. N. Bizzari and M. Blagoev. *Chemical Industries Newsletter CEH Marketing Research Report Abstract- Hydrogen.* Tech. rep. SRI Consulting, Oct. 2007. URL: http://chemical.ihs.com/nl/Public/2007Oct.pdf.

[22] J.R. Rostrup-Nielsen, J. Sehested, and Jens Kehlet Nørskov. "Hydrogen and Synthesis gas by Steam- and CO2 reforming". In: *Advances in Catalysis.* Vol. 47. 2002.

[23] Axel Düker. "Hydrogen- Production and Application in Industry". In: *Presentation Süd-Chemie.* Süd-Chemie AG. 2011.

[24] J. Zhu, D. Zhang, and K.D. King. "Reforming of CH4 by partial oxidation: thermodynamic and kinetic analyses". In: *Fuel* 80.7 (2001), pp. 899 –905. URL: http://www.sciencedirect.com/science/article/pii/S0016236100001654.

[25] Mojdeh Ashrafi. "Hydrogen-Rich Gas and Production through and Steam Reforming and of Biogas". PhD thesis. Technische Universität Wien, 2008.

[26] J.R. Rostrup-Nielsen and J.H.B. Hansen. "CO2-Reforming of Methane over Transition Metals". In: *Journal of Catalysis* 144.1 (1993), pp. 38 –49. URL: http://www.sciencedirect.com/science/article/pii/S0021951783713126.

[27] Mariana de Mattos V. M. Souza and Martin Schmal. "Supported Nickel Catalysts for Steam Reforming of Methane". In: *2nd Mercosur Congress on Chemical Engineering* (2005). URL: http://www.enpromer2005.eq.ufrj.br/nukleo/pdfs/0141_enpromer_141.pdf.

[28] Haldor Topsøe A/S. *Catalyst Portfolio.* Web. retrieved on 11.8.2013. 2013. URL: http://www.topsoe.com/products/CatalystPortfolio.aspx.

[29] Jens R. Rostrup-Nielsen. "40 years in catalysis". In: *Catalysis Today* 111.1–2 (2006). Frontiers in Catalysis: A Molecular View of Industrial Catalysis, pp. 4 –11. URL: http://www.sciencedirect.com/science/article/pii/S0920586105007017.

[30] Calvin H. Bartholomew. "Mechanisms of catalyst deactivation". In: *Applied Catalysis A* 212 (2001), pp. 17–60.

[31] Jens Sehested. "Four challenges for nickel steam-reforming catalysts". In: *Catalysis Today* 111.1–2 (2006). Frontiers in Catalysis: A Molecular View of Industrial Catalysis, pp. 103 –110. URL: http://www.sciencedirect.com/science/article/pii/S092058610500708X.

[32] Kim Aasberg-Petersen et al. "Recent developments in autothermal reforming and pre-reforming for synthesis gas production in GTL applications". In: *Fuel Processing Technology* 83.1–3 (2003), pp. 253 –261. URL: http://www.sciencedirect.com/science/article/pii/S0378382003000730.

[33] Zhongxiang Chen, Yibin Yan, and Said S.E.H. Elnashaie. "Catalyst deactivation and engineering control for steam reforming of higher hydrocarbons in a novel membrane reformer". In: *Chemical Engineering Science* 59.10 (2004), pp. 1965 –1978. URL: http://www.sciencedirect.com/science/article/pii/S0009250904001071.

[34] J. R. Rostrup-Nielsen. "Sulfur-Passivated Nickel Catalysts for Carbon-Free Steam Reforming of Methane". In: *Journal of Catalysis* 85 (1984), pp. 31–43.

[35] Jens R. Rostrup-Nielsen. "Syngas in perspective". In: *Catalysis Today* 71.3–4 (2002), pp. 243 –247. URL: http://www.sciencedirect.com/science/article/pii/S0920586101004540.

[36] Jens R. Rostrup-Nielsen. "Chemisorption of hydrogen sulfide on a supported nickel catalyst". In: *Journal of Catalysis* 11.3 (1968), pp. 220 –227. URL: http://www.sciencedirect.com/science/article/pii/0021951768900353.

[37] Meghana Rangan, Matthew M. Yung, and J. William Medlin. "Experimental and computational investigations of sulfur-resistant bimetallic catalysts for reforming of biomass gasification products". In: *Journal of Catalysis* 282.2 (2011), pp. 249 –257. URL: http://www.sciencedirect.com/science/article/pii/S0021951711001953.

[38] Kazuhiro Sato and Kaoru Fujimoto. "Development of new nickel based catalyst for tar reforming with superior resistance to sulfur poisoning and coking in biomass gasification". In: *Catalysis Communications* 8.11 (2007), pp. 1697 –1701. URL: http://www.sciencedirect.com/science/article/pii/S1566736707000349.

[39] Christian Hulteberg. "Sulphur-tolerant catalysts in small-scale hydrogen production, a review". In: *International Journal of Hydrogen Energy* 37.5 (2012), pp. 3978 –3992. URL: http://www.sciencedirect.com/science/article/pii/S0360319911026516.

[40] Kaimin Shih and James O. Leckie. "Nickel aluminate spinel formation during sintering of simulated Ni-laden sludge and kaolinite". In: *Journal of the European Ceramic Society* 27 (2007), pp. 91–99.

[41] Ulla Lassi. *Catalyst deactivation mechanisms*. Web. retrieved on 13.8.2013. 2003. URL: http://herkules.oulu.fi/isbn9514269543/html/x546.html.

[42] Forschungszentrum Jülich. *Reformierung*. Web. retrieved on 14.3.2013. 2013. URL: http://www.fz-juelich.de/iek/iek-3/DE/Forschung/BGS/Brennstoffzellenseiten/Reformierung/_node.html.

[43] R. Zennaro, F. Hugues, and E. Caprani. *Synthesis Gas Chemistry*. Tech. rep. Eni, IFP, Axens, 2006. URL: http://www.dgmk.de/petrochemistry/abstracts_content14/Zennaro.pdf.

[44] Inyong Kang, Joongmyeon Bae, and Gyujong Bae. "Performance comparison of autothermal reforming for liquid hydrocarbons, gasoline and diesel for fuel cell applications". In: *Journal of Power Sources* 163.1 (2006), pp. 538 –546. URL: http://www.sciencedirect.com/science/article/pii/S0378775306019409.

[45] MKS Instruments GmbH. *1179A Mass-Flo*. Web. retrieved on 11.07.2013. July 2013. URL: http://www.mksinst.com/product/Product.aspx?ProductID=68.

[46] Bronkhorst High-Tech B.V. *Digital Mass Flow / Pressure Meters and Controllers Specification Sheet*. Bronkhorst High-Tech B.V. 2013.

[47] Bronkhorst High-Tech B.V. *LIQUI-FLOW® Specification Sheet*. Bronkhorst High-Tech B.V. 2013.

[48] Bronkhorst High-Tech B.V. *Liquid Delivery System with Vapour Control Specification Sheet*. Bronkhorst High-Tech B.V. 2013.

[49] Elster-Instromet Vertriebsges. m.b.H. *BK-G2,5 und BK-G2,5T*. Jan. 2010. URL: www.elster-instromet.com.

[50] Emerson Process Management. *Instruction Manual NGA 2000 MLT Hardware*. 2008. URL: http://www2.emersonprocess.com/siteadmincenter/PM%20Rosemount%20Analytical%20Documents/PGA_Manual_MLT_CAT200_HW_200804.pdf.

[51] José David Martinez Cerezo. "Heterogeneous modeling of steam reforming of methane". MA thesis. Technical University of Cartagena (Spain), 2007. URL: http://repositorio.bib.upct.es/dspace/bitstream/10317/89/1/pfc2270.pdf.

[52] AZoM. *Silicon Dioxide (SiO2)*. Web. retrieved on 11.07.2013. June 2013. URL: http://www.azom.com/article.aspx?ArticleID=1114.

[53] MakeItFrom. *Aluminum Oxide (Al2O3)*. Web. retrieved on 11.07.2013. July 2013. URL: http://www.makeitfrom.com/material-data/?for=Alumina-Aluminum-Oxide-Al2O3.

List of Figures

A Appendix

A.1 Abbreviations

Symbol	Description
CHP	combined heat and power
CO	carbon monoxide
CO_2	carbon dioxide
CH_4	methane
COS	carbonyl sulfide
DFB	dual fluidized bed
GC	gas chromatography
GCF	gas correction factor
GHSV	gas hourly spacevelocity
H_2	hydrogen
H_2O	water
H_2S	hydrogen sulfide
MFC	massflow controller
Ni	nickel
O_2	oxygen
ppm	parts per million; 10^{-6}
SV	spacevelocity
TEM	transmission electron microscopy
TU	Technische Universität, technical university
vol-%	volume-fraction in percent

A.2 Symbols and Units

Symbol	Unit	Description
c_x	[vol-%]	concentration of substance x
H_2/CO	[-]	ratio between H_2 and CO gas concentration
$\dot{m}_i$	[g/h]	mass-flow of substance i in gram per hour
$\dot{n}_i$	[mol/s]	mole-flow of substance i in mole per second
S/V	[mol/mol]	steam-to-carbon ratio, see 3.4.1
SV	[h^{-1}]	spacevelocity, see 3.4.1
t	[s] or [h]	time
T	[°C]	temperature in °C
$\dot{V}$	[L/h]	volume flow
V	[L]	volume
X_i	[%]	conversion of substance i
Y_i	[-]	volume-fraction of substance i

A.3 Results Datasheets

A.3.1 Gas Mixture 1

Parameter				Outlet Concentration					Difference Outlet-Inlet Concentration					Conversion X (in % of [mol/h]				
SC	SV	T	H_2S	CO	CO_2	CH_4	H_2	N_2/Rest	CO	CO_2	CH_4	H_2	N_2/Rest	CO	CO_2	CH_4	H_2	N_2/Rest
[-]	[1/h]	[°C]	[ppm]	[vol-%]	[vol-%]	[vol-%]	[vol-%]	[vol-%]	[vol-%]	[vol-%]	[vol-%]	[vol-%]	[vol-%]	[%]	[%]	[%]	[%]	[%]
1.6	9997	647		19.11	16.95	8.92	36.70	18.36	-0.3	0.4	0.7	-2.6	1.8	-3.5	0.7	5.7	-9.5	7.2
1.6	9996	706		19.93	16.33	8.72	37.11	17.95	-1.2	1.0	0.9	-3.0	2.2	-8.0	4.3	7.8	-10.7	9.3
1.6	9997	776		21.13	15.20	7.71	38.96	17.03	-2.4	2.2	1.9	-4.8	3.1	-17.0	9.1	16.7	-18.7	12.1
1.6	10001	833		22.87	13.55	5.96	41.85	15.77	-4.1	3.8	3.7	-7.7	4.4	-31.5	15.7	33.1	-32.5	15.4
1.6	9999	882		24.53	12.03	4.46	43.96	15.00	-5.8	5.3	5.2	-9.8	5.1	-45.8	22.8	48.3	-43.8	16.9
2.5	9938	817		21.21	13.57	3.74	44.87	16.59	-2.4	3.8	5.9	-10.8	3.6	-34.2	7.2	53.8	-56.3	2.1
2.5	8933	818		20.43	13.74	3.47	45.07	17.27	-1.7	3.6	6.1	-10.9	2.9	-32.3	3.8	56.1	-60.6	-4.2
2.4	7891	828		20.14	13.49	3.19	44.94	18.23	-1.4	3.9	6.4	-10.8	1.9	-33.3	3.5	58.7	-63.7	-12.5
2.4	6914	827		19.62	13.25	2.95	44.50	19.66	-0.8	4.1	6.7	-10.4	0.5	-33.5	2.6	60.8	-66.7	-24.7
2.3	5965	825		19.23	12.86	2.88	43.53	21.49	-0.5	4.5	6.7	-9.4	-1.3	-34.1	3.1	60.9	-67.0	-39.6
0.7	9551	824		27.18	11.20	4.92	43.00	13.72	-8.5	6.1	4.7	-8.9	6.6	-53.0	31.9	46.0	-33.1	28.8
1.3	10004	829		24.83	12.16	4.32	44.03	14.66	-6.1	5.2	5.3	-10.0	5.7	-46.5	22.4	50.2	-42.8	20.3
1.8	10015	826		22.28	13.36	3.88	44.94	15.54	-3.5	4.0	5.7	-10.9	4.8	-37.4	10.9	53.3	-52.4	11.7
2.4	10021	827		21.69	13.39	3.59	45.08	16.25	-3.0	3.9	6.0	-11.0	4.1	-36.8	8.8	55.9	-56.3	5.6
3.0	10021	830		20.62	13.63	3.61	44.61	17.54	-1.9	3.7	6.0	-10.5	2.8	-32.7	5.1	54.7	-57.9	-4.0
3.2	9985	688		16.39	17.17	6.12	41.20	19.15	1.8	-0.4	3.2	-7.9	3.3	-0.7	-14.0	26.6	-37.8	4.9
3.2	10014	744		18.51	15.47	4.73	43.32	17.99	-0.4	1.3	4.6	-10.0	4.5	-16.6	-5.3	41.8	-48.5	8.4
3.2	10012	800		19.78	14.42	4.00	44.22	17.59	-1.6	2.4	5.3	-10.9	4.9	-26.2	0.6	50.1	-53.6	9.3
3.2	10015	829		19.84	14.18	3.40	45.30	17.28	-1.7	2.6	5.9	-12.0	5.2	-29.2	0.2	56.8	-60.6	9.0
3.2	10011	883		19.88	14.06	2.89	46.40	16.78	-1.7	2.7	6.4	-13.1	5.7	-31.6	-0.6	62.7	-67.2	10.2

Table A.1: Results for gas mixture 1

A.3.2 Gas Mixture 2

Parameter				Outlet Concentration					Difference Outlet-Inlet Concentration					Conversion X (in % of [mol/h]				
SC	SV	T	H_2S	CO	CO_2	CH_4	H_2	N_2/Rest	CO	CO_2	CH_4	H_2	N_2/Rest	CO	CO_2	CH_4	H_2	N_2/Rest
[-]	[1/h]	[°C]	[ppm]	[vol-%]	[vol-%]	[vol-%]	[vol-%]	[vol-%]	[vol-%]	[vol-%]	[vol-%]	[vol-%]	[vol-%]	[%]	[%]	[%]	[%]	[%]
1.9	10006	680		19.33	27.69	11.03	40.85	1.2	2.3	-1.4	0.3	-0.9	-0.3	8.9	-7.5	0.4	-4.2	-31.9
1.9	10008	740		19.31	26.70	10.36	42.65	1.1	2.3	-0.4	0.9	-2.7	-0.1	6.2	-6.7	3.7	-12.0	-21.0
1.9	9998	789		20.59	24.82	8.56	45.41	0.7	1.0	1.5	2.7	-5.4	0.2	-4.4	-3.6	16.9	-24.6	17.9
1.9	10005	838		22.49	23.19	6.12	48.05	0.2	-0.9	3.1	5.2	-8.1	0.7	-18.8	-0.9	38.1	-37.4	75.0
1.9	10005	887		24.22	22.17	4.96	48.73	-0.1	-2.6	4.1	6.3	-8.8	1.0	-29.1	2.7	49.4	-40.5	106.4
0.9	9998	847		27.71	20.49	5.95	45.91	-0.02	-5.4	6.1	5.6	-7.0	0.8	-38.5	13.9	42.4	-31.5	102.6
1.4	10008	850		24.76	22.13	5.59	47.54	0.03	-2.5	4.4	5.9	-8.6	0.7	-27.8	4.1	44.2	-40.5	95.7
1.9	10004	847		22.66	23.24	5.35	48.73	0.06	-0.4	3.3	6.2	-9.8	0.7	-19.7	-3.1	45.3	-47.4	91.3
2.4	10011	851		21.11	24.00	5.10	49.81	0.03	1.2	2.5	6.4	-10.9	0.8	-13.9	-8.7	46.8	-53.8	96.0
2.8	10010	848		19.68	24.75	4.77	50.91	-0.05	2.6	1.8	6.8	-12.0	0.8	-8.3	-14.4	49.3	-60.5	108.3
1.9	11003	846		22.65	22.72	5.30	48.11	1.44	-0.2	3.5	6.2	-9.7	0.2	-19.6	-3.1	45.3	-48.6	-5.5
1.9	10004	845		23.23	22.17	4.85	48.55	1.42	-0.6	4.0	6.7	-10.3	0.3	-23.2	-1.8	49.6	-52.3	1.1
1.9	9014	851		23.98	21.48	4.28	49.01	1.46	-1.6	4.5	7.1	-10.4	0.3	-28.6	0.5	55.0	-52.5	2.5
1.9	8006	852		24.10	21.32	4.17	49.14	1.22	-1.8	4.6	7.2	-10.4	0.7	-29.9	1.1	56.0	-52.7	21.8
1.9	7008	858		24.20	21.24	4.03	49.27	1.20	-1.9	4.7	7.3	-10.4	0.4	-30.8	1.5	57.2	-52.6	11.6
1.9	6016	860		24.30	20.99	4.05	49.36	1.23	-2.1	4.9	7.3	-10.3	0.4	-31.8	2.3	57.0	-52.0	7.0
1.0	9993	695		22.15	26.10	11.45	40.42	-0.05	-0.2	0.2	0.2	0.4	-0.5	-1.3	0.4	1.4	0.7	90.6
1.0	9992	808		26.06	23.02	9.06	42.29	-0.36	-4.1	3.2	2.6	-1.5	-0.2	-22.4	9.8	20.0	-6.7	28.9
1.0	10005	900		30.81	19.54	6.26	44.04	-0.61	-8.9	6.7	5.4	-3.3	0.1	-48.6	21.4	43.2	-14.1	-24.3
2.9	10005	697		18.67	27.94	10.96	42.72	-0.22	3.1	-1.6	0.6	-2.0	-0.1	11.2	-9.9	1.6	-8.5	31.8
2.9	10008	804		18.34	27.43	8.38	46.02	-0.12	3.4	-1.1	3.2	-5.2	-0.2	7.2	-14.7	20.0	-24.3	60.5
2.9	10017	894		21.53	24.36	4.98	48.76	0.40	0.2	2.0	6.6	-8.0	-0.7	-15.9	-8.5	49.4	-40.2	242.2

Table A.2: Results for gas mixture 2

A.3.3 H_2S Gas Mixture

Parameter				Outlet Concentration					Difference Outlet-Inlet Concentration					Conversion X (in % of [mol/h]				
SC	SV	T	H_2S	CO	CO_2	CH_4	H_2	N_2/Rest	CO	CO_2	CH_4	H_2	N_2/Rest	CO	CO_2	CH_4	H_2	N_2/Rest
[-]	[1/h]	[°C]	[ppm]	[vol-%]	[vol-%]	[vol-%]	[vol-%]	[vol-%]	[vol-%]	[vol-%]	[vol-%]	[vol-%]	[vol-%]	[%]	[%]	[%]	[%]	[%]
1.9	10039	685	163	20.57	25.61	11.57	38.89	3.43	0.3	-0.3	0.0	-0.1	0.0	1.3	-1.1	0.2	-0.5	1.0
1.9	10039	743	163	20.95	25.58	11.58	38.50	3.46	-0.1	0.0	0.0	0.0	0.1	-0.1	0.0	0.3	0.1	1.5
1.9	10040	795	163	21.36	25.48	11.47	38.29	3.48	0.1	0.3	0.4	-0.9	0.1	-1.1	-0.1	2.2	-3.9	0.9
1.9	10021	853	163	21.28	25.79	11.09	38.12	3.79	0.1	0.4	0.8	-1.5	0.1	-1.7	-0.8	4.8	-6.4	0.2
1.9	10024	887	163	23.37	24.20	9.56	39.54	3.41	-1.9	1.6	2.3	-2.2	0.2	-12.9	3.0	16.8	-9.5	0.9
1.4	10010	842	163	22.28	25.28	11.34	38.02	3.16	-0.4	0.9	0.8	-1.4	0.1	-3.9	1.2	4.4	-6.0	2.0
1.9	10021	853	163	21.28	25.79	11.09	38.12	3.79	0.1	0.4	0.8	-1.5	0.1	-1.7	-0.8	4.8	-6.4	0.2
2.4	10010	845	163	19.96	26.50	11.00	39.04	3.57	1.4	-0.6	0.8	-1.8	0.1	3.9	-5.2	4.4	-7.7	0.9
2.9	10044	836	163	20.15	26.11	10.64	38.99	4.17	0.9	0.3	1.0	-2.4	0.2	0.6	-2.7	5.0	-10.8	-0.2
1.9	11011	844	163	21.07	25.98	11.25	38.46	3.33	0.4	-0.2	0.6	-0.9	0.1	0.5	-2.2	3.9	-4.0	1.5
1.9	10021	853	163	21.28	25.79	11.09	38.12	3.79	0.1	0.4	0.8	-1.5	0.1	-1.7	-0.8	4.8	-6.4	0.2
1.9	9021	857	163	21.57	25.67	11.08	37.92	3.84	-0.2	0.5	0.8	-1.3	0.0	-2.8	0.0	5.1	-5.5	-0.8
1.9	7991	856	163	21.41	25.68	10.92	38.16	3.90	0.1	0.1	1.0	-1.3	0.1	-1.8	-1.5	6.5	-5.7	-0.3
1.9	7030	847	163	21.12	25.69	10.94	38.38	3.94	0.3	0.2	0.9	-1.6	0.1	-1.1	-1.7	5.6	-7.1	-0.1
1.9	6027	852	163	21.37	25.51	10.68	38.50	4.00	0.0	0.4	1.2	-1.7	0.1	-2.7	-1.3	7.6	-7.3	0.2
1.9	6012	835	163	20.79	25.75	10.89	39.24	3.40	0.7	-0.4	1.0	-1.5	0.2	1.1	-4.0	6.5	-6.4	2.3
1.9	9994	847	0	22.62	23.66	6.20	47.38	0.2	-1.2	2.6	5.1	-6.3	-0.2	-18.1	-2.5	39.4	-28.9	196.9
1.9	10000	849	25	22.77	23.51	6.20	47.05	0.5	-1.4	2.7	5.1	-5.9	-0.6	-18.9	-1.8	39.4	-28.0	100.0
1.9	9999	850	50	22.35	23.83	6.78	45.74	1.4	-0.9	2.4	4.5	-4.6	-1.4	-15.6	-2.3	34.4	-23.3	100.0
1.9	9994	850	75	21.41	25.92	9.98	41.52	1.2	0.0	0.3	1.3	-0.4	-1.3	-2.4	-2.8	10.8	-3.4	100.0
1.9	10000	849	100	21.29	26.09	10.50	40.59	1.6	0.1	0.1	0.8	0.5	-1.7	-0.8	-2.5	7.0	-0.1	100.0
1.9	9999	849	150	20.92	26.17	10.71	39.92	2.3	0.5	0.1	0.6	1.2	-2.4	0.8	-2.9	5.0	1.4	100.0
1.9	10007	849	200	20.73	26.04	10.77	39.43	3.1	0.7	0.2	0.6	1.7	-3.2	1.3	-2.9	4.1	2.2	100.0

Table A.3: Results for H_2S gas mixture

A.3.4 Product Gas

Parameter				Outlet Concentration					Difference Outlet-Inlet Concentration					Conversion X (in % of [mol/h]				
SC	SV	T	H_2S	CO	CO_2	CH_4	H_2	N_2/Rest	CO	CO_2	CH_4	H_2	N_2/Rest	CO	CO_2	CH_4	H_2	N_2/Rest
[-]	[1/h]	[°C]	[ppm]	[vol-%]	[vol-%]	[vol-%]	[vol-%]	[vol-%]	[vol-%]	[vol-%]	[vol-%]	[vol-%]	[vol-%]	[%]	[%]	[%]	[%]	[%]
2.5	10997	845		16.73	19.55	6.11	42.13	15.52	-0.7	1.3	2.4	-7.8	4.8	-11.9	-0.5	23.5	-31.7	18.2
2.5	9974	846		16.33	19.54	6.03	41.97	16.15	-0.4	1.2	2.5	-7.7	4.3	-10.4	-1.6	23.5	-32.1	14.7
2.4	9001	849		19.09	18.51	6.30	42.37	13.75	-2.6	3.0	2.5	-6.9	4.1	-23.3	8.2	23.7	-27.3	17.7
2.4	8005	850		18.76	18.42	6.12	42.41	14.31	-2.4	3.0	2.6	-7.0	3.8	-22.9	7.5	24.7	-28.6	15.2
2.4	7003	846		18.20	18.40	6.03	42.14	15.23	-2.1	2.4	2.5	-7.7	4.9	-20.7	5.7	25.0	-30.5	19.5
2.4	5996	848		18.88	17.40	5.77	41.68	16.29	-3.0	3.2	2.7	-7.3	4.4	-27.1	9.9	26.9	-29.4	15.7
1.2	9999	843		21.88	17.47	7.10	41.20	12.41	-5.0	4.5	1.9	-4.8	3.4	-33.5	18.1	18.7	-16.9	18.8
1.8	9985	846		19.70	17.52	6.49	40.70	15.65	-3.6	3.3	2.1	-6.3	4.4	-27.3	12.4	21.2	-23.3	18.8
2.4	10006	845		18.02	18.38	6.32	40.99	16.36	-2.0	2.2	2.2	-6.9	4.5	-19.1	5.9	21.5	-26.9	17.4
3.0	10020	847		17.24	18.58	6.12	41.03	17.09	-1.4	1.8	2.3	-7.3	4.7	-16.1	3.2	22.5	-29.4	16.6
3.7	10003	848		16.14	19.02	5.95	41.15	17.79	-0.5	1.1	2.3	-7.8	4.9	-10.9	-1.1	23.1	-32.2	15.8
2.4	9999	698		16.21	20.23	7.93	37.12	18.59	-0.2	0.5	0.6	-3.0	2.2	-3.2	0.4	5.1	-10.8	9.0
2.4	9998	750		16.68	19.73	7.58	38.34	17.75	-0.7	1.0	0.9	-4.2	3.0	-7.1	2.0	8.5	-15.4	12.3
2.4	9998	799		17.11	19.22	7.08	39.54	17.11	-1.1	1.5	1.4	-5.4	3.7	-11.4	3.3	13.4	-20.6	14.4
2.4	9996	850		18.23	18.09	6.20	40.97	16.55	-2.2	2.6	2.3	-6.9	4.2	-21.2	7.1	22.6	-27.6	15.4
2.4	10000	903		19.73	16.59	4.86	42.79	16.07	-3.7	4.1	3.7	-8.7	4.7	-35.4	12.0	37.4	-37.6	15.2

Table A.4: Results for product gas